Section 2

Better Knowledge of Objects

Proceedings of Metal 2004 National Museum of Australia Canberra ACT 4–8 October 2004
ABN 70 592 297 967

Solder on silver: historical usage and the problem of fretting

M.J.T.M. van Bellegem[a], H.A. Ankersmit[b], R. van Langh[c] and W. Wei[d]

[a] Westerstraat 242-II, NL-1015 MT Amsterdam, The Netherlands,
[b, d] Netherlands Institute for Cultural Heritage, P.O. Box 76709, NL-1070 KA Amsterdam, The Netherlands.
[c] Rijksmuseum Amsterdam, P.O. Box 74888, NL-1070 DN Amsterdam, The Netherlands.

Abstract

A preliminary study is being conducted in order to determine the cause of fretting of silver objects by tin-based solders. The microstructures of reproductions of historic solder joints as well as model samples are being examined using optical and scanning electron microscopy (SEM). Thus far, it has been found that soldering, which generally occurs at approximately 200 °C, appears to result in the formation of an Ag_3Sn layer as a result of the dissolution of silver by tin. Above 221 °C, the Ag_3Sn layer goes partially into solution and is in equilibrium with a Sn rich liquid phase. Thus, typical methods to remove solder by reheating above the soldering temperature only partially remove the Ag_3Sn layer and allow free tin to further dissolve silver. This dissolution is slow enough that it is not obvious to the naked eye. During the restoration of a soldered joint by brazing, temperatures rise above 480 °C. At these temperatures, the Ag_3Sn layer has completely decomposed. Free tin dissolves silver, but now at a much higher rate, resulting in fretting. In order to avoid fretting, it is thus important to find a method to remove the Ag_3Sn layer before brazing.

Keywords: (soft) solder, brazing, silver, tin, lead, fretting, intermetallic compounds

1. Introduction

Silverware, which has been repaired using soft solders, based on alloys of tin (Sn) and lead (Pb) poses several problems to conservators. The solder has often been applied extensively, thus disturbing the surface and the colour of the object. The solder joints are often weak in comparison to joints executed with silver brazes, and are thus more prone to failure. It should be taken into account that the desired strength for a repair depends the function of the object. The solder may also be the cause of a form of damage to the silver object known as fretting (Brehpohl 1996; Untracht 1975; Urs Stussi 1988; Cuzner 1965; Wylie Davidson 1913). Fretting is a term used to indicate the damage caused by the dissolution of silver by tin-lead solders, the silver being "eaten away" as it were. Fretting appears as dark spongy spots in the silver surface, (see for example, Figure 4 in Niemeyer,1997, p191). Replacing the soldered joint with silver brazing often results in failure due to fretting.

Corresponding author: TEL: +31204704746, metalsconservation@yahoo.com

The conservator or silversmith thus has several options for repairing soldered joints:
1. Reapplication of solder.
2. Removal of solder using mechanical or chemical methods, followed by brazing.
3. Removal of solder using mechanical or chemical methods, followed by gluing.
4. Removal of the affected area of silver and replacement with a new piece of silver.

Currently, conservators and many silversmiths find the use of solder on silver unnecessary and undesirable (conservators also find brazing to be undesirable). Gluing is a possibility (often used with fiber reinforcement), and is generally the preferred alternative (Costa 2001). However, gluing (third option above), as well as reapplication of solder (first option), have the disadvantage that the resulting joint is still weak. This can be a problem in cultural collections where objects may still have a functional use. However, for objects in a museum collection, the demands on usage are different and choices will often be made in favor of a weaker joint so that it will fail preferentially in order to avoid damaging the original parts of the object. The fourth option, replacing the affected area of silver, is more complex and is fraught with ethical issues. The second option is thought to provide a stronger joint and to result in the least amount of damage to the silver object, though in most cases. However, the phenomenon of

fretting when brazing former solder joints is well-known by gold- and silversmiths and has prevented brazing from being more widely accepted.

It is not clear from the literature whether fretting is caused during soldering, or later, for example during removal of the solder and subsequent brazing. A microstructural study is thus being conducted to determine the cause of fretting and to find solutions for avoiding the problem.

2. Experimental procedure

Microstructural studies are being conducted on reproductions of historical solder joints, and on model solder samples where soldering conditions are systematically varied. To study the soldering process and the influence of various parameters on the interaction between solder and silver alloy during soldering, a series of reproductions have been carried out. 925/000 (sterling) silver discs (Degussa), 5 mm diameter and 1 mm thick were soldered in the centre of 30 x 30 x 1 mm 925/000 silver sheet (Degussa) specimens using a propane/oxygen gas torch. Various combinations of fluxes and solders as found in historical sources were used, see Table 1.

Table 1

Solder / Flux combinations used in historic reproductions
(compositions in wt.%)

Solder	Flux
50Sn-50Pb	S-39 flux (containing ZnCl)
50Sn-50Pb	one of the following: • tallow • colophonium
60Sn-40Pb	S-39 flux (containing ZnCl)
96.5Ag-3.5Sn	flux for Sn-Ag solder (Felder GmbH, containing zinc chloride, ammonium chloride, hydrochloric acid, isopropanol and water)

Before soldering, the surfaces were polished with 800 grit paper and then cleaned with ethanol. Soldering was conducted using a propane/oxygen torch. The temperature of the backside of the silver sheet (away from the solder) was measured with a thermocouple (Testo 925™). After soldering, the specimens were cooled in air and the flux remnants were rinsed off with tap water.

The repair of a solder joint by brazing was also simulated. The solder was removed from the 50Sn-50Pb specimen by melting, shaking as much solder as possible off, and wiping the rest off with a cloth. The silver disc was then reattached using a soft silver braze with borax as the flux.

Based on the results of the reproductions, the interaction of soldering materials with silver was studied. 50Sn-50Pb solder, pure Sn, or pure Pb were melted and held at various temperatures on 925/000 silver or pure silver sheet specimens cast from fine silver granules (Degussa; 30 x 30 x 1 mm), see Table 2. The experiments were conducted in a Carbolite™ oven. After heating for the specified time, the specimens were cooled in air.

Table 2

Test parameters for investigation of interaction between solder materials and silver
(compositions in wt.%)

- 50Sn-50Pb on 925/000 silver sheet specimens, held for 4 minutes at 200, 400, 600 or 800 °C
- Pure Sn on fine silver sheet specimens held for 4 minutes at 400, 600 and 800 °C
- Pure Pb on fine silver sheet specimens held for 4 minutes at 400, 600 and 800 °C

Cross sections were cut from the soldered specimens and prepared metallographically using techniques recommended by Struers. The sections were embedded in Specifix Resin, ground using Hermes waterproof paper (220, 800, 1600 and 3200 grit) polished with nine, three, and 1 μm diamond spray using DP-Lubricant blue, green and red on MD-Largo and MD-mol polishing cloths. For this initial work, results are given for the unetched condition. The microstructure of the reproduction solder joints, and the interaction zones between soldering materials and silver were examined using a JEOL- JSM 5910-LV scanning electron microscope (SEM) with a

Vantage Termonoram energy dispersive spectroscopy (EDS) system at high vacuum and 20 kV accelerating voltage. Line scans were made across the solder/silver interfaces to investigate the diffusion of the various elements between the solder alloy and the silver substrate. Elemental mapping and analyses were conducted using EDS to determine phase relationships in the microstructure. Any loss of silver due to fretting or other attack was measured as the loss in thickness of the silver sheet.

3. Results

Typical temperature-time curves for the various soldered joint reproductions are shown in Figure 1 for 50Sn-50Pb solder using S-39 flux, tallow, or colophonium as flux. All of the other tested soldering processes showed similar temperature behavior. The maximum temperature was reached within 15 seconds, and cooling in air took up to five minutes. This behavior would be expected for hand soldering, where the part would be heated only until the moment that the solder melted and flowed. It should be noted that the measured temperatures, especially the maximum around 200 °C, are probably lower than the actual temperatures, since the thermocouple was placed on the reverse side of the silver sheet, away from the soldering process.

The loss in thickness of the silver sheet in selected samples is given in Table 3. In spite of the reaction of Sn with Ag, it can be seen that the soldering process results in only a small loss in thickness of 16 μm for the 50Sn-50Pb (nr. 1 in Table 3). This value falls within the uncertainty of the measurement of the thickness of the unsoldered sheet material. A 96.5Sn-3.5 Ag solder tested in this programme also showed a similar loss in thickness (nr. 2 in Table 3). Removal of the solder by remelting, removal of the disc, shaking, and wiping resulted in further loss of silver to a total of about 50 μm (nr. 1a). Brazing the disc back onto the silver sheet increased the total loss to over 90 μm, in spite of the fact that no additional Sn-Pb solder was used. The temperature during brazing reached over 480 °C, and remained above the temperature for soldering (around 200 °C) for almost two minutes. At higher temperatures the reactivity of Sn can be seen by the large thickness losses for specimen nrs. 4 and 5 in the table. Pb on the other hand, does not show a reaction layer with Ag even at 400 °C. The small thickness loss value shown, (nr. 3) is also within the uncertainty of the measurement of the original thickness of the Ag sheet.

Table 3

Loss in thickness of silver sheet after soldering

Nr.	Sample	Loss of thickness (μm)
1	Ag disc soldered onto Ag sheet using 50Sn-50Pb solder with S-39 flux	16
1a	Ag disc soldered onto Ag sheet using 50Sn-50Pb solder with S-39 flux; removal of the solder	50
1b	Ag disc soldered onto Ag sheet using 50Sn-50Pb solder with S-39 flux; removal of the solder; brazed	92
2	Ag disc soldered onto Ag sheet using 96.5Sn-3.5 Ag solder with S-39 flux	19
3	Pb on Ag held for 4 min. at 400° C	12
4	Sn on Ag held for 4 min. at 400° C	101
5	Sn on Ag held for 4 min. at 800° C	439

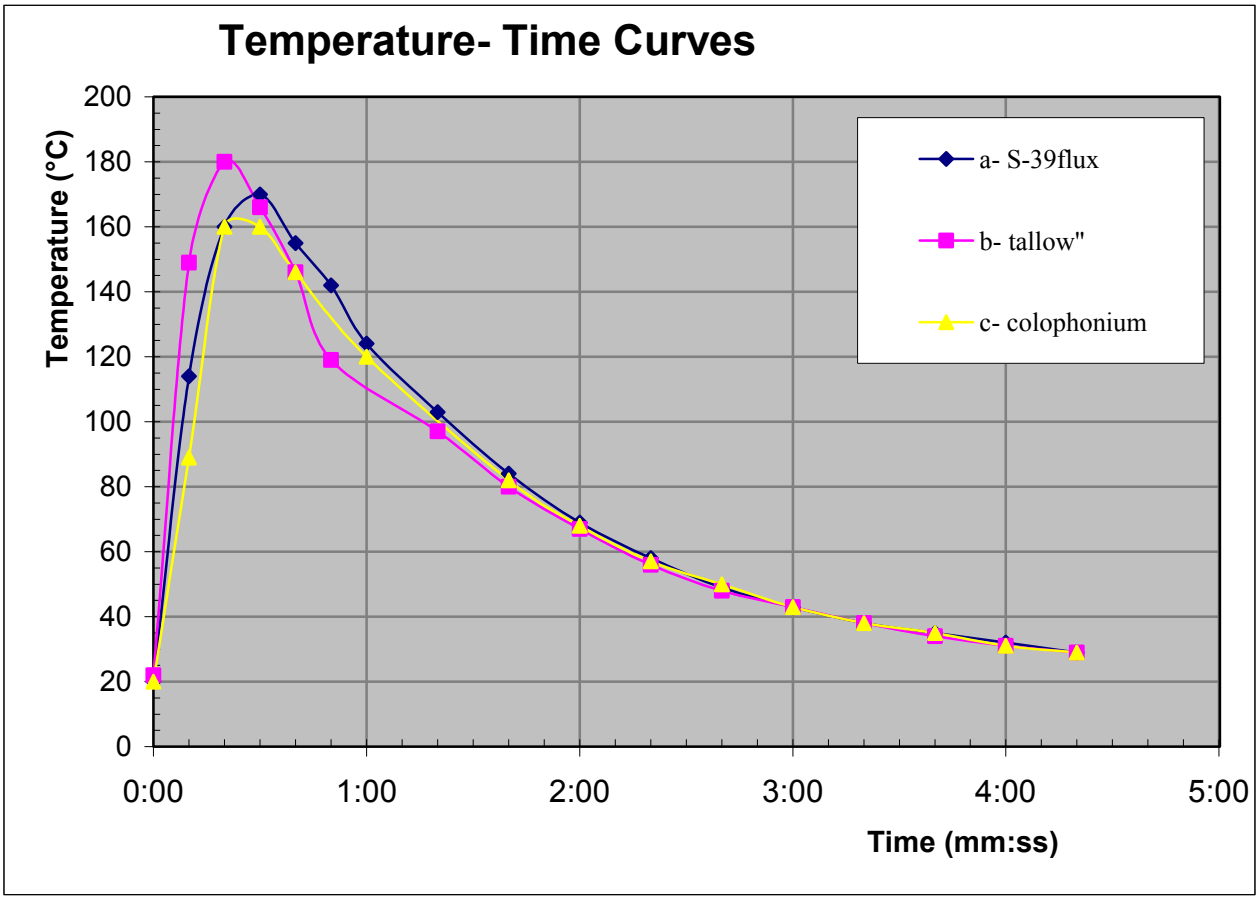

Figure 1 - Typical temperature-time curves during the soldering process with 50Sn-50Pb solder using the following fluxes:

a) S-39 flux
b) tallow
c) colophonium

An SEM-micrograph of soldered joint reproduction using 60Sn-40Pb solder and 925/1000 silver is shown in Figure 2 along with corresponding elemental maps for Ag, Cu, Pb and Sn. To the left, one can see the silver sheet with a dark elongated Cu-rich phase, typical for rolled material. To the right, the eutectic structure typical for Sn-Pb solders can be seen, where the white phase is Pb-rich phase.

The interface in the centre of the micrograph has an irregular finger-like structure, see arrows in Figure 2. The fingers have a length of 2-3 μm. The elemental maps, Figs. 3bcde show that Ag and Sn overlap in this region, with the overlap corresponding exactly to the finger-like structure. EDS analyses, Figure 2f and line scans of these fingers show a chemical composition of approximately 75 wt.% Ag, 25% wt. Sn. This corresponds to the composition of the intermetallic phase, Ag_3Sn, often found in electronic solder joints (see for example, Humpston 1993, Unsworth and Mackay 1973, Bulwith and Mackay 1985). The interface of 50Sn-50Pb specimen had a similar appearance.

In Figure 3, a 50Sn-50Pb specimen is shown after trying to remove the solder. Figure 3a shows that there is still a layer of material attached to the silver sheet. Elemental mapping, Figures 3bc and EDS analysis show that this is again a mixture of Ag and Sn in the ratio expected for the Ag_3Sn intermetallic phase. Traces of Cu and Pb are also to be found in the outer surface of this layer. This possibly indicates that Cu has also reacted with Sn, and that some solder (as evidenced by the Pb) remains on the surface.

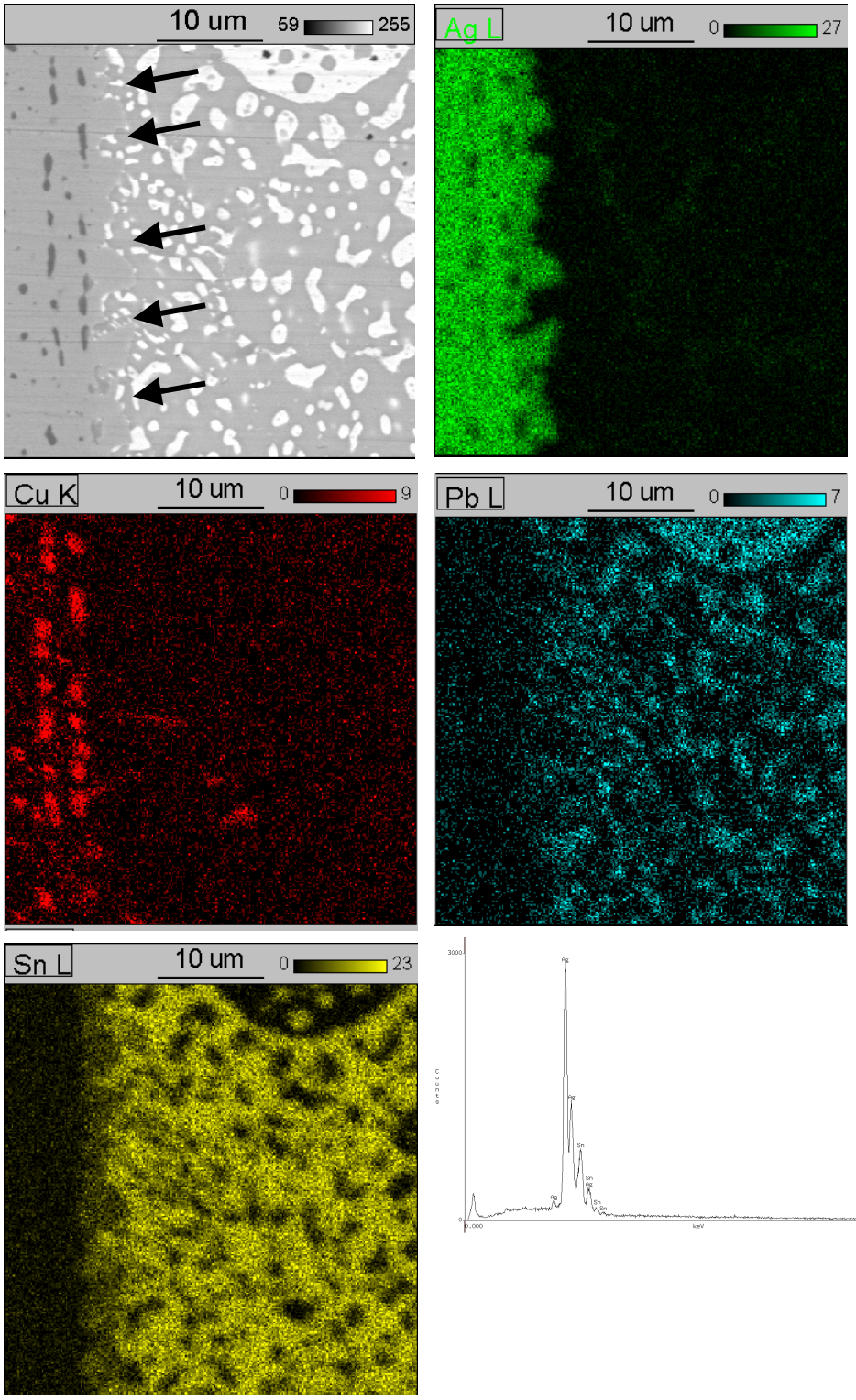

Figure 2 - SEM micrograph and elemental maps for a specimen soldered with 60Sn-40Pb and S-39 flux.
a)-SEM micrograph- arrow shows finger structure described in text
b)- Ag map
c)- Cu map
d)-Pb map
e)- Sn map
f) EDS spectrum from one of the fingers (arrow)

a

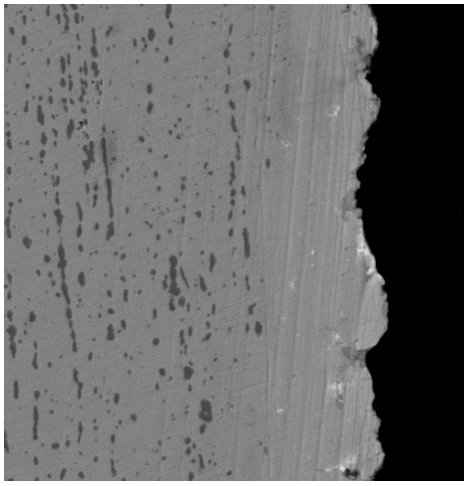

b

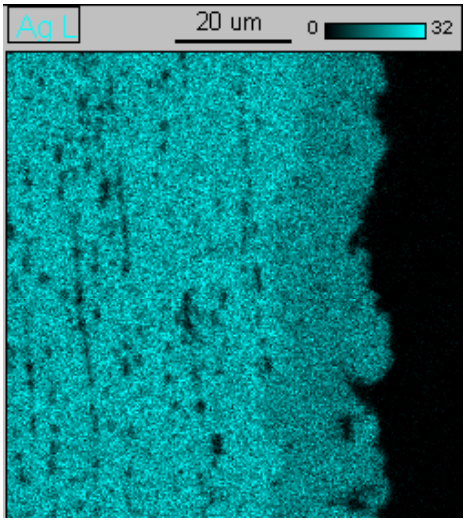

c

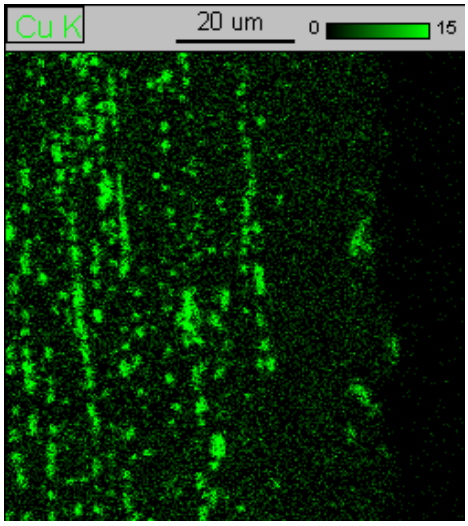

d

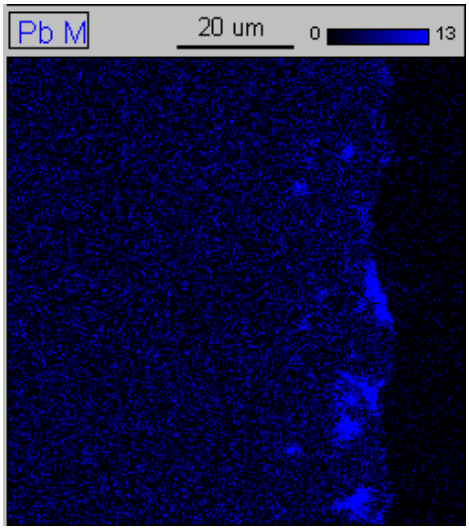

e

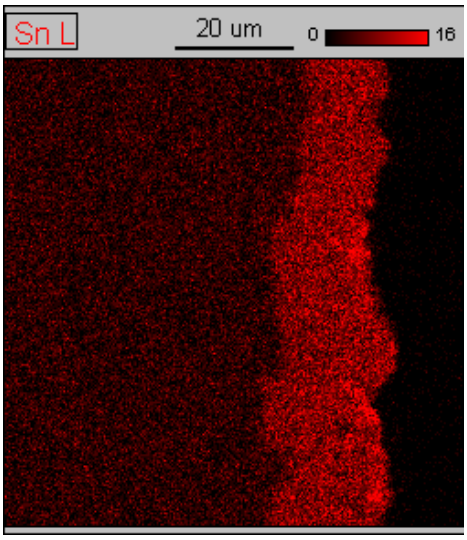

Figure 3 - SEM micrograph and elemental maps for a specimen soldered with 50Sn-50Pb solder, where the solder was then "removed" by remelting, shaking and wiping.
a) SEM micrograph
b) Ag map
c) Cu map
d) Pb map
e) Sn map

4. Discussion

The initial results of this study show that historical methods of soldering silver objects result in the reaction of Sn with Ag, creating a thin reaction layer most likely consisting of the intermetallic phase, Ag_3Sn. Removal of the solder by remelting, shaking, and wiping does not appear to be successful, as the intermetallic layer remains, Figure 3a. In addition, there is a slight additional attack of the silver by Sn. Brazing on top of the remaining solder causes further attack, with the thickness loss being almost the same as for the combined processes of soldering and cleaning. This additional attack would be the fretting attack commonly experienced by conservators.

The explanation for the further attack of Sn, in spite of the fact that no additional solder is used in brazing, and obviously when removing the original solder, can be found by considering the equilibrium phase diagram for the Ag-Sn system, see Figure 4.

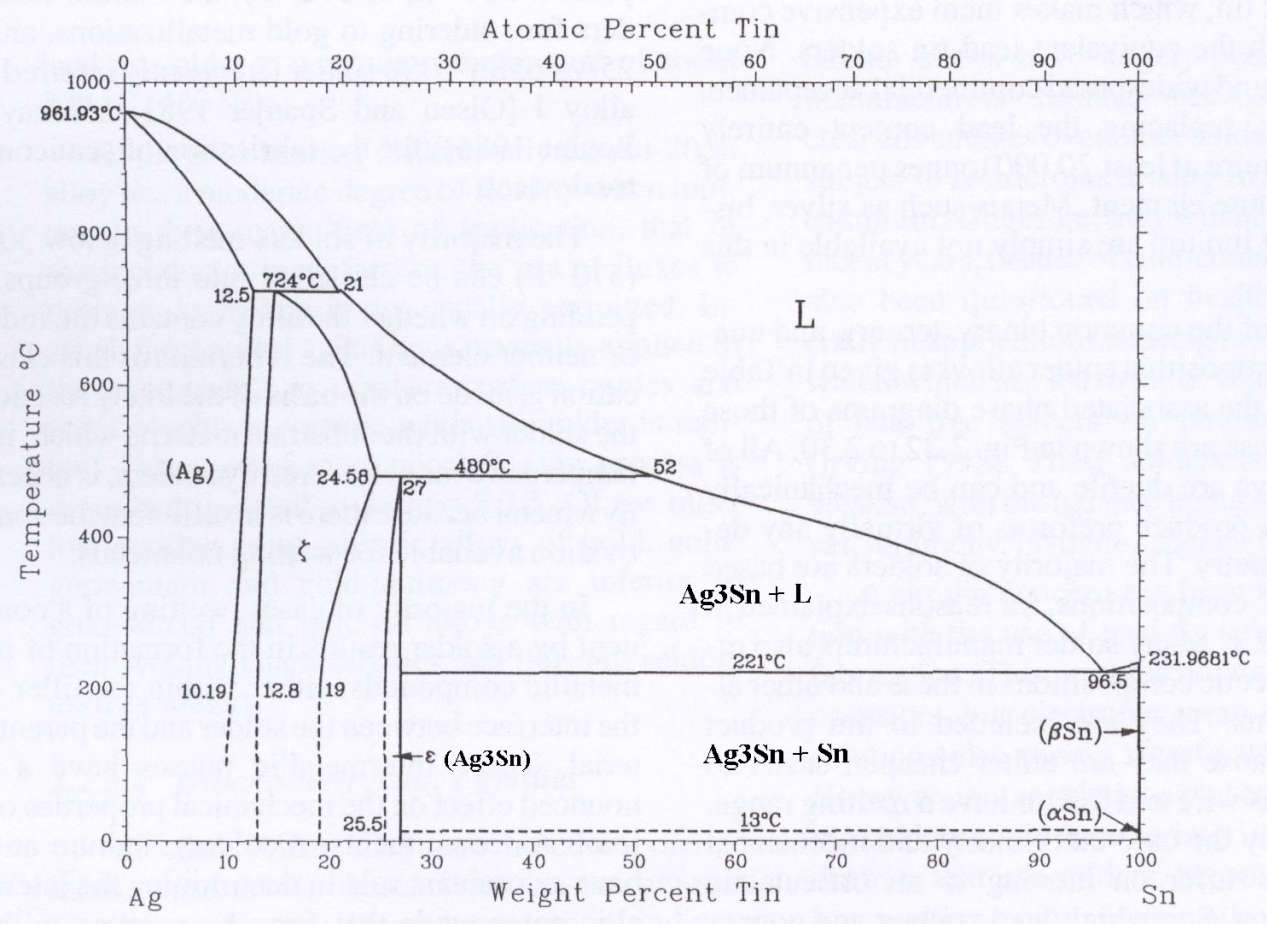

Figure 4 - The Ag-Sn equilibrium phase diagram. Adapted from Humpston 1993, p.78

During soldering by hand, temperatures can rise above 200 °C, resulting in a two-phase equilibrium between Ag_3Sn and a Sn rich liquid. This Sn liquid phase will dissolve Ag. Upon solidifying, the intermetallic phase Ag_3Sn will form as part of the reaction layer. However, the equilibrium diagram shows that below 221° C, a eutectic mixture of Ag_3Sn and a Sn-rich phase are to be expected. An equilibrium phase diagram cannot be used to describe a dynamic process such as cooling, but given that solder joints are generally cooled in still air, there may be enough time for some of the Sn-rich phase to form.

When traditional methods are used to remove the solder, the joint is probably heated to temperatures similar to those used for soldering, around or above 200 °C. This will be sufficient to melt any unreacted solder lying above the reaction zone. However, the eutectic temperature for Ag-Sn is 221 °C. The Ag_3Sn - Sn eutectic microstructure most likely remains in the solid state. If the temperature should rise above 221 °C, only a small amount of the eutectic will melt, and that would initially be the Sn-rich phase. Thus the Ag_3Sn layer remains on the surface and the Sn-rich phase is free to react with the Ag.

When brazing silver, much higher temperatures are used, well above 450 °C (which is the generally accepted difference between soldering (< 450 °C) and brazing (> 450 °C) (Humpston 1993)). At those temperatures, much of the Ag_3Sn will have melted, again releasing Sn into the liquid phase. Thus the solder, which was not removed, that is, that in the reactive layer, is again aggressive. However, the temperatures are now much higher than for soldering.

The model specimens show that the reaction of Sn with Ag is much higher at higher temperatures, 400 ° and 800 °C This agrees qualitatively with the literature, which shows that the solubility of Ag in Sn increases with temperature according to an Arrhenius relationship (see Bader 1969, Unsworth and Mackay 1973, Bulwith 1985, Klein Wassink 1989 and Humpston 1993). Pb does not appear to attack Ag, at least at 400 °C (merely 12 μm of penetration, see table 3 nr.3). Thus, the Sn remaining on the material under the braze will be highly reactive, and "fretting" will occur.

The origins of the problem of "fretting" of silver objects by solder can be understood by looking briefly at the history of the soldering and brazing of silver. The historical development of soldering and brazing techniques has been reviewed, among others, by Allen 1978, 1984; Wolters 1983ab and Schmidt 1993. The Greeks and Romans are known to have used tin-lead alloys for soldering (Allen 1978). Schmidt (1993) mentions that tin-lead alloys and pure tin were used on silver, in particular, objects of the Hildesheimer Silberfund. Wolters (1983) discusses the use of brazes on silver, including a silver-tin alloy described in the *Mappae Clavicule* (ca. 825 A.D.) with a liquidus of 937 °C and silver-copper-tin alloys used in the Middle Ages.

In the late medieval period, brazing became more important. This can be seen in guild specifications for the amount of noble metals to be used in brazes (Weber 1959, p.65; Fock 1983, p.42). It is known that silver objects had to be assayed for the amount of silver used in the alloy. Silver objects were often a way of investing money. When necessary they could be melted down and made into coins. This was more difficult if solder had been used on an object. Impurities of lead or tin in gold or silver alloys could lead to a brittle alloy (Wolters 1981, p.49 and 63; Brehpohl 1996, p.303) and present problems when working with these alloys. The use of solder on silver would therefore be undesirable.

The 18th century provides more documentation about soldering and brazing techniques. The treatise of the Dutch silversmith, Willem van Laer (1674-1722) does not mention the use of solders on silver (see reprint, Laer 1967). However, Laer does mention a 'soldeer-lamp', which he designed for use on small failures or holes in joints. The advantage of that lamp was that the work did not need to be placed into the full flame of a coal fire with the risk of melting previous joints. The work was heated in the coal fire until it glowed, then was taken out of the fire, and locally joined by directing the flame with a blowpipe. Based on that description, the lamp was probably used for brazing with silver brazes. In 1760, Johann Georg Friedrich Klein described the use of a 'Lóthlampe' (lóth = soldering/ brazing) (see reprint, Klein 1987). The lamp was mounted on a wooden box with little drawers used to hold 'Schlagloth, Borax und anderes kleines Lóthgeráthe' (brazes, borax and other small soldering tools). This indicates that this type of lamp was used for brazing, since borax is a flux used for brazing. Klein also describes other methods for soldering, including

- casting on parts by pewterers
- the use of a soldering bit by tinkers
- use of thin wires of solder and a blowpipe for directing a flame, used mainly by pewterers, possibly derived from techniques used by gold- and silversmiths
- use of colophonium to help solder flow on an object placed in a coal fire, used mainly by coppersmiths
- heating small objects on top of small iron-melting furnaces, used by 'Zinnknopfmachern' (tin button makers).

Further improvements in the method of heating the work came in the 19th century with the invention of the gas burner by Bunsen (Fock 1983) and the development of the electric soldering bit.

Literature from the twentieth century presents different views about soldering. Some sources claim that it can be used for all metals (Cuzner 1965; Diebener's Handbuch 1936). Others say it should be used only as a last resort on gold or silver (Untracht 1975, Fachkunde Edelmetallgewerbe 1981, Brehpohl 1969, Urs Stussi 1988, Braun-Feldweg 1968, Wylie Davidson 1913) or that it should not be used on gold or silverware at all (Finegold 1983, Staton Abbey 1968, Weber 1959). In general it can be said that the use of solder during the manufacture of historical silver objects is limited, which means that the presence of solder on historical silver objects is generally due to repairs.

From this brief review of the soldering and brazing of silver, it is clear that in conservation, this work is performed by hand with no accurate means for temperature control, that being not only which temperature, but also time at temperature. The application of solder on silver could have been done by either conservators or gold- or silversmiths who saw no other possibility than using solder, or by untrained workers. The results of the current research programme indicate that it is virtually impossible to remove solder from a silver object using traditional methods. Any attempt to resolder, clean, and/or braze will release some, if not, all of the tin bound in the reactive layer, allowing it to further attack the silver. This can occur at any temperature above the eutectic temperature for Ag_3Sn - Sn, 221 °C, but is more rapid at the high temperatures used in brazing. However, the fact that there is a range of temperatures where fretting is observed, could be a cause for the confusion in the literature and in seemingly conflicting anecdotal stories about fretting.

The best solution to the problem of fretting is, in any case, to find a method for removing all remnants of solder, including the Ag_3Sn reaction layer. These could include a combination of mechanical and/or chemical techniques. However, they will all require knowledge of how deep the solder has attacked the silver. There will also be a number of important practical and ethical issues associated with possible solutions.

5. Conclusions

An experimental study has been conducted to determine the cause of fretting of silver during the restoration of solder joints by brazing. Microstructural analysis was performed on historical reproductions of soldered joints, joints repaired by brazing, and samples modelling the soldering and brazing processes. The results indicate that the original soldering process itself does not lead to fretting. However, there is limited dissolution of silver by tin from the solder, which results in the formation of an Ag_3Sn layer at the interface between the solder material and the silver object. At temperatures above 221 °C, that is, just above the soldering temperature, this Ag_3Sn layer goes partly into solution, creating a two-phase equilibrium of solid Ag_3Sn and a Sn-rich liquid. Thus, the solder and reaction layer cannot be removed by merely melting and removing it mechanically. This Sn-rich phase can attack the silver object further. At temperatures common for brazing (well above 400 °C), this dissolution process occurs at a much faster rate, resulting in the visually apparent problem of fretting. Mechanical and or chemical methods must be developed to completely remove this Ag_3Sn layer before brazing in order to avoid fretting.

Acknowledgements

This paper is the result of a thesis project conducted by the first author for a diploma in conservation at the Netherlands Institute for Cultural Heritage (ICN), Amsterdam. He would like to thank the Rijksmuseum Amsterdam for providing the facilities for the work. In addition he would like to extend his appreciation to Ineke Joosten (ICN) for assistance with the SEM work, P. Hallebeek (ICN) for x-ray analyses, and Ilonne de Groot, Ink de Pree, and Loes Siedenburg (all ICN), Russell Wanhill (Netherlands Laboratory for Aerospace Research), Antoinette Verhage, and Camiel Aalberts for their assistance and helpful discussions.

References

Allen, B. M. (1978) *Discovering soft-soldering history,*. The Metallurgist and Materials Technologist, October 1978, (London) p.537-540.

Allen, B.M. (1984) *Bibliography of books on soft soldering (1760-1983),* In: Klein Wassink, R.J. (ed.). Soldering in Electronics, (Ayr: Electrochemical Publications Limited) p.454-458

Bader, W.G. (1969) *Dissolution of Au, Ag, Pd, Pt, Cu and Ni in a molten tin-lead solder*. Tests indicate that palladium, copper, silver and gold are unsuitable for thin-film applications if they are to serve as substrate films for 60Sn-40Pb solder'. Welding Journal; Welding Research Supplement, Vol. 48, p.551-557s.

Brehpohl, E. (1996) *Theorie und Praxis des Goldschmieds* (Leipzig: Fachbuchverlag)

Braun Feldweg, W.(1968) *Metal, Werkformen und Arbeitsweisen* (Ravensburger: Otto Maier Verlag)

Bulwith, R.A. and Mackay, C.A. (1985) *Silver scavenging inhibition of some silver loaded solders*. The results of experiments show that silver dissolved in a solder alloy has an inhibiting effect on the scavenging of silver from silver substrate'. Welding Journal; Welding Research Supplement, March 1985, p.86-90s.

Costa, V. (2001) *The deterioration of silver alloys and some aspects of their conservation,* Reviews in Conservation, number 2, (London), p.18-34.

Cuzner, B. (1965) *A Silversmith's Manual, treating of the designing and making of the simpler pieces of* domestic *silverware*, (London: N.A.G. Press, Ltd).

Diebeners Handbuch Des Goldschmieds, ein werkstattbuch fur die Praxis, (1936). (Leipzig: Verlag von Wilhelm Diebener)

Finegold, R. and Seitz, W.(1983) *Silver smithing*, (Radnor:Chilton Book Company)

Fock, W (1983) *Technieken in de kunstnijverheid, 1 goud en zilver*, (Leiden: Kunsthistorisch instituut, Rijksuniversiteit Leiden)

Humpston, G. and J, David M. (1993) *Principles of Soldering and Brazing,* (Ohio: ASM International)

Klein, J.G. F. (1987) *Ausfũhrliche Beschreibung der Metalllothe und Lothungen, darin sowol alle Schlag- Schnell- Hart- Weich- Metall- und andere lothe zu machen; als auch alle Metalle selbst zu lõthen, angewiesen werden von Johann Georg Friedrich Klein, im Verlag des Buchladens der Realschule, Berlin 1760*, (Leipzig: Deutscher Verlag fur Schweisstechnik Gmbh).

Laer, W. van. (1967) *Weg-wyzer voor aankomende goud en zilversmeden*, (Lochem: De Tijdstroom)

Niemeyer, B. (1997) *Early 20th-century restorations and modern conservation treatments on archaeological silver objects*'. Metal 95, Proceedings of the international conference on metals conservation, (London: James & James) p.190-195.

Schmidt, H. (1993) *Übersicht zur wissenschaftlichen Literatur über das "Löten und Schweißen in der Antike/ Altertum*'. Berliner Beiträge zur Archäometrie, 12, (Mainz) p.5-53.

Staton Abbey, (1968) *The Goldsmith's and silversmith's handbook, a practical manual for all workers in gold, silver, platinum and palladium, based on the well-known handbooks by George E. Gee*, (London: The technical press Ltd.)

Unsworth, D.A., and Mackay, C.A. (1973) *A Preliminary Report on Growth of Compound Layers on Various Metal Bases Plated with Tin and its Alloys,* Transactions of the Institute of Metal Finishing, Vol 51, (London) p.85-90.

Untracht, O. (1975) *Metal Techniques for Craftsmen*, A basic manual for craftsmen on the methods of forming and decorating metals, (London: Robert Hale Limited)

Urs Stussi, F. (1988) *Schmuck, Material, Design, Herstellung*, (Ravensburger: Ravensburger Buchverlag Otto Maier GmbH)

Weber, A. (1959) *The Jeweler, directives and targets to be attained in training apprentices*, (Geneva: Office for Industrial Information, Hugo Buchser(translated from german in 1955)

Wolters, J. (1981) *Der Gold- und Silberschmied, Band 1, Werkstoffe und Materialien*, 1.Auflage (Stuttgart: Ruhle-Diebener-verlag GmbH & Co.KG)

Wolters, J. (1983a) *Zur Geschichte der Lötung von Edelmetallen, Teil 1: Historische Entwicklung der Lotlegierungen,* Zeitschrift für Archäometrie 1/2. p.48-64

Wolters, J. (1983b) *Zur Geschichte der Lötung von Edelmetallen, Teil 1: Historische Entwicklung der Lotlegierungen*, Zeitschrift für Archäometrie 1/3. p.86-98

Wylie Davidson, P. (1913) *Educational Metalcraft, A practical treatise on repousse, fine chasing, silversmithing, jewellery, and enamelling, specially adapted to meet the requirements of the instructor, the student, the craftsman and the apprentice*, (London, New York, Bombay, and Calcutta: Longman's Green, and co.)

Surface analysis of corroded silver coins from the wreck of the *San Pedro De Alcantara* (1786)

I.D. MacLeod [a], E. Schindelholz [b1]

[a]Western Australian Museum, Cliff Street, Fremantle, Western Australia 6160, Australia
[b] Mariners' Museum, 100 Museum Drive, Newport News, Virginia 23606-3759

Abstract

A detailed morphological study of the corroded surfaces of seven silver "Pieces of Eight" recovered from the *San Pedro de Alcantara* shipwreck site was conducted using low pressure scanning electron microscopy (SEM) with energy dispersive spectroscopy (EDS) analysis. Mosaics of the backscattered images of the coin faces indicated that the coins consist of a solid solution of β-phase grains with α-phase inclusion and that bromian chlorargyrite is the main corrosion product. Thin surface films of hydrated iron oxides facilitated the formation of sulphide minerals on buried coins. Surfaces were heavily abraded by the harsh erosion corrosion conditions and most bear evidence of damage from impact of other artefacts on-site. Correlations exist between the surface analyses and the data from the *in-situ* corrosion measurements.

Keywords: SEM mosaics, bromian chlorargyrite, silver coins, corrosion, shipwrecks, conservation

1. Introduction

The *San Pedro de Alcantara* was a 64 gun Spanish man-of-war ship that was built in Cuba in 1770. The vessel left Peru in 1784 carrying cargo which included 420 passengers, hundreds of tons of copper and gold and more than one hundred tons of *pieces of eight* minted in Lima. Lengthy repairs in Rio de Janeiro saw the journey delayed until 1786 when the vessel sank after colliding with a rock off the coast of Portugal. One hundred and twenty-eight people, including several Peruvian prisoners, perished in the accident (Blot & Pinheiro-Blot, 1991). Given that the cargo represented 8% of Spain's total circulating currency King Charles (Carolus) III launched a salvage operation that employed 40 full-time divers for three years to recover the cargo (Blot, 2004). The diving operation was at that time the largest ever in European history and was successful in recovering the majority of the ship's cargo. The wreck site was essentially undisturbed until January 1963 when a German-built Portuguese steamship *João Diogo* ran aground less than 30 metres from the impact site of the *San Pedro de Alcantara* (Blot & Pinheiro-Blot, 1991). Salvagers blasted the hulk, which scattered the iron ore cargo and elements of the steel ship over the Spanish shipwreck site (Blot & Pinheiro-Blot, 1992).

The current site is scattered over 200 metres long in water 3-9 metres deep, lying off a rocky coast near Peniche, Portugal. The sea bottom consists of irregular rocks, with numerous cavities and crevices filled with up to 0.5 metres of stone and sand. The artefacts are mostly small objects randomly spread over the large area and located in these cavities and crevices (Blot, 1998a). The site is characterised by very high energy with waves breaking over it. Recent excavation recovered fragments of pottery, encrusted iron objects, pieces of lead sheathing, silver and gold coins, a copper ingot, and mercury deposits, and a swivel gun from the forecastle of the ship. Lead bars and iron tools related to the 18th century salvage operation were also recovered (Blot, 1998b). The maritime archaeologists developed mathematical models based on artefact distribution and the physical characteristics of the artefacts to gain insight on parameters affecting the site formation processes (Blot and Pinheiro-Blot, 1992; Blot, 1998a). The initial *in-situ* corrosion studies of silver coins focused on seven coins that represented varied geographic locations, which were subsequently recovered and these objects formed the locus of this study.

The pieces of eight (8 reales) were minted in Lima, Peru, and showed a "bust type" portrait of Carolus III on the obverse and the Spanish coat-of-arms on the reverse (Figure 1). They were minted between 1772 to 1788 when the King was succeeded by his son Carolus IV. The coins had mint dates of 1780 (no 4030), 1784 (no 4324) and 1782 for numbers 4327, 4331 and 4342 while 4315 and 4325 were too heavily abraded and could not be dated. These coins were minted on a screw press, which was operated by rotating a weighted lever that pressed an upper and lower die together with a milled or finished planchet between them (Craig *et al*., 2002). Under the intense and even pressure of the press the minters were able to produce coins with great accuracy. Their mass was 27.064 grams and the fineness of 0.90278 equated to 90.278% silver and 9.722% copper, the

[1] Corresponding author: TEL:+1 757 5917787: FAX +1 757 591 7312 e-mail: eschindelholz@mariner.org

diameter was 3.8 cm and they were 2 mm thick (Cordua, 2003). The coin weight is almost (0.955) one avoirdupois ounce.

The degree of preservation of the recovered coins related to their location on the wrecksite. Coins 4324, 4325, 4327 and 4331, which were found buried under 15cm of coarse sediment, have more or less retained their original dimensions. Coins 4315, 4030, and 4342, which were found lying atop the seabed, have lost a majority of their original surface and dimensions. There was only one coin (no.4325) with any significant amount of concretion; the deposits consisted of sand-sized to pebble-sized sedimentary particles and small shells bound together by calcareous concretion (see Figure 2). Coins 4325, 4331, 4324, and 4327 all have considerable amounts of iron corrosion products on their surfaces. Since these coins represent valuable components of Peruvian, Spanish and Portuguese cultural heritage, a non-invasive methodology of surface analysis was chosen.

Figure 1: Carolus III 1780 “bust type” piece of eight, from www.newworldtreasures.com.

A distinct and uniform mineral stratum was identified on a few coins, which may indicate physical or chemical changes in the site environment or their microenvironments over time (Robbiola *et al*, 1988). Scott (1994) has demonstrated the relationship between the composition of the corroded surfaces and the underlying original microstructures of bronze artefacts from an ancient terrestrial archaeological site and how the changes in the burial and in post-burial environments were expressed in the corroded surfaces. The authors have found related shipwreck phenomena (MacLeod, 1982; 1985; 1991; 2002) that connect the corrosion characteristics of metals with electrochemical site parameters and their metallurgical structure. Oxely (1990) stated the importance of understanding site formation processes of underwater sites with respect to artefact preservation. The same methodology was recently applied by Craig *et al.* (2002) to an 1800 Ecuadorian Spanish Piece of Eight from the wreck of the *Santa Leocadia*. Corrosion studies on marine metals have been reported by Robinson (1982), Macleod *et al.* (1986) and North and Macleod (1987) while Fox (1994) examined land corrosion.

Figure 2: Obverse surface of coin no 4325 on the left and reverse on the right.

2. Experimental Procedure

The coin surfaces were examined using reflected light microscopy and geological scanning electron microscopy (GeoSEM) in low-vacuum backscattered mode (Robinson, 1992). Backscattered image mosaics of the coin faces presented a unique view of the corrosion patterns. The primary aim of this non-destructive characterisation of the microstructure and corrosion of silver coins was to test a hypothesis on the deterioration mechanisms they underwent in the marine archaeological environment. The initial study revealed important information relating to the deterioration of the coins in the archaeological environment. Stress corrosion cracking in the form of fine fissures in the metal surface was apparent at many of the leading edges of the coins, where the raised edges are adjacent to the milled edge where distortion during striking would be at a maximum. There were numerous examples of sites where selective corrosion of the copper rich phases of the alloy had been attacked in a series of parallel lines. These were associated with stress placed on the silver during rolling of the blanks before they were cut to size. Corroded β-phase silver grains (solid solution of copper in silver) were identified on an eroded area of one coin. Redeposition of silver from a layer of corrosion products was found on the surfaces of another coin, a phenomenon that has been observed on silver coins recovered from Australian wrecks (MacLeod, 1991). Mercury and lead corrosion products, in the form of minute particles and spots, were found on the surfaces of some coins. This indicates that the coins and the original lead particles and liquid mercury existed in the same microenvironment on the wrecksite.

Each coin and their corrosion patterns were recorded with high resolution (5 mega-pixel) photographs. Images were taken of both sides of each coin using a Nikon Coolpix 5700 camera. The coins were also examined using a reflected light stereomicroscope at up to 80x magnification to provide supplementary information to the SEM/EDS analysis. Initial analyses in Australia were conducted using a Phillips XL40 scanning electron microscope with light element energy dispersive analytical x-ray detection (EDAX) and GeoSEM with low-vacuum capabilities. Although the instrument is able to work at higher pressures, stray x-ray radiation occurs when the electrons from the primary electron beam deflect off air molecules in the sample chamber and hit the specimen at considerable distances from the position of the beam (Robinson, 1992). The impact of the stray x-rays on the EDAX was minimised using a combination of between 0.2-0.8 mbar chamber pressures and a working distance of around 10 mm. The SEM was used in backscattered imaging mode to investigate the morphological and relative compositional nature of the coin surfaces. EDAX was employed to identify the elemental composition of areas of interest on the backscattered image.

Backscattered electron (BSE) photo mosaics of the coin faces were created using a software program developed by Michael Verall of CSIRO for use with the Philips XL 40. Since the typical magnifications of the BSE images of the coin surfaces cover an area of 0.04 mm^2 it was useful to have a method for gaining a composite image, since the average coin surface comprises roughly 200-300 such images. Part of the project was to see if there was any correlation between localised compositional differences and the gross features of the corroded and eroded surfaces. The software automates the SEM to capture 330 images in a string of 200x BSE pictures of the sample along a regular grid coordinate system. Although some distortion occurred around the edges of each individual image in the mosaic, the digital images of the coin faces were superimposed on the corresponding SEM mosaics using Adobe Photoshop 7.0. Using the mosaic maps with the highlighted areas of interest, a second set of SEM/EDS sessions were carried out using a Hitachi S3200 variable-pressure SEM with a Robinson backscatter detector and a light element x-ray energy dispersive spectrometer (XEDS) at the Canada Centre for Mineral and Energy Technology (CANMET) in Ottawa, Canada. The chamber pressure on the Hitachi was set to around 0.1 mbar with a working distance of 16mm.

X-ray diffraction**.** Unless otherwise stated all mineral phases were identified by x-ray diffraction. Typical 0.5 mg samples of corrosion products from coins 4342 and 4325 were placed on a zero background sample plate and run on a Phillip's Xpert MPD at 45 kilovolts and 40 milliamps for approximately one hour. The silver sulphide from the obverse of coin 4325 was adhered to the tip of a glass fiber with silicone oil and placed in Gandolfi camera and run in a helium atmosphere for 22 hours at 40 kilovolts and 22 milliamps on a Philips 2W 1010/90 generator with a cobalt source.

3. Results and discussion of the corrosion mineralogy

Calcium carbonate was abundant on every coin surface either as biogenic deposits or as inorganic crystals of magnesian calcite, ($Ca_{1-x}Mg_xCO_3$) while the polymorph magnesian aragonite was found covering large areas of coin 4327. The aragonite is in a steep pyramidal form as clusters of sharp spiked crystals (see Figure 3) The presence of this form of aragonite on coin 4327 indicates that this coin was subjected to a different microenvironment. In normal seawater of salinity 34.33% the ionic product of calcium and carbonate ions at pH 8.2 is 270 x 10^{-8}, which is much higher than the solubility product of 50 x 10^{-8} for calcium carbonate, confirms that seawater is supersaturated with respect to calcium carbonate (Horne, 1969). Any change in temperature,

salinity or pH will cause the precipitation of some form of $CaCO_3$ since the ratio of $[CO_3^{2-}]/[HCO_3^-]$ is given by the relationship,

$$log\{[CO_3^{2-}]/[HCO_3^-]\} = pH - 10.2,$$

where 10.2 is the pKa_2 of carbonic acid. In normal seawater bicarbonate is the dominant ion so any increase in the local pH will dramatically alter the activity of the carbonate ion and lead to precipitation on the coin surfaces at cathodic sites. In aerobic seawater the cathodic reduction of oxygen,

$$O_2 + 2H_2O + 4\ e^- \rightarrow 4\ OH^-$$

will cause the pH to increase on the surfaces associated with the reduction side of the corrosion process (Weier, 1971, North & MacLeod, 1987).

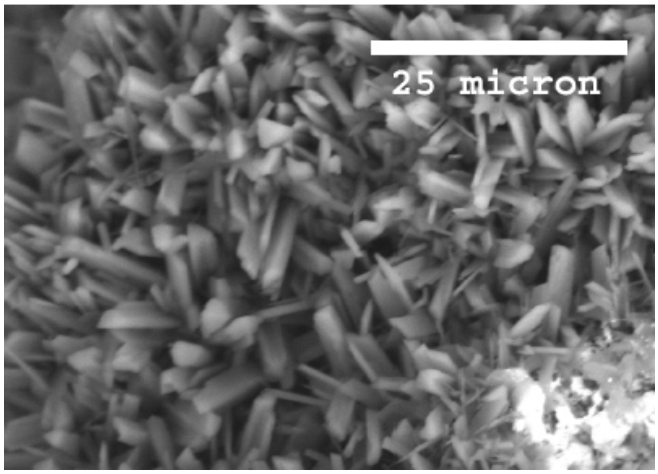

Figure 3:Field of magnesian aragonite on surface of coin no. 4327, full width 68 μm

Magnesium carbonate is much more soluble than its calcium analogue and its concentration will not normally be sufficient to allow it to precipitate. Calcareous concretions on artefacts from Australian waters are composed of a range of magnesian calcites, where 0.966 <x> 0.839 in the general formula $Ca_{(1-x)}Mg_xCO_3$ (MacLeod, 1991). The magnesium content of the calcareous deposits on the coins from the *San Pedro De Alcantara* fell in this range, with the aragonite on coin 4327 having higher levels of magnesium than the calcite on other coins. Carlson (1983) found that aragonite is the preferred mineral when higher concentrations of magnesium are present. Tribble (1993) noted that sedimentary environments rich in iron would favour aragonite formation relative to iron-deficient systems.

Milliman and Manheim (1968) reported aragonite to be the major calcium carbonate mineral in an aerobically formed concretion on an iron nail recovered from a shipwreck off the coast of Turkey. Under anaerobic conditions, when a coin is buried in the sand, or when there is a coherent layer of iron oxy-hydroxides preventing direct access of the dissolved oxygen to the corroding surface, sulphide ions from sulphate reducing bacteria are precipitated as silver sulphide (Ag_2S). The presence of iron oxides on coin 4327 provides a good rationale for the large amounts of silver sulphide present on the surfaces, and the preferential growth of aragonite on this coin. The absence of aragonite on coin 4325, which also exhibits major iron oxide and silver sulphide deposits is simply a reflection of an alternative cathodic reduction process that does not produce hydroxide ions.

The large amounts of iron found in the concretions and as distinct films on the coins recovered from a buried microenvironment is consistent with the history of the site. The majority of the surfaces of coins 4325, 4327, and 4331 were covered with a layer of pure hydrated iron oxides, such as $FeOOH.xH_2O$. The films are compact and of relatively uniform thickness. The deposition of this material is likely to have occurred during the salvaging of the *João Diogo* as a continuous film that was subsequently eroded/corroded away in areas to reveal underlying layers of silver halides. The absence of iron on coins 4315, 4030 and 4342 is a reflection that these coins are highly eroded and corroded and have very little concretion.

Redeposited silver is present on coins 4324, 4342, and 4325 as crystals that have grown on top of the crystalline primary corrosion products and on top of amorphous deposits. The exposed silver sulphide stratum underneath the iron film on coin 4325 exhibits numerous inclusions of redeposited silver crystals averaging 15 microns in length (see Figure 4). Redeposited silver crystals are commonly found underneath iron oxide films on silver coins from marine shipwrecks in Australia (MacLeod, 1991). The formation of silver crystals can be due to the poor electrical and ionic conduction properties of iron oxide films, which can limit oxygen access to the corroding metal surface and favours alternative reduction reactions such as

$$AgCl + Cu \rightarrow CuCl + Ag\downarrow$$

At chloride ion activity of 0.32 M, the cell potential for the above reaction would be around 94 mV (MacLeod, 1981). The formation of redeposited silver on coin 4324, which has a small amount of iron oxide film covering its surface, and 4342, which lacks a film, can be attributed to a different process. On these coins the redeposited silver is in the form of 5-10 micron amorphous inclusions in Ag(Cl,Br) pavements. The inclusions were only found in the smooth abraded areas of the pavements, which may be due to the fact that, during BSE examination, the abraded surfaces provided areas of higher visibility for the bright silver inclusions compared to the surrounding rough, non-abraded pavement. Both coins also contained a large amount of mercury, usually in a silver amalgam.

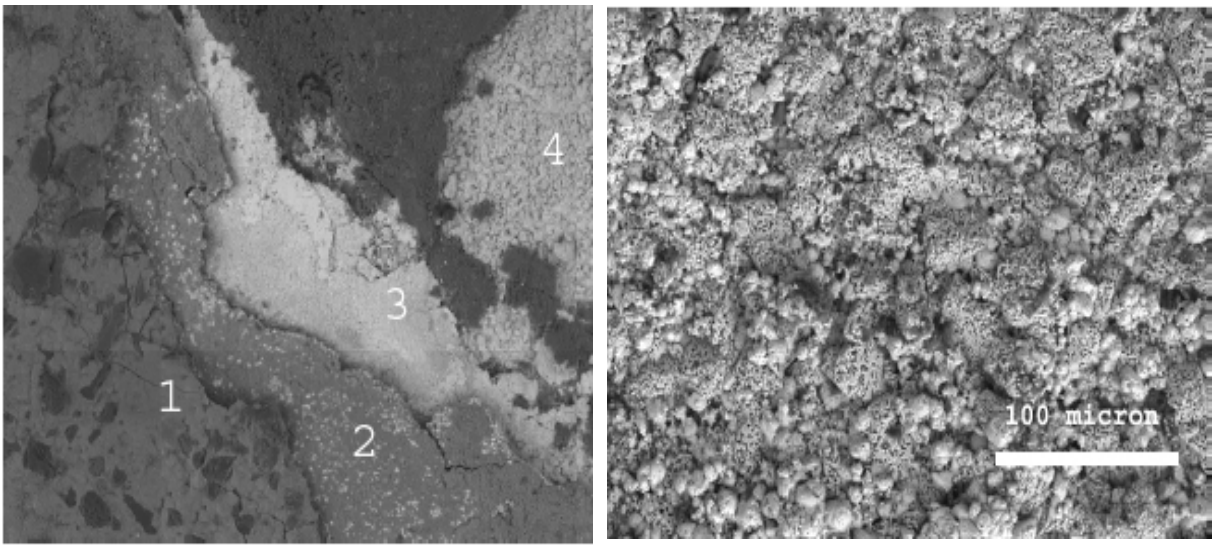

Figure 4: Left SEM photomosaic of coin 4325 showing layer 1: (lower left) hydrated iron oxides with silica inclusions, layer 2: mixed silver and copper halides, layer 3: silver sulphides, layer 4: silver halides overlaying the dark grey $CaCO_3$ deposits (image width 1100 μm). The right SEM image shows corroded redeposited silver intermixed with silver halides, width 800 μm,

The presence of mercury on these coins is not surprising given the archaeologists found a few hundred grams of mercury in the hollow of a rock on the *San Pedro de Alcantara* site, which they attributed to the mercury samples the ship was transporting when it sank (Blot & Pinheiro-Blot, 1991). The smallest amalgam deposits on coins 4324 and 4342 were discovered on the abraded areas of the Ag(Cl,Br) pavements and are identical in shape and size to the redeposited silver on these coins. From these findings, it can be hypothesized that the formation of redeposited silver inclusions involved the reduction of silver corrosion products by mercury. When mercury came in contact with the silver halides it reduced the silver and formed soluble mercuric halides. One such reaction that may have occurred is as follows:

$$2\ AgCl + Hg \rightarrow 2Ag + HgCl_2$$

The standard potential for this reaction is 62 mV, which is sufficient to allow the reaction to proceed. Mercuric chloride ($HgCl_2$) is highly soluble in seawater and would have been diffused from the reaction site. Excess mercury may have then amalgamated with the reduced secondary (redeposited) silver and the exposed underlying primary core silver, which would account for the silver amalgam inclusions as shown in Figure 5. Coins 4342 and 4324 exhibit spheres of silver amalgam between 300-500 microns in diameter resting on top of Ag(Cl,Br) pavements The ratio of mercury to silver in these alloys was determined to be 1:1 using EDS analysis. It is possible that the mercury had volatilized after excavation and during SEM examination, but it can be understood that these deposits contained at least 50% mercury at the time of their recovery. The spheres were also found to be quite porous and some have silicon inclusions. The formation process for the amalgam spheres would have been the same as that for the small amalgam inclusions discussed above.

The spherical shape of these deposits is attributed to the high surface tension of mercury and alludes to drops of mercury sitting on the surface of the coins and amalgamating the underlying primary silver. Relatively large non-spherical deposits of 1:1 amalgam are present on coins 4342, 4315, and 4030. The edges of the amalgam deposits on all of these coins are rounded hinting at the influence of surface tension on their formation. The obverse of 4030 is covered with a discontinuous layer of amalgam that contains large amounts of silicon inclusions. This coin may have at one time been sitting in a pool of mercury on the site. In addition to the amalgam on these coins, an anomalous non-spherical deposit of virtually pure mercury sits on top of an

Ag(Cl,Br) matrix on the obverse of coin 4342 The failure of the amalgam formation is likely to be due to the deposition of a siliceous organism on the coin surface which acts as an insulator.

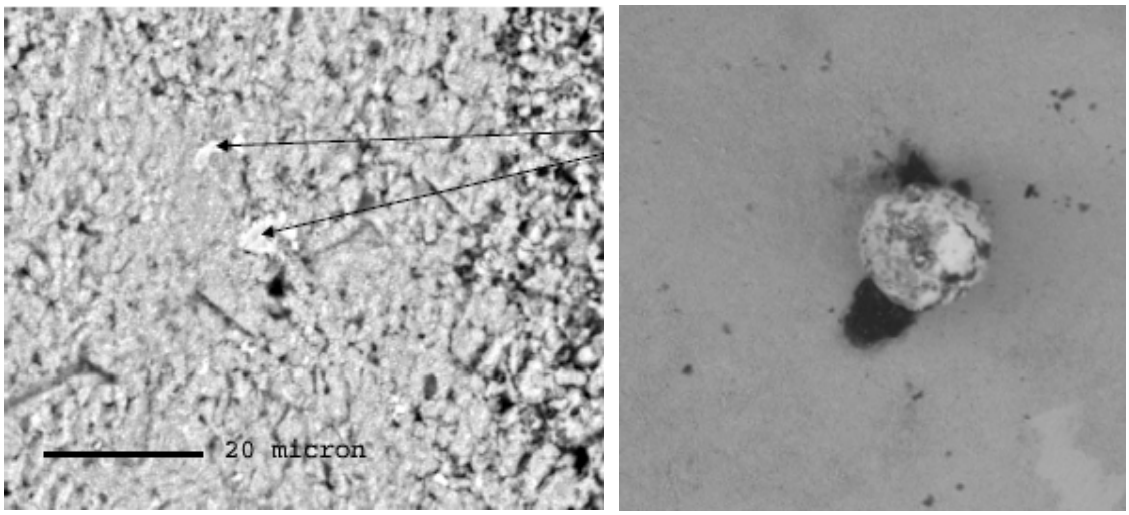

Figure 5: The left image shows the BSE images of obverse of coin no 4342, of silver amalgam (arrowed) in a silver halide matrix (image width 70 μm), right BSE image showing an amalgam sphere on coin 4342, approximate diameter 110 μm.

The major silver corrosion product found on every coin in this study is embolite Ag(Cl,Br), otherwise known as bromian chlorargyrite, with minor amounts of chlorargyrite (AgCl). The presence of these minerals is to be expected given the coins are from a shallow and energetic ocean site. Bromian chlorargyrite has been found in quantity on archaeological silver artefacts from both terrestrial and underwater environments. Since the silver ion concentration needed to precipitate AgCl from seawater is $2.92x10^{-10}$ and for AgBr it is $5.04x10^{-10}$ the coprecipitation of both halides is not unexpected. Kolthoff and Yutzy, Hedges (1976) speculated that the ratio of bromide to chloride in silver halide corrosion products from a marine environment would be on the order of 0.33 on a molar basis and analysis of a Spanish piece of eight found a similar ratio. Coins from the *San Pedro De Alcantara* site had molar ratios of bromine to chlorine in chlorargyrite from 0 to 1.0 on a molar basis, with the mode ratio being 1.0. There are two distinct phases of bromian chlorargyrite on all of the coins: amorphous particles that occur as pavements and larger isometric crystals. Except for the heavily eroded coins (4315, 4030, 4342), the coins display pavements of amorphous particles overlying a stratum of large Ag(Cl,Br) crystals measuring up to 50 microns. The large crystals are lamellar in structure and appear to be the product of recrystallisation (see Figure 6). EDS analysis of the two phases revealed no difference of Cl:Br ratios between them. Cubic crystals of chlorargyrite are present on the coins in limited quantity and were usually found intermixed with the amorphous Ag(Cl,Br) pavements. Bromargyrite (AgBr) was not observed on any of the coins in this study.

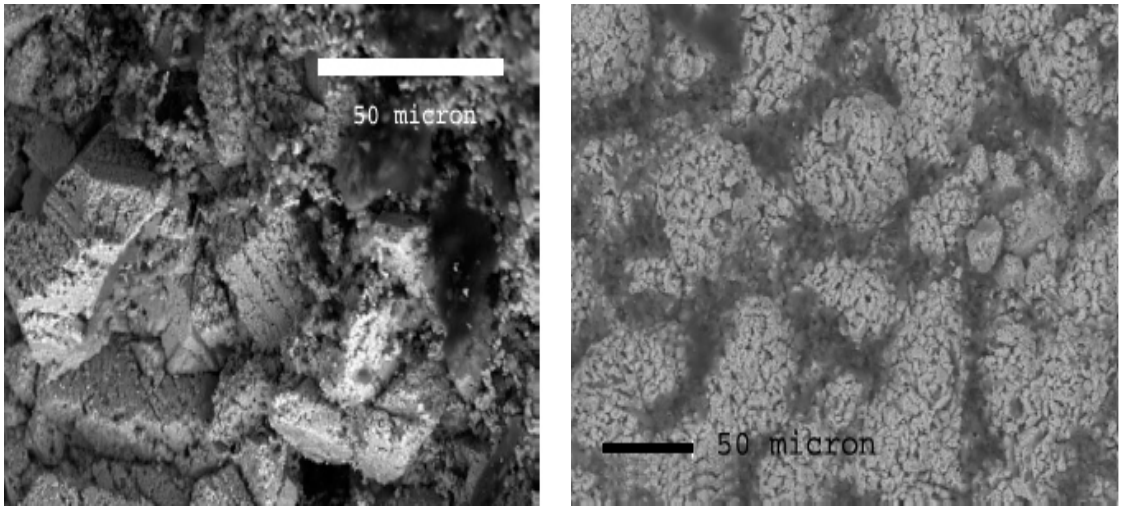

Figure 6: Left BSE micrograph of coin 4331 showing lamellar structure of large Ag(Cl,Br) crystals, image width 140 μm and the right image from the reverse of coin 4325 showing crystals in the process of recrystallising, image width 300 μm

Deposits of silver sulphide (Ag_2S) are present on coins 4325 and 4327 as distinct layers (that also contain small amounts of copper) were found under hydrated iron oxide films. The silver sulphide layer (see layer 2 from the left image in Figure.4) on the obverse of coin 4325 consisted of monoclinic acanthite (Ag_2S) and the presence of some argentite. This body-centered cubic polymorph of acanthite, is indicated by the presence of very similar lines, since the 2θ angles for argentite are very close to certain angles in the acanthite pattern. Both Ag_2S forms have been found on silver-copper alloys artefacts from shipwreck sites in Australia (North and MacLeod, 1987) with acanthite the dominant sulphide corrosion products on coins from the *Rapid* shipwreck (MacLeod, 1991). Given that no other reports of naturally occurring argentite have been encountered in the biosphere, it is likely that the inherently unstable argentite could be explained by the stabilization of argentite by copper atoms (McNeil and Little, 1992) Argentite, but not acanthite, can accommodate up to approximately 30% copper in its lattice structure which could make it more stable on a silver-copper alloy coin (McNeil and Little, 1999). This could explain the presence of copper in the silver sulphide layer on coin 4325 and the lack of copper sulphides or silver copper sulphides in the XRD analysis results. The large number of silver-copper-sulphide corrosion products on shipwreck artefacts is due to the ubiquitous presence of sulphide ions resulting from the metabolic activity of sulphate reducing bacteria as noted by Craig *et al.* (2002). The presence of silver sulphide layers underneath iron corrosion products on coins 4325 and 4327 is consistent with an anaerobic microenvironment under the iron while the coins were in an aerobic environment (McNeil and Little, 1999). Alternating cycles of burial and exposure can also explain the presence of Ag(Cl,Br) layers underneath the silver sulphide layers on both coins.

Apart from possible copper sulphides on coins 4325 and 4327, aerobic copper corrosion products cover large areas of the surface of every coin in this study. Generally the minerals exist as small and numerous deposits intermixed with the Ag(Cl,Br) matrices or as large overlying deposits on the surface of the coins. XRD and EDS analysis show the compounds consist of a variety of copper (II) chloride compounds and copper oxides, including clinoatacamite, $Cu_2Cl(OH)_3$. The greater mobility of copper chloride complexes such as $CuCl_2^-$ accounts for the overlying copper corrosion deposits on the coins. Raised islands of copper corrosion products overlying the silver halide surfaces are present on the heavily deteriorated coins. The greater Mohs' hardness of copper oxides and chlorides (3 hardness) compared with silver halides (1.5-2 hardness), would leave islands of copper corrosion products in an erosion situation that reflects the extremely turbulent nature of the *San Pedro De Alcantara* wrecksite.

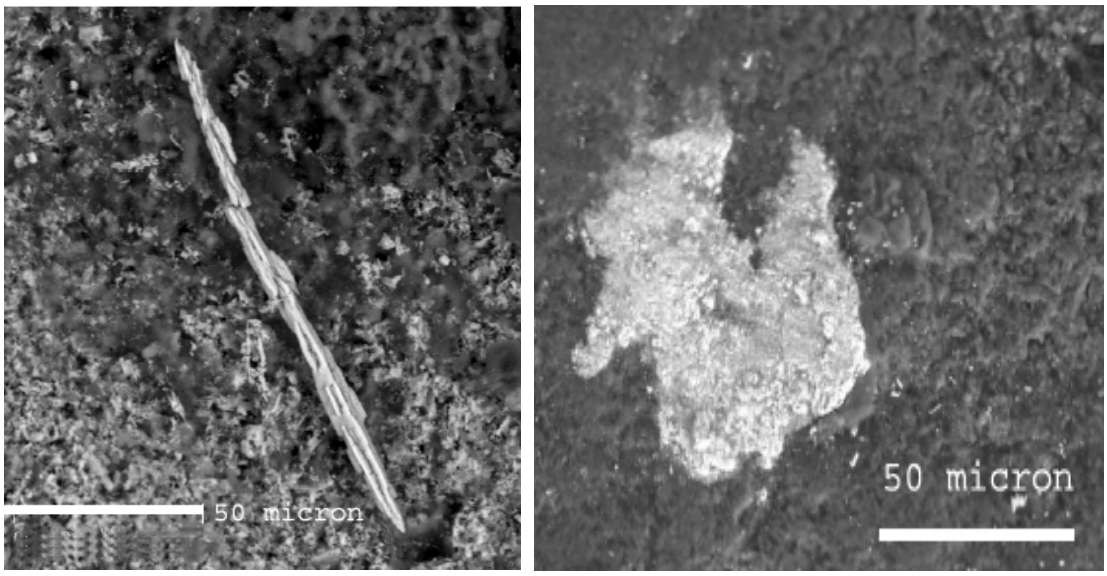

Figure 7: Left BSE image of the reverse surface of coin no 4030 showing an anglesite crystal, image width 140μm and on the right, an image from the obverse of the same coin on the obverse showing laurionite in a calcium carbonate matrix, width of 110 μm

Many anglesite ($PbSO_4$) crystals were found on the surface of coin 4030 along with deposits of laurionite (PbClOH) in the iron-bearing calcium carbonate concretions. Anglesite crystals covering the enormous range of 2-200 μm in length were found on both faces of the coin and have a tabular bladed appearance dominated by large pinacoid faces (see Figure 7). Most of the anglesite was found sitting on top of or intermixed with loose sand debris and calcite crystals in the niches of calcareous concretions. Laurionite was found as discrete amorphous deposits in the iron-bearing calcareous concretions on the obverse of this coin, mainly on the concretion edges. Coin 4030 is the only coin of the seven that bears lead minerals. Although it was not found near any lead artefacts, it could be postulated that the coin was at one time in close association with lead since both minerals are highly insoluble in seawater. Large crystals of calcium sulphate ($CaSO_4$) present on coins 4324, 4327, and 4331 are a likely consequence of iron corrosion products acting as ion exchange sites, which regularly concentrates sulphate ions so that the normally soluble minerals would precipitate on the coin surfaces.

3.2 Erosion Corrosion

Erosion corrosion is indicated by an increased rate of deterioration on a metal because of the relative movement between a corrosive fluid and a metal surface (Shrier, 1976). Since the *San Pedro de Alcantara* site is an area of constant and aggressive surge action, erosion corrosion plays a major role in the deterioration of metals on this site. The coins 4342, 4030 and 4315 were found lying on top of the sediment and their much higher mass loss is a measure of the erosion effect. Prior to recovery, coin 4315 was lying flat on top of a thin layer of sediment in a shallow bedrock hole, which meant it was fully exposed to water and sediment movement, and this resulted in more than a 60% mass loss. The majority of the coin is covered with a thin pavement of amorphous Ag(Cl,Br) with inclusions of copper corrosion products but in some areas the core metal of the coin is actually exposed since the erosion was so severe as to prevent precipitation of corrosion products. There are a few small remnants of raised calcareous concretions on the coin that are resting on eroded and corroded silver halide pedestals, the shape of which indicates that they were being eroded and corroded away in preference to the concretions, since calcite and aragonite have Mohs' hardness of 3 compared with 1.5-2 for bromian chlorargyrite. Two other heavily deteriorated coins, 4342 and 4030, display a similar concretion pattern.

Although hardness is a fairly good criterion for resistance to mechanical erosion or abrasion, it does not necessarily succeed as a good criterion for predicting resistance to erosion corrosion. The ability of a surface film or layer to passivate the underlying metal is also an important factor. Calcareous concretions, especially those that grow in tropical waters tend to be somewhat porous and good conductors for the corroding metal they cover (MacLeod, 1982). In contrast, iron oxide films tend to be poor ionic and electrical conductors and can passivate the underlying corroding metal. There is a clear discrepancy between the preservation of those coin surfaces that are covered by iron oxide films and those that are not. Where the surface of coins 4325 is covered by an iron oxide film the raised design is well preserved, while the surfaces without the protective iron have the design obliterated. Clearly the iron oxide films are providing erosion and corrosion resistance to the coin surfaces they cover. It appears that the combination of the hardness of the marine iron oxides, from 4.5 to 6 on the Moh's scale, and their low conductivity accounts for the protection against erosion corrosion.

An unusual erosion corrosion phenomenon is found on many of the coins where the iron oxide films or thin calcareous concretions that were covering the raised lettering and design have worn away. In most of these areas there is only a hole that perfectly conforms to the shape of the eroded and corroded away raised design surrounded by an iron oxide film or concretion. The formation of these negative concavities most likely involved multiple steps, as indicated in Figure 8 for coin 4327, with the initial step involving the selective erosion of the topographical high points of the film or concretion.

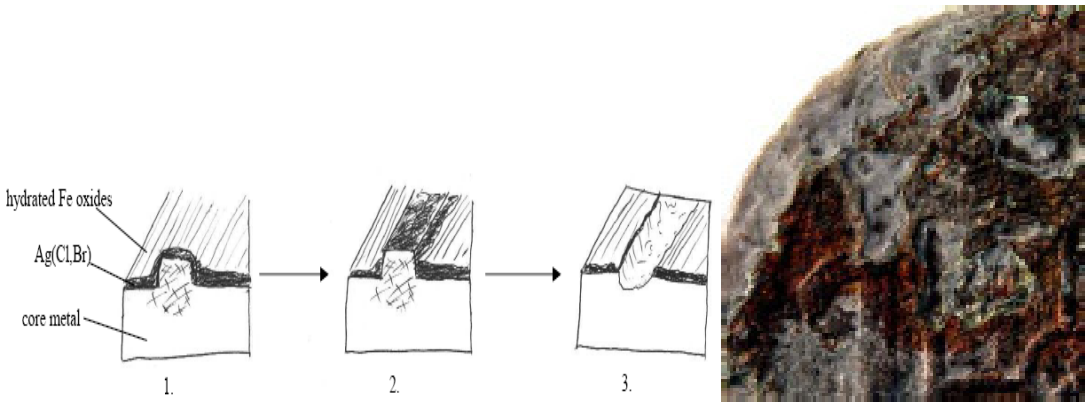

Figure 8: Erosion corrosion mechanism for preferential deterioration of raised surfaces on coin 4327.

The likely second step involved the erosion corrosion of the softer and more conductive silver corrosion products that were exposed from step one. Due to the inherent stress (hatch marks in Figure 8) in the raised areas of the coins that was caused by cold-stamping, the raised points were probably corroded in preference to their surroundings

3.3 Metallurgical Evidence

An example of stress related deterioration is seen on coin 4315, which exhibits strain lines on one edge of its obverse side (see left side of Figure 9). The strain lines, manifested by epitaxial copper (II) chloride growth in an amorphous Ag(Cl,Br) pavement, are evidence of residual stress caused during manufacture (Allen, 1969). The epitaxial growth of copper corrosion products is due to the fact that strain and slip lines can act as barriers for the migration of impurities in an alloy, causing these constituents to accumulate in those regions (Costa, 2001).

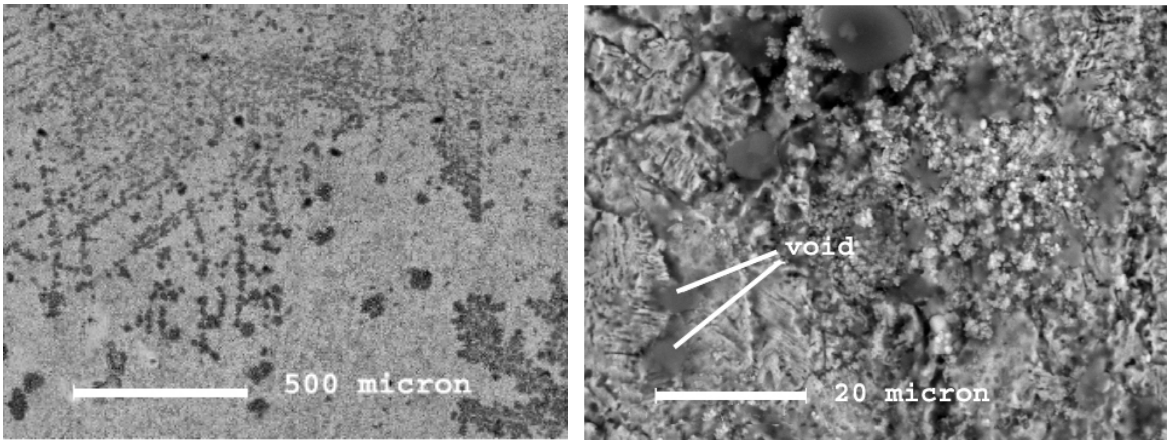

Figure 9: Left, BSE image from the obverse of coin 4315 showing Cu(II) chloride inclusions in an Ag(Cl,Br) pavement, image width 1650 μm, right image, the same surface showing exposed primary β silver grains, width of 80 μm.

The impurity in this case would be copper, given the room temperature solubility of copper in silver is only 0.1% (Butts, 1967). The precipitation of copper, usually along grain boundaries, from a solid silver-copper solution has been observed to occur on an archaeological time scale (Scott, 1991b). Additional evidence of manufacture is seen on the exposed core metal on the obverse of coin 4315, where the metallurgical grain structure is apparent, as seen in Figure 9. The microstructure of the coin was originally composed of a solid solution of β-phase grains with α-phase inclusions, which are now voids, in and surrounding the grains. This type of microstructure is characteristic of silver-copper alloys with copper contents between 5-10% *(*Costa, 2001). The absence of the α-phase (silver in copper) can be attributed to the selective corrosion of copper due to galvanic effects. Analysis of the area shown in the right hand image in Figure 9 showed it to consist of pure silver.

3.4 *In-Situ* Corrosion Potentials

The *in-situ* corrosion potentials of eleven coins, including those in this study were measured along with the pH, temperature and water depth. This data has previously been reported and it was found that there was a linear relationship between the corrosion potential (E_{corr}) and the water depth, according to the linear relationship,

$$E_{corr} = -0.273 - 0.024\, d$$

Where *d* is the water depth in metres. The square of the correlation coefficient for the nine coins described in the above equation was 0.6946, which indicates a moderate correlation between the data points and this is seen in the errors associated with the intercept value of –0.273±0.032 and the slope value is –0.024±0.006 (MacLeod, 2002a). Despite these limitations the data appears to follow the general trend observed on iron fastenings of a linear decrease in the value of E_{corr} with water depth (MacLeod, 1989). The weight of the excavated coins used

in this study and their corrosion potentials are listed in Table 1. Since all the coins had the same original weight and shape, the weight loss is a measure of the combined effects of erosion and corrosion. The data in Table 1 approximated a linear relationship between the weight loss and the corrosion potential,

$$\text{Weight loss (grams)} = 40.7 + 79\ E_{corr},$$

where the square of the correlation coefficient was 0.9222 for all but the coin 4315, which was exposed to breaking waves during heavy seas and had higher weight loss than predicted by the above equation. Despite the relatively large errors associated with the intercept (± 4.74 g) and the error in the slope (± 11.5) the data indicates that the net weight loss is linked to the corrosion potentials of the coins and thus the water depth. The apparent linear relationship between weight loss for coins and the water depth, via the E_{corr} data, indicates that different corrosion processes control the decay of the coins compared with those observed on iron shipwrecks in open waters and those in Chuuk Lagoon (MacLeod, 2002b) where there is a linear relationship between the log of the corrosion rate and water depth.

Table 1: Corrosion parameters for the silver coins

Coin reference	4315	4325	4331	4327	4342	4324	4030
Ecorr volt vs. Ag/AgCl	-0.408	-0.454	-0.452	-0.422	-0.380	-0.386	-0.374
Weight, gram	10.980	23.150	21.180	20.030	15.350	17.260	16.650

More measurements are needed before any definitive comments can be made on the relative importance of abrasion and corrosion of coins on this shipwreck site. Despite the fact that changes in microenvironment, such as coin movement and wave action, can dramatically change the corrosion potential, this preliminary study indicates that further work is likely to assist in clarifying the deterioration mechanisms.

4. Conclusion

The corrosion mineralogy and metallurgy of seven coins from the *San Pedro de Alcantara* shipwreck site in Portugal has been characterised through a combination of light and scanning electron microscopic techniques with mineral characterisation through application of quantitative x-ray analysis by EDAX and by x-ray diffraction. The physical location of the coins on the wreck site was found to be closely correlated with the specific corrosion microenvironment that was reflected in the vary degrees of corrosion, as measured by weight loss and loss of surface profile. When coins had been recovered from a similar burial environment their physical mass was similar. Aerobic environments dominate the wrecksite and this is reflected in the presence of bromian chlorargyrite, chlorargyrite, and copper (II) chlorides and oxides on the coins. Distinct layers of silver sulphide overlay bromian chlorargyrite strata on coins that were protected by the deposition of dense and electrically insulating hydrated iron-oxide films. Since the iron-oxide films are much harder than the underlying silver and copper corrosion products they provide erosion resistance. Similarly the concretions also protect the coins from erosion corrosion. The deposition of inorganic calcite is attributed to the increased pH associated with cathodic reduction of oxygen on the surfaces of the coins. Inorganic aragonite was only found on coin 4327, which is likely to be due to the large amounts of iron oxides and sulphide minerals on this coin. The site can produce such harsh erosion corrosion conditions that some surfaces were completely stripped of corrosion products. Signs of residual stress from the manufacture of the coins were apparent, which demonstrated that the coin had not been annealed after being minted. Mercury, coming from the original cargo, and its resultant silver amalgam were found on top of and sometimes intermixed with the bromian chlorargyrite pavements on the unburied coins. The discovery of large amounts of lead minerals on the surface of coin 4030 attested to its former close proximity to corroding lead objects. It was found that the weight loss of the coins could be regarded as a measure of the degradation rate and that there was a direct relationship between the corrosion potential and the weight loss of the coins.

Acknowledgements

We are deeply indebted to Bruce Robinson and Michael Verall of the Electron Beam Laboratory at the Commonwealth Scientific and Industrial Research Organization (CSIRO), Australia; and Rolando Lastra of the Canada Centre for Mineral and Energy Technology (CANMET) Mining and Mineral Science Laboratories for providing countless hours of assistance with the SEM analysis and for their insight. Special thanks to Alan Grant of Queen's University for providing his time and aid in carrying out the XRD analysis and to Alison Murray and Vera de La Cruz for their counsel. Without the inspiration of Jean-Yves Blot of the Portuguese

Institute of Archaeology, who supplied the coins from *San Pedro de Alcantara* shipwreck, this project would never have been initiated.

References

Allen, D. K., (1969) *Metallurgy Theory and Practice.* Chicago: American Technical Society.

Blot, J.-Y., Pinheiro-Blot, M.L., (1991) *Le naufrage de San Pedro de Alcantara*. La Recherche 230 Mars 22: 334-342.

Blot, J.-Y., Pinheiro-Blot, M.L., (1992) *O "interface" história-arqueologia: O caso do "San Pedro de Alcantara" 1786.* Lisbon: Academia de Marinha.

Blot, J.-Y., "San Pedro de Alcantara," http://www.abc.se/~pa/mar/spa.htm (Accessed January 25, 2004).

Blot, J.-Y., (1998a) *First steps in the analysis of ship overload*. Archaeological Computing Newsletter 51: 1-12.

Blot, J.-Y., (1998b) *From Peru to Europe (1784-1786): field and model analysis of a ship overload*. Bulletin of the Australian Institute for Maritime Archaeology 22: 21-34.

Butts, A, (ed.), (1967) *Silver: Economics, Metallurgy and Use.* Princeton, NJ: Van Nostrand.

Carlson, W.D., (1983) *The polymorphs of $CaCO_3$ and the aragonite-calcite transformation.* In Reviews in Mineralogy, vol. 11, ed. Richard J. Reeder, 191-225. Washington, D.C.: Mineralogical Society of America.

Cordua, W. S., (2003) *Pieces of eight minerals*. Leaverite news<http://www.uwrf.edu/~wc01/leaverite.html>

Costa, V., (2001) *The deterioration of silver alloys and some aspects of their conservation.* Reviews in Conservation *1.2: 18-34.*

Craig, J. R., *et al*. (2002) *Corrosion mineralogy of an 1800 Spanish piece of eight*. The Canadian Mineralogist 40: 585-594.

Fox, G. L., (1994) *Cupreous metal corrosion at a Bronze Age marine archaeological site: a study of site processes at Tel Nami, Israel*. The International Journal of Nautical Archaeology 23 (1): 41-47.

Hedges, R.E.M., (1976) *On the occurrence of bromine in corroded silver*. Studies in Conservation 21: 44-46.

Horne, R. A., (1969) *Marine Chemistry; The Structure of Water and the Chemistry of the Hydrosphere.* New York: Wiley-Interscience.

Kolthoff, I.M., Yutzy, H.C., *Studies on aging precipitates XV: the mechanism of the interaction between dissolved bromide and solid silver chloride*. Journal of the American Chemical Society 59: 2029-2032.

MacLeod, I.D., (1981) *Shipwrecks and applied electrochemistry.* Journal of Electroanalytical Chemistry 118: 291-303.

MacLeod, I.D., (1982) *The formation of marine concretions on copper and its alloys*. International Journal of Nautical Archaeology and Underwater Exploration 11: 267-275

MacLeod, I.D., (1985) *The effects of concretion on the corrosion of non-ferrous metals*. Corrosion Australasia 10 (4): 10-13.

MacLeod, I.D., (1989). *Electrochemistry and conservation of iron in sea water*, Chemistry in Australia, 56(7). 227-229.

MacLeod, I.D., (1991) *Identification of corrosion products on non-ferrous metal artefacts recovered from shipwrecks*. Studies in Conservation *36: 222-234.*

MacLeod, I.D., (2002a) *Effects of structure and composition on the performance of gold and silver alloys on shipwrecks*. Proceedings of International Congress on the Conservation and Restoration for Archaeological Objects. 178-185. Tokyo: National Research Institute for Cultural Properties.

MacLeod, I.D., (2002b) *In situ corrosion measurements and management of shipwreck sites*. In International Handbook of Underwater Archaeology, eds. Carol V. Ruppé and Janet F. Barstad, 697-714. New York: Kluwer Academic/Plenum Publishers.

MacLeod, I.D., (2003) "*Metal corrosion in Chuuk Lagoon: A survey of iron shipwrecks and aluminium aircraft,* Report to the US National Parks Authority, Pacific Division, San Francisco, USA, pp 1-92.

MacLeod, I.D., *et al. 1986. The excavation, analysis, and conservation of shipwreck sites.* In Preventive Measures During Excavation and Site Protection, *113-132. Rome: ICCROM.* McNeil, B. Michael and Brenda J. Little. (1992) *Corrosion mechanisms for copper and silver objects in near surface environments.* Journal of the American Institute for Conservation 31 (3): 355-366.
–
McNeill, & Little (1999) *The use of mineralogical data in interpretation of long-term microbiological corrosion processes: sulfiding reactions*. Journal of the American Institute for Conservation 38.2: 186-199.

Milliman, J. D., Manheim, F. T. (1968) *Submarine encrustation of a Byzantine nail*. Journal of Sedimentary Petrology 38.3: 950-953.

New World Treasures. (2003) <www.newworldtreasures.com> (Accessed April 12, 2004).

North, N. A., MacLeod I. D., (1987) *Corrosion of metals*. In Conservation of Marine Archaeological Objects, ed. Colin Pearson, 68-99. London: Butterworths.

Oxley, I., (1990) *Factors affecting the preservation of underwater archaeological sites*. International Journal of Nautical Archaeology*, 19.4: 340-341.*

Robbiola, L., et al. (1988) *Etude de la corrosion de bronzes archéologiques du Fort-Harrouard: altération externe et mécanisme d'altération stratifiée*. Studies in Conservation 33 (4): 205-215.

Robinson, B.W., (1992) *The "GeoSEM": a low-vacuum SEM optimized for geology and metallurgy*. Journal of Computer-Assisted Microscopy, 4 (3): 235-239.

Robinson, W. S., (1981) *First Aid for Marine Finds. London: The Trustees of the National Maritime Museum.*

Robinson, W. S., (1982) *The corrosion and preservation of ancient metals from marine sites*. The International Journal of Nautical Archaeology 2 (3): 221-231.

Scott, D.A., (1991a) *Metallography and Microstructure of Ancient and Historic Metals.* Santa Monica: Getty Conservation Institute.

Scott, D.A., (1991b). *A technical and analytical study of two silver plates in the collection of the J. Paul Getty Museum*. In Materials Issues in Art and Archaeology II, eds. Pamela B. Vandiver *et al.*, 665-690. 68

Scott, D.A., (1994) *An examination of the patina and corrosion morphology of some Roman bronzes*. Journal of the American Institute for Conservation 33 (1): 1-23.

Shrier, L.L., ed. (1976) *Corrosion,2nd ed., vols. 1&2., Newnes-Butterworths, London:*.

Tribble, G. W., (1993) *Organic matter oxidation and aragonite diagenesis in a coral reef.* Journal of Sedimentary Petrology 63.3: 523-527.

Weier, L.E., (1971) *The Deterioration of Inorganic Materials under the Sea.* London: University of London, Institute of Archaeology

ABN 70 592 297 967

A local microscopic model for the formation of silver mirroring on black and white photographs

G. Di Pietro [a, 1]

[a] Division of Health, Science and Design, University of Canberra, Canberra ACT 2601 Australia

Abstract (English)

Black and white photographs are made of a gelatine emulsion containing silver grains laid on a support material that can be glass, plastic or paper. Due to the small size of the silver grains, the corrosion of the silver grains is the starting point for a variety of degradation forms appearing visually different like yellowing, silver mirroring and red spots. In this paper we focus our attention on the formation of silver mirroring, a bluish metallic sheen commonly seen on silver gelatine glass negatives. As a result of the analysis of the composition of the silver mirroring particles and of the structure of the silver mirroring layer we suggest a modification of the current model for the formation of silver mirroring. This model enables us to understand what are the characteristics that differentiate the formation of silver mirroring from the formation of other corrosion based photographic degradation forms.

Résumé

Les photographies en noir et blanc sont constituées d'une émulsion de gélatine contenant des grains d'argent, étalée sur un support matériel constitué de verre, ou bien de plastique ou encore de papier. Les grains d'argent connaissent un processus de corrosion qui, à cause de la petite taille des grains, aboutit à différentes formes de dégradation se manifestant visuellement de plusieurs façons, comme le jaunissement, le miroir d'argent (*silver mirroring*), et les taches rouges. Cet article porte sur la formation du miroir d'argent, un reflet métallique bleuté communément observé sur les négatifs en verre. Nous proposons une modification du modèle courant de formation du miroir d'argent, basée sur l'analyse de la composition des particules et de la structure de la couche du miroir d'argent. Ce nouveau modèle nous permet d'identifier les caractéristiques qui différencient la formation du miroir d'argent de la formation des autres formes de dégradation des photographies basées sur la corrosion.

Keywords: black and white photographs, degradation of photographs, silver mirroring.

1. Introduction

Black and white (B&W) photographs are made of a gelatine emulsion containing silver halide crystals that are turned to silver grains during processing. The emulsion resides on a support material that can be paper, plastic or glass. The silver grains have dimensions of the order of microns and, in photographs chemically developed, a complex dendritic form. Their small dimension and the presence of kinks result in them having a very large surface area. This explains their susceptibility to undergo reactions and corrosion processes. Indeed, the oxidation of the silver grains and the subsequent reduction of their dimension and formation of silver ions in the emulsion are of the basis for at least three visually different degradation forms of B&W photographs: the shift towards a yellow tone in the image areas, the formation of red spots and the formation of silver mirroring, a bluish metallic sheen mostly present at the edges of the photograph (Figure 1).

In this paper we shall focus our attention on the formation of silver mirroring with the aim of understanding the detailed mechanism leading to its formation, and be able to identify which compounds and reaction conditions are likely to result in silver mirroring or in other corrosion based degradation phenomena.

[1] Corresponding author: TEL: +61 2 62012121: FAX: +61 2 6201 2048: email: Giovanna.Di.Pietro@canberra.edu.au

Figure 1 Silver gelatine glass negative with wide silver mirroring stain, partially obscuring the image. Cueni study collection (~1910).

1.1 Historical review of the models on silver mirroring formation

The first account of silver mirroring dates back to the 1882 (British Journal of Photography 1982), just two years after the invention of modern B&W photography. Even in these early stages silver mirroring was attributed to the action of hydrogen sulphide ("sulphuretted hydrogen") (British Journal of Photography 1901), and the formation of silver mirroring was defined as a "slow sulphiding" (British Journal of Photography 1918). A key date in the understanding of the silver mirroring process is 1963. In this year Henn and Wiest (1963) proposed a model, called here the Oxidation-Migration-Re-aggregation model (OMR). According to the OMR model the silver image particles are first oxidized, silver ions are formed, and then migrate in the gelatine. When the silver ions are reduced to silver they either re-aggregate within the emulsion forming small particles appearing as red spots, or they re-aggregate at the emulsion top surface forming silver mirroring. The analysis of the composition of mirrored areas with an electron microprobe concluded that they contain "appreciable but highly variable amounts of silver sulphide".

Feldman (1981) published the first transmission electron micrographs of mirrored photographs. Later Hendriks of the Public Archives of Canada (Hendriks 1984, Hendriks 1991a), showed, by using TEM images, that silver mirroring not only consists of a layer of colloidal particles clustered at the emulsion top surface but also that mirrored emulsions have a number of signs of corrosion: the image silver grains are smaller, they have a more rounded shape, and they are surrounded by very small particles. The compounds responsible for such degradation were thought to be a large category of oxidizing and reducing compounds present either in the photograph itself as a result of improper processing, or in the surrounding air, or in the filing enclosure. Although he did not publish results on the chemical composition of the mirroring particles, he believed them to be made of a very thin layer of elementary silver centred on a silver sulphide nucleus. The mechanism leading to the formation of a surface layer of particles, the peculiarity of silver mirroring, was not explained in detail. An attempt to solve this matter was done by Nielsen and Lavedrine (Nilesen and Lavedrine 1993) who showed by analysing TEM images that underneath the mirroring layer a distribution of smaller particles existed. Such particles are considered to be proof for a migration of the silver salts towards the surface although no driving force for this movement was suggested.

1.2 Open questions

In conclusion: the OMR model and its subsequent refinements still leave two main questions unanswered regarding the formation of silver mirroring. These are: the chemical composition of the silver mirroring particles and the driving force for the formation and /or aggregation of particles at the emulsion top surface.

Answering the first question is crucial in understanding which compounds are actually responsible for the formation of silver mirroring. If the silver mirroring particles are made of elementary silver (Ag) then the compounds responsible for silver mirroring, apart from oxidant compounds, have to be searched for among silver reducing substances (e.g. aldehydes) while if they are made of silver sulphide (Ag_2S) they have to be searched for among sulphur containing substances (e.g. hydrogen sulphide H_2S).

Answering the second question is crucial to distinguishing the formation of silver mirroring, which microscopically has been shown to be layer of colloidal particles clustered at the emulsion top surface, from the other corrosion based degradation forms of black and white photographs, which microscopically consist of small particles aggregated within the emulsion bulk.

The first question will be answered by analysing the chemical composition of the silver mirroring layer.

The second question will be answered by analysing the particle shape and the density of the particle distribution underneath the mirroring layer. The particle shape and the density of particles are properties inherited by the mechanism of formation of silver mirroring. A surface layer of particles, like silver mirroring, can result either from particles formed within the emulsion bulk and then migrating towards the emulsion surface or from particles formed directly at the emulsion surface. These two mechanisms lead to two different trends for the particle shape. In the first case, the particle shape is predicted to be spherical at great distances from the surface and ellipsoidal close to the surface as colloidal particles cannot escape from the emulsion and cluster once their spatial density is sufficiently high. In the second case, particles would be formed by the reaction between silver ions, results of the oxidation of the image grains, and an external compound and, as the reaction has not a preferred direction, their shape is predicted to be spherical at any distance from the surface.

2. Experimental Procedure

The following experiments were performed on silver gelatine glass negatives. These formed the most common class of negative photographic processes between the 1880s and the 1920s. Silver gelatine glass negatives are particularly prone to silver mirroring because they have a relatively thick, non-hardened emulsion, and because they were mostly not lacquered. The negatives examined belong to the Cueni study collection, a collection of about 150 glass plate negatives of the Swiss painter and amateur photographer Adolf Cueni active in the Basel region in the years 1910s -1920s. The Laboratory of Image and Media Technology of the University of Basel presently owns the plates.

2.1 Chemical composition of silver mirroring

The spectroscopic methods suited to determine the chemical composition of silver mirroring have to fulfil two requisites. The first requisite is that they have to distinguish between compounds present in the mirroring layer, with thicknesses of the order of hundred nanometres, and compounds present in the emulsion bulk, of thickness of the order of fifty microns. The second requirement is that they have to be able to detect silver sulphide, which means either determination of the amount of sulphur and silver in the mirroring layer or detection of the presence of silver sulphide directly. The simple detection of sulphur is not sufficient to draw definitive conclusions because sulphur compounds can arise from the protein cystine, one of the constituent proteins of the gelatine, and from the incomplete removal of sodium thiosulphate ($Na_2S_2O_3$), the usual fixing agent.

These criteria suggested that successful analysing techniques might be X-Ray Diffractometry (XRD) on powder samples and X-Ray Photoelectron Spectroscopy (XPS). Both techniques satisfy the second criteria because XRD detects the crystalline structure of silver sulphide and XPS provides quantitative results of the sample atomic composition. Moreover, XPS is a truly surface analysis because the electrons used in the apparatus have energy of only few hundreds of electron volts. This energy is so small that uniquely the electrons emitted from atoms distant at maximum 10 nanometres from the sample surface can escape and be detected. X-Ray Diffraction on the surface of mirrored emulsions and Scanning Electron Microscopy with Energy Dispersive X-ray analysis (SEM-EDX) were also tested but did not give reliable results. Indeed the penetration depth of X-rays with energies of the order of 8 KeV (typical of the XRD apparatus) and the penetration depth of electrons with energy of 20 KeV (typical of the SEM apparatus) largely exceed the thickness of silver mirroring layer. Table 1 summarizes the spectroscopic analyses performed.

XRD analysis

The XRD analysis on powder samples was performed at the XRD facilities of the Netherlands Institute for Cultural Heritage (ICN), Amsterdam, under the supervision of Mr. P. Hallebeek. The XRD instrument is composed of an X-ray generator (Philips PW 1010) using a Cukα X-Ray source at wavelength λ=1.5406 Å and energy E=8.041 keV and of a Debey-Scherrer powder camera with a double coated CEA Reflex 25 film. The sample, consisting of few powder grains, is fixed on the tip of a glass fibre with cedar oil and it is continuously rotated during the measuring time (order of a few hours) to cover all the possible mutual positions between the incoming beam and the crystal planes within the sample. This instrument is able to detect the crystal composition of extremely minute amount of sample, of dimension of the order of 0.5 mm^2. The silver mirroring was scratched off the plates with a scalpel under a loupe, with careful attention in removing only the mirroring layer and not the underlying emulsion. The total amount of material was of the order of few powder grains.

XPS analysis

The measurements were performed at the XPS laboratory, Institute of Physics, University of Basel, under the direction of Prof. P. Oelhafen with an in-house built XPS apparatus. The samples, of dimensions approximately of 1cm*2 cm, are fixed with metal screws on a metal holder and inserted in the spectrometer where an air pressure of 10^{-9} millibar is reached in 10 hours. In spite of the high vacuum attained during the measurement, no damage was visible on the samples. The samples are then bombarded with X-ray and the spectra recorded in a few minutes. Due to high surface charging effects it was possible to record spectra only from the silver mirroring areas close to the metal screws. In these areas the surface charging was minimised because the electrons could diffuse to the metal holder and dissipate. The percentage atomic composition M_i of the sample can be calculated from the XPS spectrum (a graph of the number of the emitted electrons against the detected energies) because the area A_i of the peaks is proportional to the amount of atoms ejecting the electrons. It is given by the following formula:

$$M_i = \frac{A_i}{C_i} \times \frac{1}{\sum \frac{A_i}{C_i}} \qquad [1]$$

where C_i is the photoionization cross-section for the atomic core electron i

Table 1 Spectroscopic analyses

Samples	Analysis
Plate 1	
1a	XRD powder
Plate 2	
2a	XRD powder
2b	XRD flat
2c	XPS flat
2d	SEM-EDX
Plate 3	
3a	XRD flat
3b	XPS flat
Plate 4	
4a	SEM-EDX

2.2 Size and shape distributions of the silver mirroring particles

The size and shape distributions of the silver mirroring particles were analysed by using Transmission Electron Micrographs (TEM) with a LEO EM 912 microscope available at the Interdivisional Electron Microscopy Laboratory of the University of Basel. Small portions (dimension 1×2 mm^2) of mirrored emulsion of a historical non-processed glass negative were removed by immerging the plate in a solution of water and alcohol and using a knife blade and tweezers under the loupe. The samples were then embedded in a resin, a standard mixture of epoxy embedding medium,

hardener (DDSA and MNA) and accelerator (BDMA) all produced by Fluka. They were laid flat on a resin drop and, after removing the water in excess on the emulsion, they were covered with a second drop of resin and inserted in an oven at 60 degrees for about 8 hours. Afterwards, slices of 70 nm thickness were cut in the cross-section direction with an ultra microtome. The slices were transferred on a grid and they were inserted in the microscope where images with magnification of the order of 10000 times were taken. As the negative was a non-processed plate, long electron exposures had to be avoided in order not to develop the silver bromide grains physically. The TEM micrographs were digitised and the digital images analysed with the software NIH Image®. The software Mathematica® was used in the statistics analysis of the data.

3 Results

3.1 Results on the chemical composition of silver mirroring

The XRD analysis on powder samples has shown that the silver mirroring scratched off from plates 1 and 2 is composed at 100% of silver sulphide Ag_2S. No other crystalline compounds were detected. In the case of the detection of a single compound the error in the mass composition of the sample attained by the instrument used in this measurement is of the order of 5-10%.

The XPS analysis revealed in sample 2c (Figure 2) the presence of the following elements: carbon C (40%), oxygen O (11%), silver Ag (29%), sulphur S (14%), iodine I (4%) and mercury Hg (2%). The percentages refer to the relative atomic composition and are calculated from the spectra using formula [1]. In sample 3b carbon C (49%), oxygen O (10.5%), silver Ag (25%), sulphur S (11%), bromine Br (3%), iodine (1%) and mercury Hg (0.5%) were detected. As the spectral resolution of the spectrometer, measured as the full width at half maximum (FWHM) of the Ag 3d5/2 core-level signal is 0.93 eV, the error in the atomic composition is of the order of 10%.

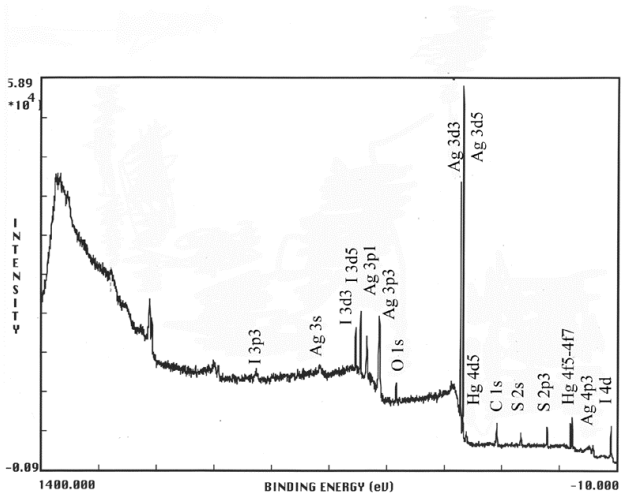

Figure 2. XPS spectrum of sample 2c.

In both samples the main component is carbon, arising from the collagen contained in the gelatine emulsion. Other major constituents are silver and sulphur. The ratio between the amount of silver and the amount of sulphur in the mirrored areas ranges between 2.07 and 2.27: almost the stoichiometric ratio for silver sulphide Ag_2S. Moreover the S(2p) peak has in both cases a negative shift (ranging from –4.5 to –6.3 eV) suggesting that sulphur is in the S^{2-} state (Hammond et al. 1975). This indicates that silver sulphide is present in the mirroring areas. The detected amount of oxygen arises probably from the collagen present in the emulsion; indeed, the absence of the O(1s) peak at 529 eV excludes the presence of silver oxide AgO or silver dioxide Ag_2O. The presence of bromine in sample 3b is consistent with the fact that plate 3 is a non-processed negative.

The results are summarized in Table 2.

Table 2 Results of the analysis of the chemical composition of silver mirroring

Sample	XRD Powder	XPS
1a	Ag_2S	
2a	Ag_2S	
2c		Ag_2S O,C,I,Hg
3b		Ag_2S O,C,Br,I,Hg

3.2. Results on the size and shape distribution of the silver mirroring particles

The samples were difficult to cut because of the softness of the specimen core. Although the slices often broke apart after cutting, it was possible to obtain some sections suitable for the analysis of the particle distribution (Figure 3).

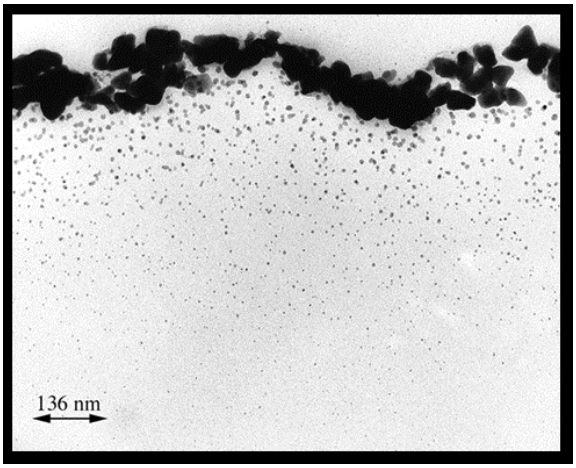

Figure 3. TEM micrograph of the cross-section of a mirrored area on a non-processed glass negative

The micrograph shown in Figure 3 was digitised and used to analyse the variation of area, density and sphericity of the small silver mirroring particles residing underneath the main layer. With the help of the software Adobe® Photoshop® the upper silver mirroring particles were removed and the image was divided in five stripes. With the help of the software NIH Image® each stripe was converted in a binary (black-white) image (Figure 4).

In each stripe the particle were counted and the particle mean area a (cm^2) and the length of the axes of the ellipse best fitting each particle were calculated. Figure 5 show the resulting depth profile of the silver mirroring spatial particle density while Figure 6 show the resulting depth profile of spherical and ellipsoidal particles. The percentage of spherical particles (star symbols) is almost constant in the emulsion and equal to the 60%. The particles with axes ratio bigger than two (triangle symbols) are always less than the 20% and show a slight increase in the uppermost 200 nm.

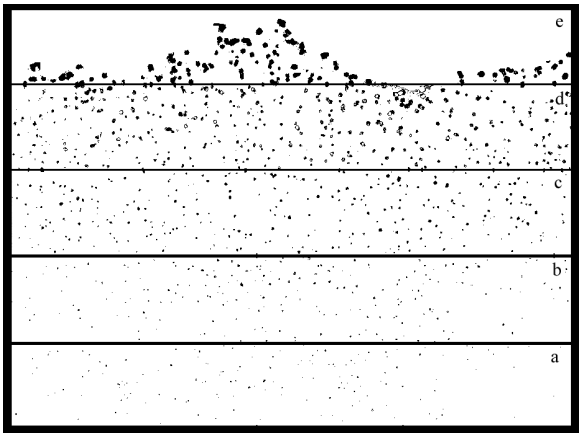

Figure 4. Result of the division in five stripes and of the binary conversion of Figure 3.

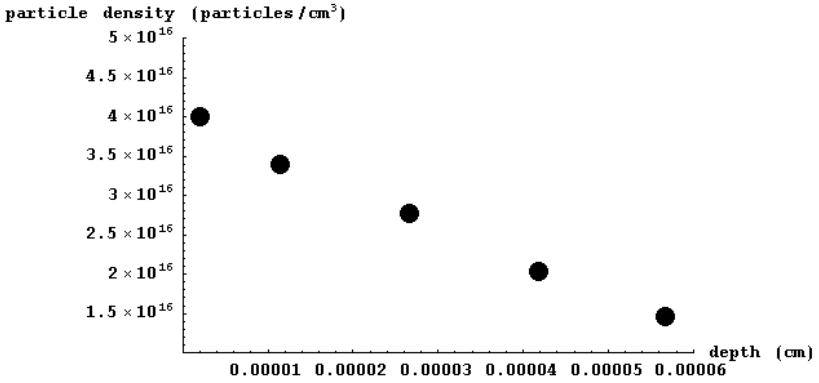

Figure 5. Depth profile of silver mirroring particle density.

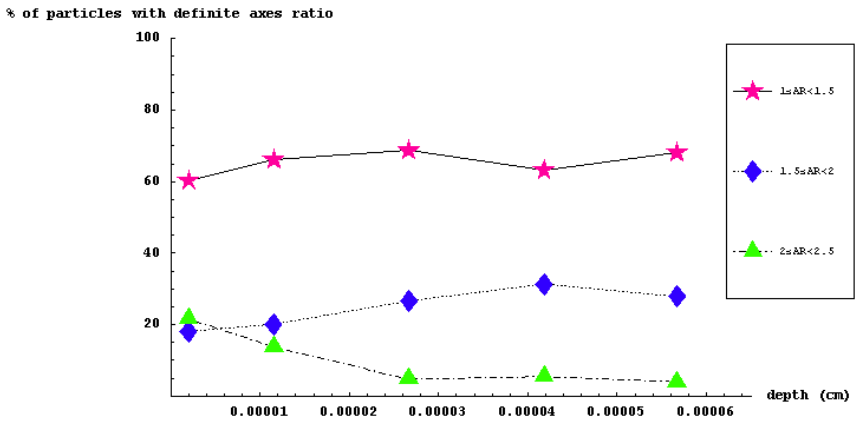

Figure 6. Depth profile of the percentage of spherical (with ratio between the lengths of the ellipse axes between 1 and 1.5) and ellipsoidal particles.

4. Discussion

The experiments have shown that the material contributing to silver mirroring is silver sulphide and that the majority of the particles beneath the main silver mirroring layer have a spherical shape up to the area closest to the emulsion surface. This allows us concluding that silver mirroring is due to the reaction between silver ions, product of the oxidation of the image grains, with environmental sulphur containing compound, possibly hydrogen sulphide, and that this reaction takes place at the emulsion top surface. On the contrary yellow discoloration takes place if the reactants are present within the emulsion. This happens either if they are the result of processing steps, so they are somehow born with the photograph, or if they can penetrate into the emulsion due to their high solubility and to their low reaction rates.

The OMR model for the formation of silver mirroring can be modified in a model consisting of the following steps: Oxidation, Diffusion of silver ions, Reaction with external sulphur compounds and Growth of silver sulphide particles (ODRG).

Oxidation

As in the classic OMR model the first step in the formation of silver mirroring is the oxidation of the image silver grains. This step has already been described in detail by other authors (Henn and Wiest 1963, Brandt 1987, Hendriks 1991b). Here I add only two comments relative to the case in which the oxidant compound is hydrogen peroxide.

For hydrogen peroxide partial pressures typically found in museums (of the order of ppbs), the amount of hydrogen peroxide dissolved in an emulsion is of the order of 10^{-6} mol cm^{-3}, which is calculated assuming that the hydrogen peroxide is dissolved in the water contained in the emulsion and applying the Henry's law [2]:

$$c_0 = p \times H^* \times mc \times W_{H_2O_2} \qquad [2]$$

where p is the partial pressure of hydrogen peroxide, H* is the Henry's coefficient (H*= 1.8×10^2 mol cm^{-3} atm^{-1}), mc (-) is the moisture content of the gelatine and W_{H2O2} (g mol^{-1}) is the molecular weight of hydrogen peroxide (W_{H2O2} =34 g mol^{-1}). The amount of hydrogen peroxide dissolved in the emulsion is two orders of magnitude lower than the amount of silver on average found in an emulsion, of the order of 10^{-2} g cm^{-3}, which corresponds to 2×10^{-4} mol cm^{-3}. This means that the oxidation step is always under the control of the amount of hydrogen peroxide

The second comment is concerned with the trend of the amount of hydrogen peroxide dissolved in the emulsion with changing relative humidity and changing degree of gelatine cross-linking. This follows the trend of the moisture content of gelatine (McCormick-Goodhart 1995, Yapel et al. 1994) and it is plotted in Figure 7.

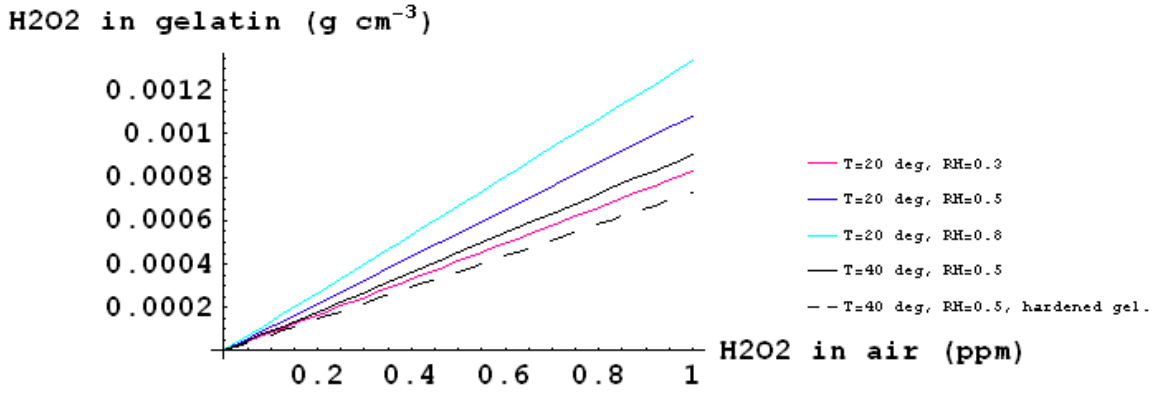

Figure 7. Equilibrium hydrogen peroxide concentration in the emulsion against hydrogen peroxide partial pressure in air for different RH, T and degree of gelatine cross-linking.

Diffusion of silver ions

The second step in the formation of silver mirroring is the diffusion of silver ions in the gelatine driven by the difference of silver ion concentration between the areas closest to the image silver grains and the emulsion bulk. The diffusion of silver ions in water-soaked emulsions is very fast. Curtis and Leaist (1998) report that in wet gelatine gel at room temperature the diffusion constant of silver ions $D(Ag^+)$ is 1.6×10^{-5} cm^2 s^{-1}. However, silver mirroring is formed in normal museum conditions where the moisture content of the emulsion is of the order of 20% maximum. From the work of Tanaka and co-workers (1973) on the conductivity K (ohm^{-1} cm^{-1}) and the silver ions transport number τ(-) in silver-silver nitrate ($AgNO_3$) films kept at 79% RH and 25° C the diffusion constant of silver ions can be calculated (Moore 1972, chapter 10 sec. 13):

$$D(Ag^+) = \frac{RT}{F^2} \times \frac{K_{tot} \times \tau}{m(Ag^+)} \quad [3]$$

where R is the gas constant (R = 8.3143 J K^{-1} mol^{-1}), T (K) is the absolute temperature, F is the Faraday constant (F = 96487 C mol^{-1}), K_{tot} (Ω^{-1} cm^{-1}) is the total film conductivity and $m(Ag^+)$ (mol cm^{-3}) is the silver ions molar concentration in the film.

Inserting Tanaka's data for τ, K_{tot} and $m(Ag^+)$ in equation [3], the diffusion constant of silver ions in gelatine films kept at 79% RH and 25 C results as being of the order of 5×10^{-11} cm^2 s^{-1}.

Assuming a diffusion law of the kind

$$\Delta L = \sqrt{D \times \Delta t} \quad [4]$$

where ΔL (cm) is the space travelled in a time Δt (s) by species with diffusion constant D (cm^2 s^{-1}), silver ions in emulsions at 79% RH and 25° C travel 50 μm (typical emulsion thickness in glass plates) in about 6 days. This time is short in comparison with the observed time scale of silver mirroring formation under normal archive conditions, which is of the order of months or few years maximum. This allows us to conclude that, in typical archive conditions, silver ions diffuse rather fast in the emulsion and they can be responsible of the formation of silver mirroring.

Reaction with external sulphur compounds

Once silver ions are produced and diffuse homogeneously in the emulsion, they will react with external sulphur based compound to produce silver sulphide seeds. Among environmental gases the most probable gas is hydrogen sulphide H_2S, a second possibility is carbonyl sulphide (OCS).

It is possible to envisage the following pathway for the dissolution of hydrogen sulphide in water followed by the reaction with silver ions:

a) $H_2S \rightarrow H^+ + HS^-$
b) $HS^- \rightarrow H^+ + S^{2-}$
c) $2\,Ag^+ + S^{2-} \rightarrow Ag_2S$

As the solubility constant of silver sulphide is very low ($k_{sp}=[Ag^+]^2 \times [S^{2-}]=6.89 \times 10^{-50}$), precipitation of silver sulphide will occur as soon as S^{2-} ions will be in solution. This, added to the fact that the emulsion surface is the region where the reactants first meet, explains why silver sulphide seeds are produced at the emulsion upper surface and not in the emulsion bulk.

Growth of silver sulphide particles

The final step in the formation of silver mirroring is the growth of the silver sulphide particles. The silver sulphide seeds grow because of the reaction between silver ions and hydrogen sulphide molecules on them. The reaction does not have a preferential direction, therefore the final shape of the particles is spherical. Further exposure to hydrogen sulphide will provoke the growth of the seeds without increasing of their number. This is supported by two different kinds of studies found in the literature. The first kind of studies is concerned with the tarnishing of silver plates. Bennet and co-workers (1969) have shown that silver sulphide clumps on silver plates nucleated on initial exposure to hydrogen sulphide and that further reaction occurred on the initially formed clumps. Graedel and co-workers (1985) also report the same reaction dynamics.

The second kind of studies is related to the photographic processes called diffusion transfer processes (typically used in Polaroid photographs). In these processes silver sulphide particles are used to catalyse the reaction between the developer and the silver ions (James 1939, Eggert 1947, Shuman and James 1971, Levenson and Twist 1973) either by adsorbing the developer onto the colloidal particles, or by stabilising a single silver atom using the electrical conductivity of the colloidal particle. The

stabilisation of silver atoms by silver aggregates has also been the object of more recent studies[2]. Although diffusion transfer processes differ from silver mirroring because the reaction takes place between silver ions and hydrogen sulphide instead of between silver ions and developer, colloidal silver sulphide particles could play the same catalytic function.

The difference of size between the particles at the interface emulsion-air and the particles underneath can be explained because the particles at the interface grow relatively fast as they are directly exposed to the environmental hydrogen sulphide and the more they grow, the more they fill the emulsion surface hindering the penetration of the gas into the emulsion. When the surface is completely covered, the amount of hydrogen sulphide entering the emulsion is zero and the growth of the particles underneath the surface is blocked.

Conclusions

This work allows us to conclude that silver mirroring is formed of a surface layer of silver sulphide particles a result of the reaction between silver ions and an environmental sulphur based compound, most probably hydrogen sulphide

Acknowledgements

I would like to thank the colleagues of the laboratories where the experimental measurements were performed, Ulla B. Nielsen Kejser of the Danish National Library for providing literature and Frank Ligterink of the Instituut Collectie Netherlands for many useful discussions.

References

Belloni, J. et al. 1991. Quantum size effects and photographic development. *Journal of imaging science* 35: 68-74.

Bennett, H. E. et al. 1969. Formation and growth of tarnish on evaporated silver films. *Journal of applied physics* 40 (8): 3351-3360.

Brandt, E. S. 1987. Mechanistic studies of image stability. 3. Oxidation of silver from the vantage point of corrosion theory. *Journal of imaging science* 31 (5):199-207.

British Journal of Photography. 1901. The permanency of toned bromide prints. *The British Journal of Photography* January 18: 39.

British Journal of Photography. 1918. Degrees of permanence in photographic prints. *The British Journal of Photography* February 15: 74-76.

British Journal of Photography. 1982. The deterioration of gelatin plates. *The British Journal of Photography* November 12: 1206.

Curtis, N. and D. G. Leaist. 1998. Interdiffusion of acqueus silver nitrate and potassium chromate and the periodic precipitation of silver chromate lisegang bands. *Berichte der Bunsen-Gesellschaft fuer Physikalische Chemie* 102 (2): 164-176.

Eggert, J. 1947. Zur katalytischen Abscheidung von Silber. *Helvetica Chimica Acta* 30: 2114-2119.

Feldman, L. H. 1981. Discoloration of black and white photographic prints. *Journal of Applied Photographic Engineering* 7 (1):1-9.

Graedel, T. E. et al. 1985. On the mechanism of silver and copper sulfidation by atmospheric H2S and OCS. *Corrosion Science* 25(12):1163-1180.

[2] It has been shown (for a review see Henglin (1993)) that the electrochemical potential for the reaction $Ag^{+}+e^{-}TAg^{0}$
is very low for single ions (-1.8 V) and it increases with the size of the silver aggregates till the value assumed on the solid metal (+ 0.799 V). For small silver aggregates quantum effects have been taken into account (Belloni et al. 1991) while for aggregates bigger than 1 nm a simple surface energy effect explains this behaviour (Plieth 1982).

Hammond, J. S. et al. 1975. X-ray photoelectron spectroscopy studies of cadmium-oxygen and silver-oxygen surfaces. *Analytical Chemistry* 47:2193-2199.

Hendriks, K. B. 1984. The preservation and restoration of photographic materials in archives and libraries: a RAMP study with guidelines. Paris: Records and Archives Management Program, UNESCO.

Hendriks, K. B. 1991a. On the mechanism of image silver degradation. In *Sauvegarde et conservation des photographies, dessins, imprimés et manuscrits*. Actes des journées internationales d'études de l'ARSAG, Paris 30 Sept.-4 Oct. 1991. ARSAG.73-77.

Hendriks, K. B. et al. 1991b. Fundamentals of photograph conservation: a study guide. Toronto: Lugus publications.

Henglein, A. 1993. Physicochemical properties of small metal particles in solution: microelectrode reactions, chemisorption, composite metal particles and the atom-to-metal transition. *Journal of Physical Chemistry* 97:5457-5471
.

Henn, R. W. and D. G. Wiest. 1963. Microscopic spots in processed microfilms: their nature and prevention. Photographic Science and Engineering 7 (5): 253-261.

James, T. H. 1939. The reduction of silver ions by hydroquinone. The Journal of the American Chemical Society, 61: 648-652.

Levenson, G. I. P. and P. J. Twist. 1973. The reduction of silver ions on nuclei by hydroquinone. The Journal of Photographic Science 21: 211-219.

McCormick-Goodhart, M. H. 1995. Moisture content isolines and the glass transition of photographic gelatin: their significance to cold storage and accelerated aging. In Research techniques in photographic conservation, Proceedings of the Conference held in Copenhagen 14-19 may 1995. Copenhagen: The Royal Danish Academy of Fine Arts. 65-69.

Moore, W. J. 1972. Physical Chemistry. London: Longman.

Nielsen, U. B. and B. Lavedrine. 1993. Etude du miroir d'argent sur les photographies. In Les documents graphiques et photographiques. Paris: Archives nationales. 131-143

Plieth, W. J. 1982. Electrochemical properties of small clusters of metal atoms and their role in surface enhancement Raman scattering. Journal of Physical Chemistry 86:3166-3170..

Shuman, D. C. and T. H. James. 1971. Kinetics of physical development. Photographic Science and Engineering 15:42-47.

Tanaka, T. et al. 1973. Drift motion of silver ions in gelatin films and its implication in the photolysis of low-pAg emulsions. In Proceedings of the symposiums on photographic sensitivity held at Gouvill & Caius College and Little Hall, Cambridge, September 1972. Cambridge: R.J.Cox. 139-147
.

Yapel, R. A. et al. 1994. Mutual and self diffusion of water in gelatin: experimental measurement and predictive test of volume-free theory. Polymer 35 (11): 2411-2416.

Proceedings of Metal 2004 National Museum of Australia Canberra ACT 4–8 October 2004
ABN 70 592 297 967

The delamination of silversulphide layers

R. van Langh [a], H.A. Ankersmit [b], I. Joosten [b]

[a] Rijksmuseum Amsterdam, P.O. Box 74888, NL-1070 DN Amsterdam, The Netherlands.
[b] Netherlands Institute for Cultural Heritage, P.O. Box 76709, NL-1070 KA Amsterdam, The Netherlands,

Abstract

The morphology of a delaminating tarnish film formed on a 17th century showplate is examined by SEM-EDS. Three different layers could be observed; *i)* the silver copper alloy, *ii)* a copper sulphide layer and on top of that a *iii)* silver sulphide layer. The original alloy shows elongated copper particles within the silver matrix, indicating a milled metal. The copper sulphide layer consists of conglomerated particles, with islands of metallic silver and possibly some metallic copper. The silver sulphide layer is stratified and contains cracks. Inside this layer several cavities and island of metallic silver are observed. The overall thickness of the stratified Ag_2S layer is typically 14 µm, while the layers that make the stratification varies from 200 – 1250 nm. The maximum silver sulphide thickness will most likely be determined by the thickness of the original fine silver layer on the object and the alloy composition.

Keywords: Silver, silversulphide, delamination

1. Introduction

Tarnishing of silver is a problem encountered in many museums throughout the world. Different preventive and active conservation strategies have been developed to minimise tarnish films growth on historic silver objects, varying from lacquering to packing in polymer films. However, some people believe that tarnish films provide protection against further damage. This, in itself, is partly true. If the increase of weight of silver (or the silver sulphide layer thickness) for the reaction between silver and low concentrations of hydrogen sulphide, is plotted against the reaction time, a square root relation is obtained (Abbott 1974). This means that the reaction rate decreases when the silver sulphide thickness increases. This can be explained by diffusion of H_2S through the tarnish film, which becomes more difficult when the layer thickness grows. If silver is reacted with a mixture of H_2S and NO_2 a linear relation is obtained (Ishino, Kishimoto et al. 1980). In both cases a more or less infinite growth of tarnish films is expected, but never observed.
The morphology of silver sulphide films has not been studied extensively. Attention is focussed on silver sulphide layers formed at high pollutant concentrations, typically at ppm levels resulting in different types of crystals (Drott 1959; Drott 1960; Fischmeister and Drott 1959; Keil and Meyer 1960).

Corresponding author: TEL: +31206747233 or +31203054662, robert.van.langh@icn.nl

Although the composition of tarnish films formed in the museum environment has been studied, the morphology of those films formed at ambient H_2S concentrations (ppt levels) has not been studied in detail.
The Rijksmuseum owns a '*Schauplatten*' (showplate) which shows the school of Athens[1] surrounded by busts of Poluxena, Zenopha, Sapho and Lucretia, and Music, expressed by eight muses playing various musical instruments. In some parts a clear delaminating tarnish layer is visible. The examination of the silver sulphide delaminating was aimed at the following issues:

- What is the composition and morphology of the tarnish layer?
- What is the typical thickness at which silver sulphide delaminates?

2. Experimental

The surface of the showplate has been examined by Leica optical microscopy using low magnification (typically 15x). Samples could easily be collected by removal of the already detached layers or by applying sticky tape directly on the tarnish surface. Cross sections were prepared according to techniques recommended by Struers™ [2]. The sections were embedded in epoxy resin, ground using waterproof paper (finish with 4000 grit), and polished with 6 and subsequently with 1 μm diamond spray.

The cross sections were examined using a JEOL- JSM 5910-LV scanning electron microscope (SEM) with a Vantage Thermo Noran energy dispersive spectroscopy (EDS) system at high vacuum and typically 20 kV accelerating voltage. Elemental mapping and analyses were conducted using EDS.

3. Results and Discussion

The plate has been in the possession of the Rijksmuseum Amsterdam since 1878. After many years in storage, the surface of the showplate is now covered by a thick black tarnish layer. This is assumed to be mainly silver sulphide (Figure 1A). As can be seen, this layer delaminates at certain places from the metal surface. At places where the silver sulphide is not present the metallic silver surface is observed (Figure 1B). On the revealed silver, new tarnish has been formed at places that were easily reached by H_2S when the tarnish was still present on the surface, *i.e.* the cracks in the Ag_2S. The black lines on the metallic silver in Figure 1B show the outline of the cracks in the original silver sulphide layer.

Figure 1A: Detail of the surface of the showplate showing the thick tarnish layer with delaminating flakes.

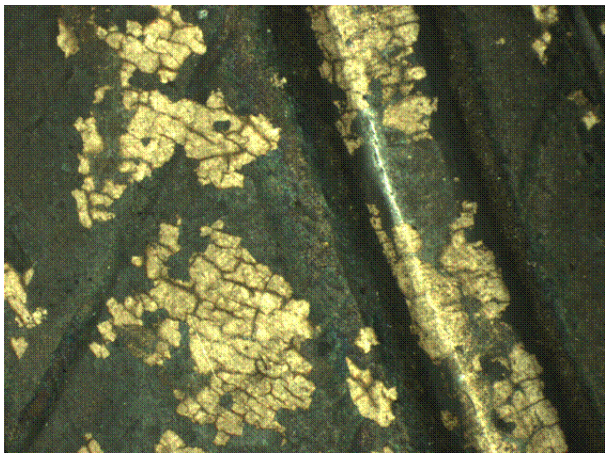

Figure 1B: Detail of 1A, showing the outline of the cracks in the original sulphide layer.

[1] The depiction is described as the School of Athens

[2] Instructions followed given through Struers (www.struers.com), abrasive grinding to 4000 grit, afterwards diamond polishing with 6 and 1 μm

Taking samples looked easy enough at first instance. Silver sulphide flakes could be removed by sticky tape. However, embedded cross sections of these, showed great disruption of the tarnish layer. One result of this way of sampling was that the boundary at which the silver sulphide flakes from the base could be analysed, showing only the presence of silver and sulphur without any copper.
Samples were also taken by cutting a small section out of the rim of the object, leaving the tarnish layer still adhered to the metal surface. Polished cross sections of these samples were studied by SEM with EDS. The silver sulphide layer which seemed attached to the silver during mounting was in fact already detached. At low magnification it can be seen that at full length of the cross section the tarnish layer is not fully adhered to the metal surface. At higher magnification three different layers can be observed in the cross section (see Figure 2), *i)* the original alloy at the bottom, *ii)* with a dark layer on top and finally *iii)* a light grey stratified layer.

Figure 2: Back scattered image, silver, copper and sulphur mappings of the cross section.

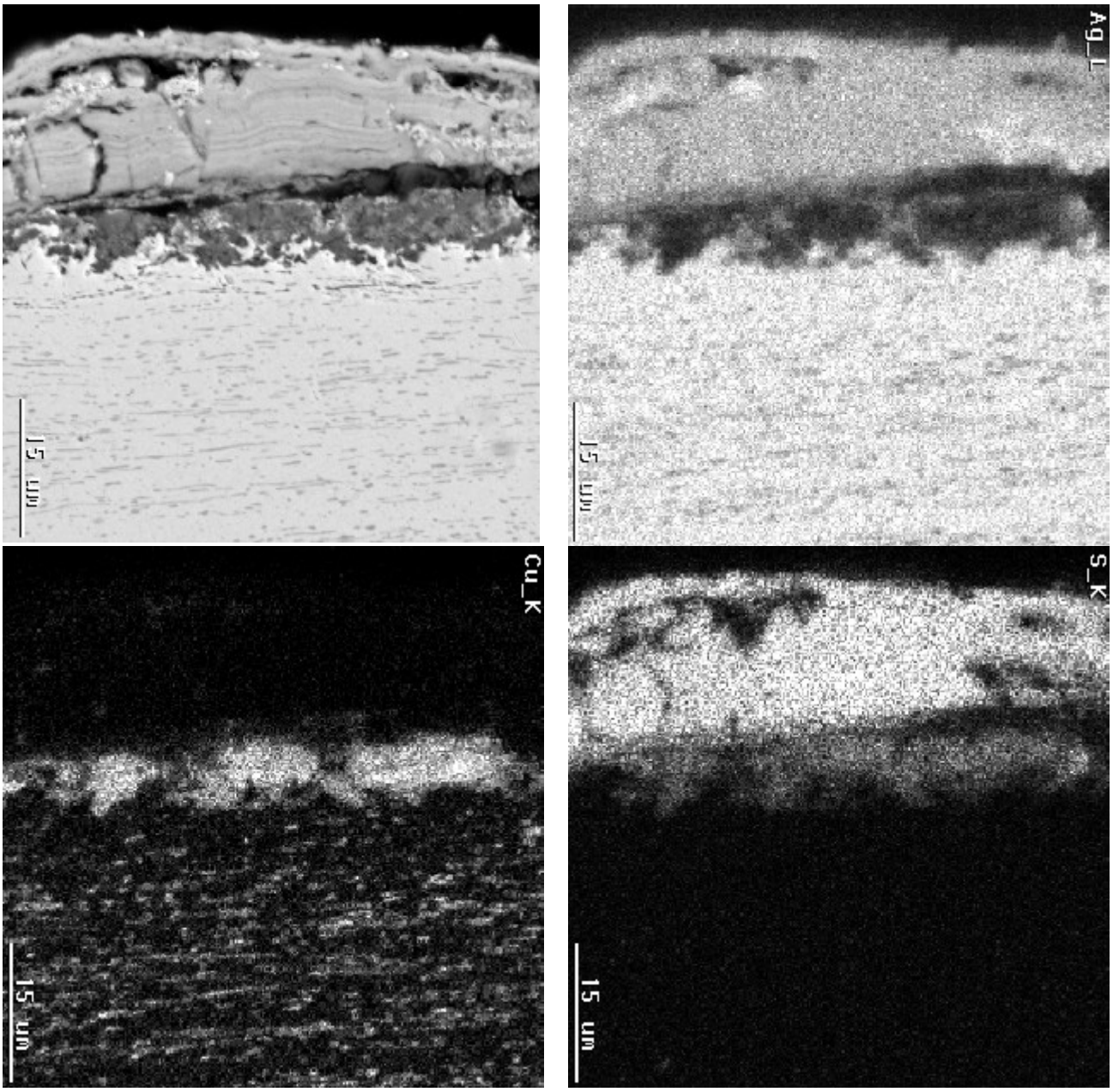

Figure 3: Backscatter electron image and line scan of tarnish layer.

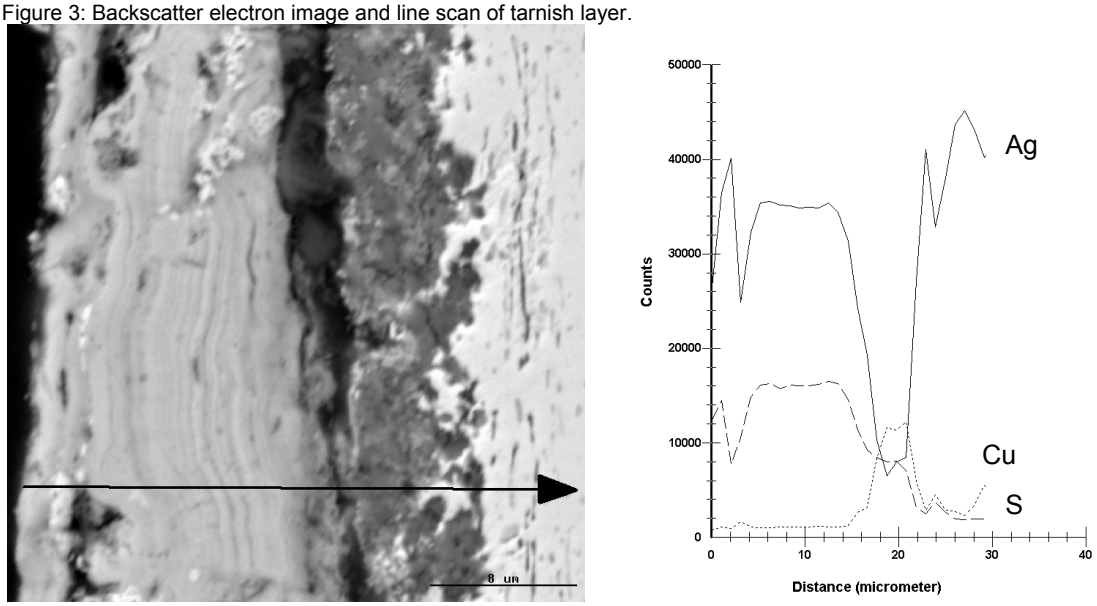

The original alloy shows elongated copper particles within the silver matrix, indicating a milled metal. When this showplate came into the possession of the Rijksmuseum in 1878, it was accompanied by 571 other objects given through the bequest of F.G.S. Baron van Brakell tot den Brakell. This showplate was mentioned as being 'new' and therefore was considered to be manufactured in the 19th century. In the beginning of this research it was even thought that it could be an electrotype of the original of a 17th century showplate[3] which is owned by the Royal Museum for Art and History (Brussels). Thus far metal milling was supposed to have only taken place from the late 17th century onwards, yet already in 1551, King Henry II had bought a rolling mill for the mechanisation of coin striking in Augsburg (Jacobi 1982). Therefore this technique must have been already available during the 16th century in Germany. It should be noted that the size of the plate being 85 by 75 cm still requires further research, because it is surprising that objects of these dimensions could be manufactured with a rolling mill.

The second layer is rather heterogeneous; showing the presence of conglomerated particles (dark grey in the back scatter image of Figure 3), islands of metallic silver (white phase in the back scatter image of Figure 3), possibly metallic copper (black particles in the back scatter image of Figure 3) and the absence of cracks. The line scan indicates the presence of copper and sulphide, which is supported by the mapping presented in Figure 2. The presence of silver and / or silver sulphide made it impossible to determine the copper / sulphur ratio accurately; it is assumed that CuS is most likely formed (Scott 2002). The metallic silver islands are concentrated near the alloy. Nearer the top all silver has leached out and has been transformed into Ag_2S. The copper enrichment of this layer is remarkable. One might have expected the presence of remnant elongated copper particles (or copper sulphide particles) within the silver sulphide layer (see below for detailed description), which is not the case. The compositional separation of these two corrosion layers, *i.e.* silver sulphide and copper sulphide is not fully understood.

The top layer, being the silver sulphide shows a layered structure with cracks running alongside the original surface and perpendicular to it. Inside this layer several cavities and island of metallic silver can be seen (Figure 2). The thickness of the stratified Ag_2S layer varied from 3.7 to 16.3 µm, but typically a thickness of approximately 14 µm was observed. The thickness of the layers that make the stratification varies from approximately 200 – 1250 nm, giving an average amount of 15 relatively thin Ag_2S layers (see also the back scatter images in Figures 2 and 3). It should be noted that a Ag_2S layer thickness of 140 Å (0.014 nm) appears yellow, while a black tarnish layer is approximately 1400 Å (140 nm) thick (Ankersmit, Doménech Carbó et al. in press).The contrast in the back scatter image within the silver sulphide layer is the result of differences in composition and / or density. Unfortunately the composition of the very thin dark grey lines in between the Ag_2S layers could not be analysed by SEM-EDS. The formation of these layers is not fully understood. However, changing environmental conditions might explain this phenomenon.

[3] Showplate with apotheoses of the arts en sciences, Hans Jakob Mair, 1674, partially gilded silver, Royal Museum for Arts and History, Inv nr. 25 II

The cracks running perpendicular to the metal surface are most likely caused by brittleness of the Ag_2S layer, combined with differences in crystal orientations and / or shrinkage and volume increase effects related to changing environmental conditions. The cracks running in between the copper sulphide and silver sulphide are most likely the result of differences in crystal packing.
The build up of the overall layers, *i.e.* Ag_2S / CuS / Ag-Cu, differs from what one would expect. Usually, historic silver objects contain a fine silver layer on top of the alloy. This enriched silver layer (approximately 10 µm thick after three times annealing and pickling) is formed by dissolving oxidised copper particles that are formed by annealing the object in vitriol (a diluted H_2SO_4 solution or tartaric acid). Tarnishing will result in a Ag_2S layer on a fine silver layer. In this case apparently all the fine silver has been consumed.

4. Conclusions

Tarnishing of silver is an ongoing process. At first the rate of tarnishing will slowly decrease in time, caused by the diffusion of H_2S that becomes more difficult through a growing tarnish layer. Long exposure of the silver showplate to ambient concentrations of gaseous sulphides resulted in the formation of a thick silver sulphide on top of a copper sulphide layer which is directly bound on the alloy. The Ag_2S layer is stratified. The underlying copper sulphide is heterogeneous. Apparently the overall tarnish layer cannot grow to an infinite thickness. At a certain point the layer flakes from the surface. It breaks in between the silver sulphide and the copper sulphide. The maximum silver sulphide thickness will most likely be determined by the overall presence of silver, *i.e.* the thickness of the original fine silver layer on the object and the alloy composition.

References

Abbott, W.H., (1974). *Effects of Industrial Air pollutants on Electrical Contact Materials*. *IEEE* Transactions on Parts, Hybrids, and Packaging **PHP-10**, 24-27
.
Ankersmit, H.A., Doménech Carbó, A., Tennent, N.H., (in press). *Tarnishing of silver: evaluation by colour measurements*. In 'ICOM-Metal'. Santiago Chile. (Ed. I, MacCleod)

Drott, J., (1959). *Reaction rate and growth forms in the reaction between silver and hydrogen sulfide.* I. The influence of water vapor pressure. *Arkiv for Kemi* **15**, 181-194
.
Drott, J., (1960) *Growth of silver sulphide whiskers*. *Acta Metallurgica* **8**, 19-22.

Fischmeister, H., Drott, J., (1959). *Reaction rate and growth forms of reaction product in the system Ag-H2S*. Acta Metallurgica **7**, 777-781.

Ishino, M., Kishimoto, M., Matsui, K., Mitani, S., (1980). *Effect of Gas Flow Velocity on tarnish Kenetics of Contact Materials*. IEEE Transactions on Components, Hybrids, and Manufactoring Technology **CHMT-3**, 63-66.

Jacobi, H.W., (1982). *De mechanisatie van het Zeeuwse muntbedrijf in 1671*. Mededelingen van het Koninklijk Zeeuwsch Genootschap der Wetenschappen, 150-175
.
Keil, A., Meyer, C-L., (1960). *Kristallwachstum bei Schwefeleinwirkung auf Silber und beim Zerfall von Silbersulfid*. Zeitschrift für Metallkunde **51**, 253-255.

Scott, D., (2002). *Copper and Bronze in Art, corrosion, colorants, conservation*. (Getty Conservation Institute)

Some news about 'Black Spots'

G. Eggert[*] [a], M. Weichert [b], H. Euler [c], B. Barbier [c]

[a] Staatl. Akademie der Bildenden Künste, Am Weißenhof 1, D-70191 Stuttgart, Germany
[b] Brandenburgisches LA für Denkmalpflege und archäol. Landesmuseum, Wünsdorfer Platz 4-5, D-15838 Wünsdorf, Germany
[c] Mineralogisch-Petrologisches Institut und Museum der Universität Bonn, Poppelsdorfer Schloss, D-53115 Bonn, Germany

Abstract

'Black spots', i.e. copper and sulphur containing efflorescences occuring during display or storage, can grow on any material which contains copper when exposed to reduced sulphur gases like hydrogen sulphide, carbonyl sulphide, and elemental sulphur. Besides mineral collections, sulphur may occur in finds from anaerobic sites directly or as a pyrite oxidation product (e.g. in wood or marine crusts), gunpowder, ancient gold hollow objects, cements, and some brands of plasticine.
While some of the black spots could be identified by X-ray diffraction as crystalline copper sulphides various (basic) copper sulphates were also found. Others are apparently X-ray amorphous, their nature needs further research with other analytical methods.

Keywords: (air) pollutants, black spots, copper sulphide, copper sulphate, (elemental) sulphur

1. Introduction

Helge Brinch Madsen (1977) was the first to note small 'black spots on bronzes' (BSoBs) consisting of copper sulphide in many major European museums and to report on them at conservation conferences in Germany (1978), Scotland (Brinch Madsen and Hjelm-Hansen 1979), and the USA (Brinch Madsen and Hjelm-Hansen 1982). It is now widely accepted that the source of sulphur reacting with copper lies within inappropriate storage and display materials (Oddy and Meeks 1982). Surprisingly, despite the frequent occurence of this phenomenon and the routine testing of display materials, only in two cases has a definite culprit been identified so far: a carpet covering the floor of a case which was woven from a mixture of nylon and wool fibres and backed with rubber (Sease 1994), and rubber bands used for packaging (Moraitou 1995). It is now clear that one has also to look at other artefacts on display as possible sources of pollutants. Besides woolen textiles (Sease 1994), a low fired ceramic vessel from an anaerobic waterlogged site (Green 1992) has been found to emit sulphurous gases. In this case hydrogen sulphide was suspected. Eggert and Sobottka-Braun (1999) showed that the sublimation of elemental sulphur has to be considered as well.

This paper will
1) update information on the corrosiveness of elemental sulphur via the gas phase
2) take a closer look on what materials BSoBs spots can grow, and
3) review the chemical nature of BSoBs.

2. Sulphur, the 'enemy of copper'

According to one theory, the word sulphur 'is derived from Sanskrit *shulbari*, meaning “enemy (*ari*) of copper (*shulba*)“' (Vira 1950). If true this would indicate a deep knowledge of chemistry which is relevant to our modern understanding of efflorescences occurring on copper containing materials in the museum and elsewhere. Sulphur has a low but measurable vapour pressure (1 ppb at 20 °C, 200 ppb at 60 °C). Under the conditions of the standard Oddy test for display materials (60 °C, 100 % relative humidity (rH)) copper coupons are visibly attacked within hours by vapours from flowers of sulphur (Eggert and Sobottka-Braun 1999). In mineral collections specimens are normally grouped according to the mineralogical system; therefore, the naturally occurring elements sulphur and copper are often displayed in the same case. To assess possible dangers of this practice, sulphur crystals from Sicily were stored in small boxes (0.225 dm³) at room temperature together with copper nuggets from Michigan in the dark (Figure 1). At 100 % rH, the first black needles growing on copper

[*] Corresponding author: TEL:+49 711 28440-217: FAX: -225: email: gerhard.eggert@abk-stuttgart.de

Figure 1 Copper nuggets, stored with sulphur crystals (middle), additional water (=100 % rH, left) and blank experiment (no sulphur, right) in polystyrene boxes, after one year.

could be observed microscopically after three days. At ambient rH it took considerably more time, although after one year the test nugget was covered with needles as well. In a display case at the University of Stuttgart collection (see below) one (out of 3) nuggets showed some BSoBs on close inspection. In consequence, sulphur should be exhibited only seperately from metals. The reason why up to now, no case of black spots on native copper displayed together with sulphur could seen in other mineralogical museums and why the two other nuggets were unaffected, is not fully understood.

While the danger by sulphur crystals is now obvious elemental sulphur might also occur hidden in artefacts. Waterlogged wood from the Mahdia shipwreck was shown to cause black spots on a modern test bronze wire on long term storage (Eggert and Sobottka-Braun 1999). EDX -SEM showed that it contained sulphur (2 $\%_{w/w}$) but no matching metal cations. Apparently it must contain elemental sulphur although XRD and extraction with pyridine could not detect it in the analysed sample. At that time, only one case where elemental sulphur was identified in wood has been reported (MacLeod and Kenna 1991): the Batavia shipwreck where it was formed as an intermediate product of pyrite (FeS_2) oxidation. Now the Vasa has been shown to contain between 0.2 and 6 $\%_{w/w}$ total sulphur in the outermost 2 cm of the wood (Sandström et al. 2002). Tonnes of elemental sulphur still left in the vessel endanger the wood by their oxidation to sulphuric acid. Marine calcium carbonate crusts on metals from similar anaerobic sites were already known to contain elemental sulphur (North and MacLeod 1987: 78, 82). Some of such crusts from the Mahdia bronzes showed black spots. If marine crusts contain reduced forms of sulphur (easily checked by the iodine/azide test, Lee and Thickett 1996: 22f.) this is an argument for removing them from copper alloys.

Some other artefacts may contain sulphur as well:
- Gunpowder may affect objects in contact or in the vicinity (Weichert et al. 2004).
- Ancient gold thin hollow objects were often filled with molten sulphur as cement for embossing and protection against mechanical damage (Eggert, Kutzke, and Wagner 1999). One ring contained BSoBs (copper cations most likely from the debased alloy or a copper wire inside) on a sulphur globule.
- Historical recipes for cements or fillers sometimes contain sulphur as an ingredient. Such a cement caused severe three dimensional silver corrosion inside a baroque game board (Hustedt-Martens 2003). Ivory-coloured inlays in Pennsylvania German furniture can consist of sulphur as well (Mass and Anderson 2003).

Another danger in display, unsuspected by most conservators (Eggert 2004), is posed by the use of ‘plasticine’ for moulding or quick mounting of metal objects. Some brands contain large amounts of elemental sulphur which, by the way, made them useful for repatinating overcleaned bronze objects (Plenderleith and Werner 1971: 261). Black spots have been found on minerals (chalcocite, Ramdohr 1980: 444), metallographic copper alloy samples (Scott 2002: 396), and a mediaeval fibula (Eggert 2004), all mounted for some time with a sulphur-containing modeling clay. Commercial brands can easily be tested for their content of elemental sulphur: gently heat a sample in a reagent tube and test the fumes with a wetted lead acetate paper (Eggert 2004). Those types containing sulphur should principally not be used in conservation departments.

To protect copper-containing objects from their 'enemy', sulphur, they should not be displayed in closed cases together with sulphur emitting substances, be they display materials or artefacts. If this is not possible (e.g. in the case of the game board where brass and cement are part of the same object), ventilation and absorbents have to be used.

3. Where do 'black spots' grow?

'Black spots on bronzes' seem to occur on all materials containing copper. Brinch Madsen found them on archaeological bronzes where they left pits in the metal beneath. Hjelm-Hansen (1984) listed cases of coated (gilding, tinning, lacquer, PVC insulation) modern copper alloys from the technical literature developing black spots. Here the spotty pattern correlates with the pores of the coating. Eggert and Sobottka-Braun (1999) reported black spots in a showcase with waterlogged wood, both on ancient bronzes and uncoated modern display materials (a copper nail and a bronze wire). Obviously, black spots can occur independent of the objects' origin, no matter if coated or not. They can also easily be grown in the laboratory. What matters are only the environmental conditions (concentration and nature of pollutant, rH, T).

Even alloys with low copper content like pewter can be affected (Weichert 2004). Small particles of finely divided copper alloy particles in paper (Daniels and Meeks 1994) react as well. A form of atmospheric copper sulphide corrosion of small inclusions has even been reported from gold coins (Linke et al.1999).

Nevertheless, the formation of black spots is not restricted to metals. Previously, Oddy and Meeks (1982) presented a case of black spots growing on corrosion products (copper carbonate and cuprous chloride). Copper minerals are often chemically identical to copper corrosion products; it is, therefore, no wonder that they also can be affected by sulphurous gases (Howie 1992), e.g. emitted by sulphur or unstable sulphide minerals, and develop black spots as well. Eggert and Sobottka-Braun (1999) described black spots occurring also on copper sulphide specimens (chalcocite, Cu_2S, and covellite, CuS). Because covellite already contains the maximum stoichiometric amount of sulphur, the latter case might even be independent of the presence of pollutant gases. To get an idea of the frequency of 'black spots' on minerals the collection of the University of Stuttgart was surveyed (Weichert 2002). In a display case with crystalline sulphur bornite (Cu_5FeS_4), chalcocite (Cu_2S), algodonite (Cu_6As), domeykite (Cu_3As), and one out of three copper nuggets showed 3-dimensional efflorescences (not only flat tarnish). In another display case without elemental sulphur covellite (CuS) was affected. All alteration products gave a medium to strong reaction with iodine/azide (i.e. contain a form of reduced sulphur). Only the efflorescence on bornite (Figure 2, digenite, Cu_9S_5) could be identified by X-ray diffraction (XRD).

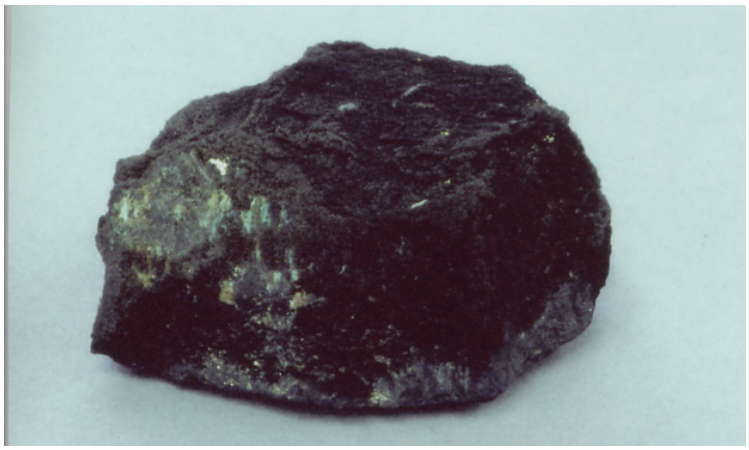

Figure2 Bornite, Cu_5FeS_4, with fuzzy tarnish of digenite, Cu_9S_5.

To further study the sensitivity of copper minerals (Howie 1992) samples of cuprite (Cu_2O), chalcocite (Cu_2S), covellite (CuS), and malachite (polished, gemstone quality) were exposed to 4 ppm hydrogen sulphide (prepared by exposing aluminum sulphide, Al_2S_3, to 100 % rH, Hjelm-Hansen 1984) over three months (Weichert 2002). All developed 'black spots'. Those of cuprite and chalcocite were analysed by XRD, covellite was found in both cases.

Copper minerals are no exception to the formation of 'black spots'; observations and descriptions in the mineralogical literature might help to further elucidate the phenomenon.

4. What are 'black spots' really?

Common conservation wisdom has it that BSoBs consist of copper sulphides. They are normally analysed by X-ray diffraction, a method which is sensitive to crystalline phases only. The first reported black spots were thus found to consist of covellite (CuS, Brinch Madsen 1977/8). Lee and Thickett (1996) reported also brown digenite (Cu_9S_5) and black chalcocite (Cu_2S). Other copper sulphide phases (see Scott 2002: 227 for a full list) could also be identified (Lee 1996) but may be difficult to distinguish in small, poorly crystalline samples.

The Pourbaix predominance area diagram for the system Cu-S (Figure 3) created with Poigdomenech's (2004) MEDUSA software shows that sulphates (depending on the pH which is decreased in the environment to slightly acid values (below the neutral pH 7, dashed line) by the presence of CO_2, SO_2, and NO_x in the air: chalcanthite $CuSO_4 \cdot 5H_2O$, antlerite $Cu_3SO_4(OH)_4$, brochantite $Cu_4SO_4(OH)_6$) are the only thermodynamically stable sulphur form in presence of air (upper region). The oxidation of sulphides to sulphates is therefore favoured.

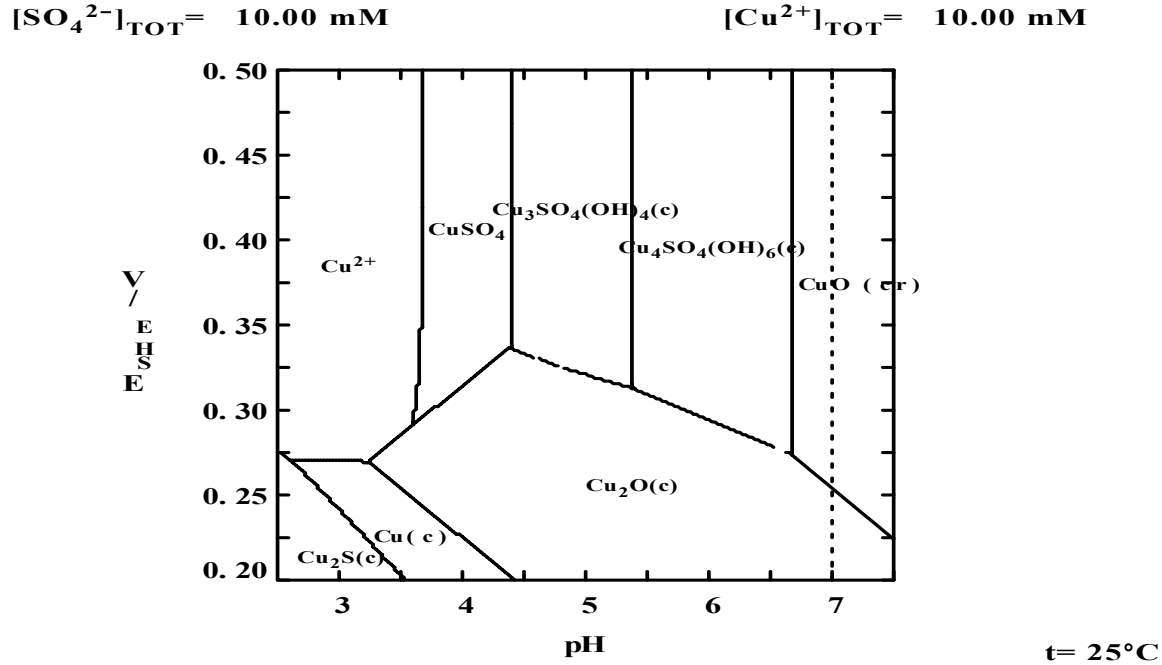

Figure 3 Pourbaix diagram showing predominant phases in the Cu-S-system (MEDUSA software, Poigdomenech 2004)

This is in accordance with the following observations:
- Freshly precipitated CuS shows oxidation to sulphate after 30 days (Babkin 1947).
- Hjelm-Hansen (1984) found covellite and brochantite in artificially grown black spots.
- Duncan and Ganiaris (1987) exposed bronze finds with golden or black sulphide patina to 80 % rH. After one week first changes were observed, after five weeks all patinas have changed. Green oxidation products were found to be the sulphates antlerite and guildite ($CuFe(SO_4)_2(OH) \cdot 4H_2O$). The amount of water might be crucial for the formation of sulphates. Steger and Desjardins (1980) exposed mineral chalcocite Cu_2S to 52 °C and 68 % rH for five weeks and found CuO and CuS, but no sulphates.
- Eggert, Kutzke, and Wagner (1999) analysed covellite and chalcanthite on BSoBs on sulphur inside a hollow gold ring.
- Twilley found primarily chalcanthite in the whiskerlike growth on metallographic sections stored on plasticine-mounted glass slides (Scott 2002: 396).
- Scott (2002: 233f.) reports namuwite, a zinc substituted brochantite in 'black spots' on brass objects.
- Weichert (2002) could replicate Hjelm-Hansen's finding of covellite and brochantite in laboratory tests on tin bronze and leaded tin bronze, but not on copper. On brass, schulenbergite $(Cu,Zn)_7(SO_4)_2(OH)_{10} \cdot 3H_2O$ was identified. All these sulphates grown in the lab formed a compact layer, no loose 'black spot' morphology. Antlerite was found in 'black spots' on a brass nail from a wooden shield (MR 82 A 2954) of the *Mary Rose*.

Clearly, some BSoBs contain copper sulphate phases. Besides attack by sulphur dioxide air pollution, the oxidation of sulphides as primary corrion products caused by reduced sulphurous gases is another reaction route to copper sulphates (schematically: $CuS + 2O_2 \rightarrow CuSO_4$). Therefore, the presence of copper sulphates alone can no longer be taken as sufficient proof for corrosion by acidic air pollution as has been done formerly, e.g. in the namuwite case. On the other hand, a negative iodine/azide test (i.e., no sulphide present) cannot totally rule out the occurrence of a BSoBs type process because initial sulphide might have totally reacted to oxidation products.

Many samples of BSoBs analysed by X-ray diffraction (XRD) showed no or nearly no signals (Figure 4) despite optimisation of the signal to noise ratio by long time measurements and computer processing of the data. Apparently, some of the black spot material is not crystalline. That BSoBs can be amorphous has been observed before (Daniels and Meeks 1994, Lee 1996) and, from our experience, seems not to be a rare phenomenon. Now knowing that oxidation can occur one cannot automatically assume that these compounds are amorphous sulphides. They might contain (non-stoichiometrically?) more or less oxygen atoms; Howie (1992: 58)

postulated (meta)-stable sulphide-oxygen-(hydroxyl)-complexes for the tarnish developing on sulphide minerals in air. Other methods (e.g. XANES or EXAFS) which can give information on the chemical surrounding of the sulphur atom are needed to get a full picture of what compounds can all hide behind the phenomenological term 'black spots'; first results are promising (Hahn 2004).

When dealing with XRD (only crystalline phases) and EDX-SEM (low sensitivity for light elements like O) analyses of BSoBs in the literature it must be kept in mind that they might show only part of the picture.

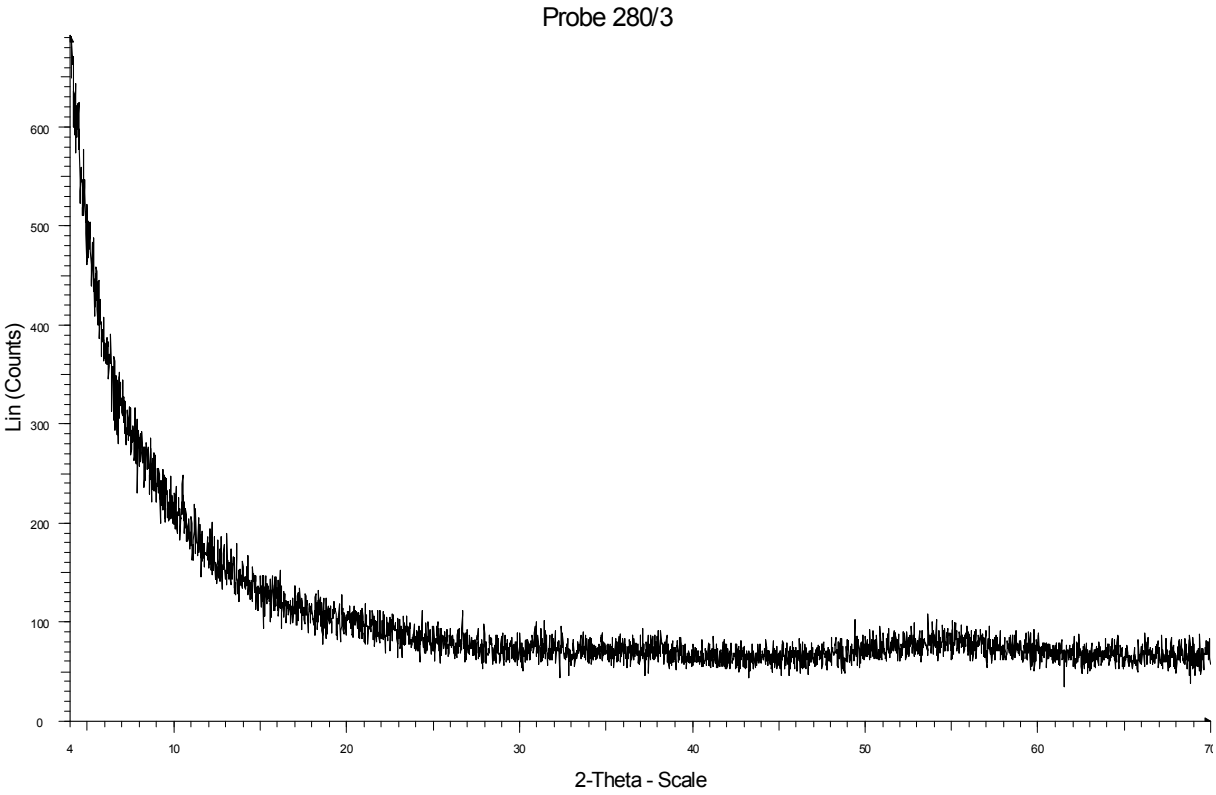

Figure 4 Powder diffractogram of X-ray amorphous ‘black spots’ from a bronze neckring, Landshut A280/3, ($4° \leq 2\theta \leq 70°$; step width 0.02°, step time 15 s, Cu radiation, Siemens D5000)

5. Summary and Conclusion

'Black spots' can occur on every material which contains copper independent of its age or previous history: metal alloys, corrosion products, minerals, and semi-precious stones all develop them when exposed to reduced sulphur gases like hydrogen sulphide, carbonyl sulphide, and elemental sulphur. Apart from mineral collections, sulphur may occur in finds from anaerobic sites directly or as a pyrite oxidation product (e.g. in wood or marine crusts). Gunpowder, ancient gold hollow objects, cements, and plasticine may contain sulphur as well. While some of the black spots could be identified as crystalline copper sulphides and others as copper sulphates, their oxidation product, others are amorphous. Their stoichiometry, including the question of if and how many oxygen atoms they contain besides copper and sulphur, needs further research., but clearly there is no general chemical formula for BSoBs.

In hindsight, the term 'Black spots on Bronzes' now used universally is not an optimal one, as it might be misleading. BSoBs are not always black: brown and other colours have been described. The term 'spot' might lead to the notion of a flat 2-dimensional phenomenon, while instead BSoBs grow 3-dimensionally like 'trees', 'bunches', or 'cauliflower' (Weichert 2004). Their occurrence is not restricted to bronzes (i.e. copper alloys), but to anything which contains copper. Therefore, the term 'Black Spots on Bronzes' should be used only in quotation marks or abbreviated form (BSoBs) or be replaced. ‘Copper-Sulphur-Efflorescence (Cu-S-F)’ might be an alternative which better represents today's knowledge.

Acknowledgements

Prof. Keller made the survey of the mineralogical collection of the University of Stuttgart possible and discussed many mineralogical questions with us.

References

Babkin, M.P. (1947) *Oxidizability of sulfides*, Zhur. Anal. Khim. 2, 118-121 (cited from CA 43(1949)5700i).

Brinch Madsen, H. (1977) *Mikrobiologisk angreb på bronzerne fra Budsene brønden*, Meddelelser om konservering **2**(9), 265-270.

Brinch Madsen, H. (1978) *Schwarze Flecken auf Bronzen*, Arbeitsblätter, **11** (Gr.2), 96-102.

Brinch Madsen, H., and Hjelm-Hansen, N. (1979) *Black spots on bronzes – a microbiogical or chemical attack*, In SSCR (ed.), The conservation and restoration of metals, p. 33-39, SSCR, Edinburgh, UK.

Brinch Madsen, H., and Hjelm-Hansen, N. (1982) *A note on black spots on bronzes*, in Brommelle, N.S., and Thomson, G. (ed.). Science and technology in the service of conservation, p. 125, IIC, London, UK.

Daniels, V.D., and Meeks, N.D. (1994) *Foxing caused by copper alloy inclusions in paper*, in Burgess, H.D. (ed.), Proceedings of Symposium 88 – Conservation of Historic and Artistic Works on Paper, p. 229-233, CCI, Ottawa, Canada.

Duncan, S.J., and Ganiaris, H., (1987) *Some sulphide corrosion products on copper alloys and lead alloys from London waterfront sites,* in Black, J., (ed.), Recent advances in the conservation and analysis of artefacts, Institute of Archaeology, Summer Schools Press, London, UK, 109-118

Eggert, G. (2004) *Another unsuspected danger in display causing black spots on bronzes*, in Ogden, J. (ed.), Postprints Exposure 2001 (Hildesheim), accepted for publication

Eggert, G., Kutzke, H., and Wagner, G. (1999) *The use of sulphur in hollow ancient gold objects*, J. Archaeol. Science **26**, 1089-92.

Eggert, G., and Sobottka-Braun, U. (1999) *Black spots on bronzes and elemental sulphur*, in ICOM-CC, 12th Triennial Meeting Lyon 29 August-3 September 1999, p. 823-827, James & James, London, UK.

Green, L.R. (1992) *Low fired ceramics and H_2S*, Museums Journal Nov. 1992, 36.

Hahn, O. (2004), BAM Berlin, private communication to G.Eggert, 29 June 2004.

Hjelm-Hansen, N. (1984) *Cleaning and stabilization of sulphide-corroded bronzes*, Studies in Cons. **29**, 17-20.

Howie, F. M. (1992) *Sulphides and allied minerals in collections*, in Howie, F.M. (ed.) The Care and Conservation of Geological Material: Minerals, Rocks, Meteorites and Lunar Finds, p.56-69, Butterworth & Heinemann, Oxford, UK.

Hustedt-Mertens, E. (2003) *Technologische Untersuchung und Restaurierung eines Brettspielkastens des 17. Jhdts*., unpublished diploma thesis, State Academy of Art and Design, Stuttgart, Germany.

Lee, L.R. (1996) *Investigation into the occurrence of 'black spot' corrosion on copper alloy objects*, internal report 1996/16 of the Conservation Research Group, British Museum, London, UK.

Lee, L.R., and Thickett, D. (1996) *Selection of materials for the storage or display of museum objects*, British Museum Occ. Paper **111**, London, UK.

Linke, R., Schreiner, M., Denk, R., and Traum, R. (1999) *Rostet Gold? Untersuchungen an „korrodierten" Goldmünzen des Wiener Münzkabinetts*, Numismat. Z. **106/7**, 173-179.

MacLeod, I.D., and Kenna, C. (1991) *Degradation of archaeological timbers by pyrite: oxidation of iron and sulphur species*, in Hoffmann, P. (ed.) Proceedings of the 4th ICOM-Group on wet organic archaeological materials conference, p. 133-141, Deutsches Schiffahrtsmuseum, Bremerhaven, Germany.

Mass, J.L., and Anderson, M.J. (2003) *Pennsylvania German sulfur-inlaid furniture: characterization, reproduction, and ageing phenomena of the inlays*, Meas. Sci. Technol. **14**, 1598-1607.

Moiraitou, G. (1995) *Mayra stigmata se chalkina antikeimena toy Moyseioy Herakleioy*, Archaiologika Analecta ex Athinon **22**(1989), 183-188.

North, N.A., and MacLeod, I.D. (1987) *Corrosion of metals*, in Pearson, C. (ed.), Conservation of marine archaeological finds, p. 68-98, Butterworths, London, UK.

Oddy, W.A., and Meeks, N.D. (1982). *Unusual phenomena in the corrosion of ancient bronzes*, in Brommelle, N.S., and Thomson, G. (ed.). Science and technology in the service of conservation, p. 119-124, IIC, London, UK.

Plenderleith, H.J., and Werner, A.E.A. (1971) *The conservation of antiquities and works of art: treatment, repair, restoration*, 2nd ed., Oxford University Press, London, UK.

Poigdomenech, I. (2004) *MEDUSA chemical equilibrium software*, downloaded from http://w1.156.telia.com/%7Eu15651596/ (12 June 2004).

Ramdohr, P. (1980) *The ore minerals and their intergrowths*, vol. 2, 2nd ed., Pergamon, Oxford, UK.

Sandström, M., Jalilehvand, F., Persson, I., Fors, Y., Damian, E., Gelius, U., Hall-Roth, I., Dal, L., Richards, V.L., and Godfrey, I. (2002) *The sulphur threat to marine archaeological artefacts: acid and iron removal from the Vasa*, in Townsend, J.H., Eremin, K., and Adriaens, A. (ed.), Conservation Science 2002, p. 79-87, Archetype, London, UK.

Scott, D.A. (2002) *Copper and bronze in art: corrosion, colorants, conservation*, Getty Conservation Institute, LA, USA.

Sease, C. (1994) *The cases of the black fuzzies*, in SSCR (ed.), Exhibitions and Conservation, p. 125-130, SSCR, Edinburgh, UK

Steger, H.F., Desjardins, L.E. (1980) *Oxidation of sulfide minerals. V. Galena, sphalerite and chalcocite*, Canadian Mineralogist **18**, 365-372.

Weichert, M. (2002) *Büschel, Bäumchen, Blumenkohl – Durch Schwefel und reduzierte Schwefelverbindungen hervorgerufene Ausblühungen auf Kupfer, kupferhaltigen Legierungen und Kupfermineralien*, unpublished diploma thesis, State Academy of Art and Design, Stuttgart, UK.

Weichert, M., Eggert, G., Jones, M., Ankersmit, H. (2004). *Trees, bunches, cauliflower – A closer look at sulphurous corrosion on copper alloys ('black spots')*, this volume.

Vira,R. (1950) *Elementary English-Indian dictionary of scientific terms,* Chandra, Nagpur, India (cited from Patterson, A.M. (1953) *Origin of "Sulphur"*, CAEN **31**, 3681.).

ABN 70 592 297 967

Trees, bunches, cauliflowers – A closer look at sulphurous corrosion on copper alloys and minerals ('Black Spots')

M. Weichert[*] [a], G. Eggert [b], A.Mark. Jones [c], H.A. Ankersmit [d]

[a] Brandenburgisches Landesamt für Denkmalpflege und Archäologisches Landesmuseum, Wünsdorfer Platz 4-5 15838 Wünsdorf, Germany
[b] State Academy of Art and Design, Stuttgart, Object Conservation, Am Weißenhof 1, 70191 Stuttgart, Germany
[c] The Mary Rose Trust, College Road, HM Naval Base, Portsmouth PO1 3LX, UK
[d] Netherlands Centre for Cultural Heritage (ICN), Gabriël Metsustraat 8, 1070 KA Amsterdam, The Netherlands

---

Abstract

'Black spots', a sulphurous copper corrosion, is not only occurring on museum objects composed of copper or copper alloys, but also on pewter and copper minerals. Severe damage such as pitting of the surface may result.

The corrosion products are not exclusively sulphidic, as previously expected, but may also contain sulphates and amorphous phases which are not yet fully investigated.

New forms of 'black spots' were discovered, showing various colours and structures, such as dendritic tufts, or a cauliflower-like appearance.

The only successful long-term strategy to avoid the development of 'black spots' on museum objects is to take preventive measures.

Résumé

Une corrosion sulfureuse, appelée aussi ‚taches noires', ne se trouve pas seulement sur des objets en cuivre ou alliage à base de cuivre, mais aussi sur des alliages à base d'étain qui contiennent des petites quantités de cuivre, et sur des minéraux. Le résultat, c'est une perte grave de la surface de l'objet. Les polluants responsables de ce processus sont le soufre élémentaire et des liaisons au sulfure gazeux. Les produits de corrosion ne sont pas exclusivement des liaisons au sulfure, comme on l'a présumé jusqu'ici, mais ils peuvent contenir aussi des phases oxydées. Ces phases ne sont pas encore étudiées entièrement.

La seule méthode couronnée de succès à prévenir la formation des 'taches noires' est l'emploi des mesures préventives.

Keywords: 'black spots' , identification guide, copper sulphides, minerals, pewter, preventive conservation, sulphur

---

1. Introduction

It is some time ago that 'black spots' were first noticed on museum objects. Brinch-Madsen (1977) was the first to publish information of this phenomenon. Since then, 'black spots' have been referred to as copper sulphides. Severe damage may be caused by this kind of corrosion; pitting visible to the naked eye can occur on previously shiny metal surfaces.

Conservators are increasingly aware of 'black spots' in museum collections, though the reason for their development is often unclear. Since 'black spots' may develop unrecognised over many years, and museum objects may be moved from one location to another, important information on the development of corrosion may be lost, and so it is often impossible to track the pollutant source, i.e. materials emitting sulphur or other reduced sulphur compounds.

This paper discusses the specific growth patterns, microscopic appearance and chemical nature of 'black spots' and provides the reader with a guide for identifying them on museum objects. Collection surveys and laboratory experiments explain which circumstances can lead to the development of 'black spots', and which objects and materials are mainly affected. In conclusion, damage caused by 'black spots' is documented and

[*] Corresponding author, TEL: +49 – 30 – 81 79 72 58, e-mail: majaweichert@gmx.de

practical advice is given on conservation treatment and preventive measures. The work was carried out for a dissertation in object conservation (Weichert, 2002).

2. Characterisation and analysis of 'black spots' - Influence of pollutants, environment and metal structure

To investigate the growth mechanisms of this extraordinary form of corrosion, 'black spots' were grown in laboratory experiments at the State Academy of Art and Design in Stuttgart and at the Netherlands Centre for Cultural Heritage (ICN) in Amsterdam. Plates of copper, copper alloys and tin alloys containing 1 to 10 % copper, were exposed to sulphur or aluminium sulphide at 100 % relative humidity (Table 1). Pollutant concentrations ranged from 1.4 ppb sulphur to approximately 4 ppm (Hjelm-Hansen 1984) hydrogen sulphide. The surfaces of the samples were prepared using sandpaper (240 and 600 grit) and glass bristle brushes. The plates were rinsed with deionised water and then cleaned with acetone in an ultrasonic bath. The samples were placed in desiccators with water filled containers.

Some of the test plates were worked using methods such as chasing, chiselling, engraving, and bending. These samples were exposed in a pollutant chamber at the ICN to 50 ppb H_2S at 65 % rh for 41 days, and to 200 ppb H_2S at 82.5 % rh for 17 days.

Alloy	Components	Material	Thickness / diameter
Copper	E-Cu Purity 99.9 %; contains 0,005 to 0.04 % oxygen SF-Cu Purity 99.9 %; free of oxygen; contains 0.015 to 0.04 % phosphor	Sheet metal	0.6 mm
Bronze	Cu 94 % Sn 6 %	Sheet metal	0.5 to 0.79 mm
Bronze	Cu 92 % Sn 8 %	Sheet metal	1 mm
Lead bronze	Cu 77 % Pb 15 % Sn 8 %	Section of cast rod	Ca. 1 cm / 3 cm
Brass	Cu 85 % Zn 15 %	Sheet metal	1 mm
Brass	Cu 72 % Zn 28 %	Sheet metal	0.79 mm
Red brass	Cu 87.5 % Zn 5.5 % Sn 4.5 % Pb 2.5 %	Section of cast piece	Ca. 1 cm
Tin alloy	Sn 90 % Cu 10 %	Section of cast rod	Ca. 1 cm / 3 cm
Tin alloy	Sn 97 % Cu 3 %	Solder, drawn wire[1]	Diameter 3 mm
Tin alloy	Sn 99 % Cu 1%	Section of cast, triangular rod	Thickness ca. 1.5 cm
Tin alloy	Sn 95 % Sb 4 % Cu 1 %	Sheet metal	0.5 to 1.7 mm

Table 1:
Samples exposed in desiccators with elemental sulphur or hydrogen sulphide

[1] Cu Rotin 3©, Felder Löttechnik GmbH, Oberhausen; DIN 1707 L-SnCu3/zh, without flux.

The comparison of test plates mainly shows a rough relationship between the copper content of an alloy and its tendency to develop 'black spots'; copper had the highest tendency to develop 'black spots', whereas on alloys with relatively low copper contents (pewter, 1 to 10 % copper), either no 'black spots', or only small areas covered with rather flat, not very distinct species, were visible. However, the development of 'black spots' did not seem to be strictly proportional to the copper content of the alloy. Other alloy components such as lead, or trace elements, could have influenced the corrosion process.

Analysis of the corrosion product was carried out by x-ray diffraction and by the iodine-azide test (results see table 2). The corrosion products were either identified as copper sulphides, or both copper sulphides and copper sulphates were present, or they were amorphous and their composition could therefore not be determined by XRD (for further discussion see Eggert et al., this volume). The iodine-azide test detected sulphur or other reduced suphur compounds in every corrosion sample. Interestingly enough, the experiments showed that tenorite may develop on copper at temperatures as low as 50°C.

Alloy	**Experimental method**	**Results of XRD analyses**	**Description of corrosion**
Copper	Exposed to elemental sulphur, at 50°C, 100 % rh, for 14 weeks (equivalent to 64 ppb S)	Tenorite (CuO) and Cuprite (Cu_2O) identified; probably other phases present	Covered with tree-like, black, partially white corrosion; powdery, loosely adhering
Bronze (Cu 94%, Zn 6%)	Exposed to aluminium sulphide, at ca. 20°C, 100 % rh, for 14 weeks (equivalent to ca. 4 ppm H_2S)	Brochantite (Cu-sulphate) and covellite (CuS) identified	Covered with black, flaking corrosion; green, flaking corrosion underneath; no growth of characteristic 'black spots'
Lead bronze (Cu 77%, Pb 15%, Zn 8%)	Exposed to aluminium sulphide, at ca. 20 °C, 100 % rh, for 14 weeks (equivalent to ca. 4 ppm H_2S)	Brochantite (Cu-sulphate), covellite (CuS) and quartz identified; presence of gerhardtite (Cu-nitrate) is possible	Covered with black, powdery or flaking corrosion; no growth of characteristic 'black spots'
Brass (Cu 85%, Zn 15%)	Exposed to elemental sulphur, at 50°C, 100 % rh, for 14 weeks (equivalent to 64 ppb S)	Probably tenorite (CuO) present, or partially tenorite with other amorphous phases	Thinly covered with dark brown, powdery corrosion; no growth of characteristic 'black spots'
Brass (Cu 72%, Zn 28%)	Exposed to elemental sulphur, at 50°C, 100 % rh, for 14 weeks (equivalent to 64 ppb S)	Mainly amorphous; probably partially covellite, with the same amount of schulenbergit (Cu-Zn-sulphate)	Thinly covered with light green corrosion; waxy to fluffy consistency; no growth of characteristic 'black spots'
Red brass (Cu 87%, Zn 5,5%, Sn 4,5%, Pb 2,5%)	Exposed to elemental sulphur, at 50°C, 100 % rh, for 14 weeks (equivalent to 64 ppb S)	Tenorite (CuO) identified	Thinly covered with black-brown, powdery corrosion; no growth of characteristic 'black spots'
Tin alloy (Sn 97%, Cu 3%)	Exposed to aluminium sulphide, at ca. 20 °C, 100 % rh, for 14 weeks (equivalent to ca. 4 ppm H_2S)	XRD (Debye Scherrer): covellite identified; at least one other crystalline phase present, could not be identified c) microchemical test: copper detected	Blue-black corrosion, growing in some areas; flat, not very distinct 'black spots'
Tin alloy (Sn 95%, Sb 4%, Cu 1%).	Exposed to aluminium sulphide, at ca. 20 °C, 100 % rh, for 14 weeks (equivalent to ca. 4 ppm H_2S)	XRD: (Debye Scherrer): covellite identified; at least one other crystalline phase present, could not be identified c) Microchemical test: copper detected	Corrosion appeared to consist of different phases; black and whitish components were visible; corrosion partially growing as characteristic, tree-like spots

Table 2:
Analyses of exposed copper and tin alloys.

2.1 Trees, bunches, cauliflowers - Identifying black spots on museum objects

'Black spots' grown in the laboratory under accelerated conditions (see chapter 2) were mainly of a tree-like structure, with a stem and a more or less branched crown. Growth patterns of 'naturally' and more slowly grown corrosion identified on museum objects, were of a greater variety. Some were of the same tree-type, though many looked like cauliflowers, or appeared as hard and glassy mushrooms. A large proportion was finely branched and loosely adhering. The corrosion either grew in spots or sometimes covered wider areas of the object. The colours ranged from black to various shades of brown, to brass-like and metallic greenish or bluish, glittering spots. The SEM-structure of the 'black spots' varied significantly. Needle-like structures were observed, as well as platelet forms, tufts and 'black spots' that looked like algae (Figures 1-3). None of these varieties could be grown in the laboratory.

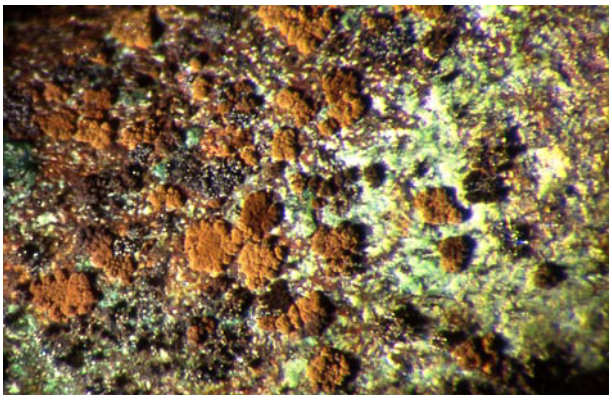

Figure 1: The 'cauliflower' type on a Roman bronze bracelet (622 a (1))[2].

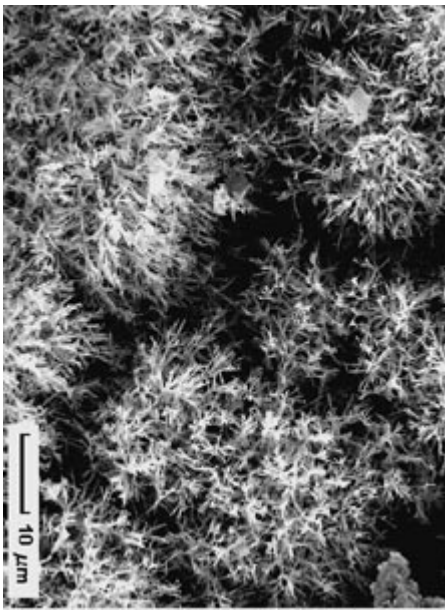

Figure 2: Needle structures on another bronze bracelet (A 626 d), probably Roman[3].

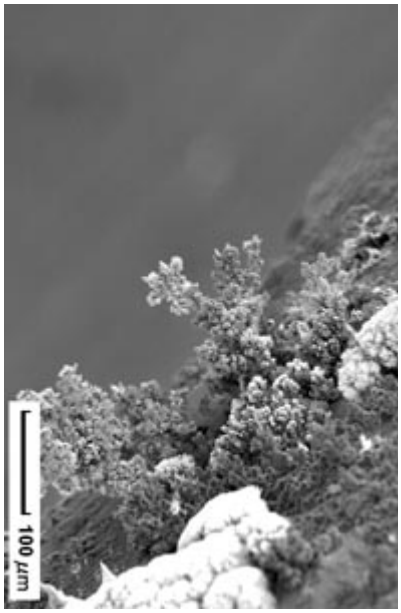

Figure 3: Dendritic growth forms on the same bracelet as in Figure 2 (A 626 d)[4].

The colour of the 'black spots' remained unchanged, regardless of whether they were still attached to the metal surface and illuminated by daylight, or removed from the object and viewed through the microscope. It is uncertain whether a certain colour or structural form of a 'black spot' can be attributed to a specific corrosion product composition. However, it is likely that there should be a connection between the colour and the dimension of the structure. On a bronze bracelet, black and brown efflorescence was visible to the naked eye. Viewed through the SEM, the single units of the structure of the black corrosion appeared smaller than those of the brown corrosion. X-ray diffraction analysis was carried out for both corrosion types; the black corrosion consisting of smaller units turned out to be covellite, the brown corrosion consisting of slightly larger units could be identified as chalcocite. This relationship between crystal size and colour was also reported by Lie and Scheifler (1982) for some whisker-like copper sulphides (chalcocite or a mixture of chalcocite and djurleite). Their crystals of a size below 0.7 µ were brown, whereas crystals of a size over 1 µ were black.

[2] Museen der Stadt Landshut, Germany; width of photo relates to 0.35 cm of the original. The corrosion product was amorphous.
[3] Museen der Stadt Landshut, Germany; SEM photo by Ineke Joosten, ICN.
[4] SEM photo by Ineke Joosten, ICN.

An easy-to-use method for identifying 'black spots' on objects is the iodine-azide test (Lee and Thickett, 1996), combined with the use of analytical test strips for copper ions (Merckoquant by Merck). The first test indicates whether sulphur or other reduced sulphur compounds are present; with the test strips, the copper content of the corrosion product can be determined qualitatively. A small amount of the corrosion is placed on the test strip, which is then wetted using deionised water. If both tests are positive, the corrosion product in question contains copper ions and a reduced form of sulphur; the presence of some copper sulphide is likely. Care must be taken not to remove part of the metal or mineral when collecting the sample material, since this may falsify the result.

2.2 Dependence of growth on metal structure

A relationship between metal structure and the growth mechanism of 'black spots' seemed likely. An evaluation of the test plates from the experiments carried out at the Stuttgart Academy (see chapter 2) showed that in some cases, metal structure disrupted due to mechanical stress such as scratching, tearing or bending, clearly proved to be the starting point for the development of 'black spots'.

Another theory is, that the growth of 'black spots' is influenced by the existence of an oxidation layer; and the formation of an oxidation layer is, in turn, influenced by the metal structure. Indeed, most of the test plates showed a relationship between a disruption of the metal structure, and the development of an oxidation layer.

To find more evidence, a survey on approximately one hundred objects made of copper alloys was carried out at the Museum of Landshut, Bavaria. Some artefacts showed a pronounced development of 'black spots' in areas of metal disruption (Figures 4 and 5). These disruptions were due to the production process of the object, such as chased decoration, or to later damage. Where forging structures were visible, the growth of 'black spots' followed them. Often a distinct grouping of 'black spots' could be observed, but without any obvious reason. In some cases, the influence of heat, heat in combination with metal distortion, or contact with other metals, was the starting point for the growing of 'black spots'. Two bracelets showed growth of 'black spots' exclusively around a modern sample drill hole, forming a neat line along the rim of the hole (Figure 6). Another bracelet had developed 'black spots' in a narrow zone around a modern solder repair.

Figure 4: 'Black spots' forming along a tear in a Roman bronze fibula (A 584 a) [5].

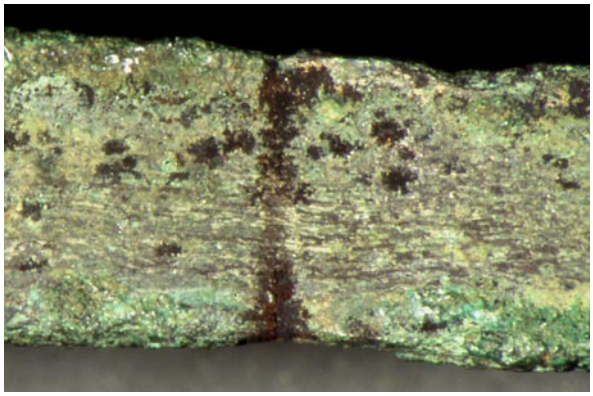

Figure 5: The development of 'black spots' on a Roman object (615 a-c) , following a disruption of the metal structure due to bending[6].

Figure 6: A modern drill hole in a Roman bronze bracelet (A 282 / 1)[7].

[5] Museen der Stadt Landshut, Germany; width of photo relates to ca. 1.5 cm of the original
[6] Museen der Stadt Landshut, Germany; width of photo relates to 1.8 cm of the original.
[7] Museen der Stadt Landshut, Germany; width of photo relates to 3 cm of the original.

The survey also showed, that 'black spots' grow on both the metal surface and corrosion layers, but seem to prefer to grow directly on metal, or in areas where existing corrosion has become dislodged.

2.3 Why the spot is a spot

As an explanation for the characteristic appearance of 'black spots', Eggert and Sobottka-Braun (1999) suggested the local migration of copper ions from the metal into sulphide crystals which had formed on the metal surface; these crystals act as a nucleus for the development of a 'black spot'. Since copper sulphides are slightly conductive, copper ions can move within the sulphide crystal. At the surface of the crystal, copper ions may react with sulphur from the atmosphere; copper ions following up from the base will keep this mechanism going.

It is in any case characteristic for 'black spots' to spread from the point where their growth began. The question is, why certain areas of the object are more prone to the formation of nucleus crystals than others. One answer would be the microscopic disruption of the metal structure as discussed above. Another explanation could be the locally restricted attack of gas molecules, as observed in the form of pores in protective coatings (Weichert, 2002) or cable insulations (Kawawata and Ogura, 1971), or pores in corrosion layers.

3. What damage do 'black spots' cause, and which objects and alloys are in danger of being affected?

'Black spots' are a severe conservation problem. They disturb the appearance of the object before and after removal (Figure 7); underneath a black spot, the metal can be bright and shiny, in contrast to an otherwise dark and oxidised surface. Black spots cause pitting on metal surfaces (Figure 8); eventually, the surface of an object can partially be destroyed.

Figure 7: 'Black spots' covering large parts of a medieval bronze fibula (KN 116)[8]

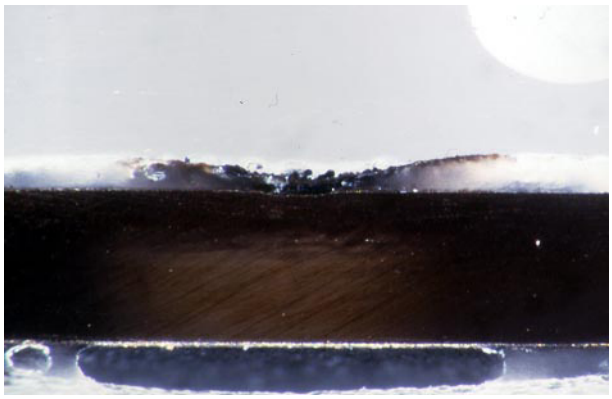

Figure 8: Copper test plate coated with microcrystalline wax COSMOLLOID H80©; a black, sulphurous corrosion had grown through a pore in the coating after exposure at ca. 4 ppm hydrogen sulphide for several weeks. A slight depression in the metal surface is visible[9].

3.1 Susceptibility of different copper alloys and tin alloys containing small amounts of copper (pewter)

'Black spots' on copper and copper alloys are now a known phenomenon. With laboratory experiments, described in chapter 2, the assumption was now verified, that copper sulphide corrosion can occur on alloys with a very low copper content of 1 to 3 %, when exposed to a very high concentration of hydrogen sulphide (4 ppm) over a period of several weeks. The identified crystalline phase was covellite, though other crystalline and possibly amorphous phases were present. Pewter with a significantly higher copper content (10 %) did not develop corrosion visible to the naked eye under the same experimental conditions. Presumably, a corrosion nucleus is necessary to initiate this kind of corrosion on pewter, as was observed in one experiment with corroded copper alloys and uncorroded pewter (copper content between 1 and 3 %), exposed to 4 ppm hydrogen

[8] Museum der Stadt Konstanz; width of photo relates to 0.9 cm of the original.
[9] Width of photo relates to 0.9 cm of the original.

sulphide. The corrosion started to spread to the pewter, from a point where the two plates touched (Figure 9). The corrosion spread over a distance of approximately 3 cm.

One experiment, which needs verification, showed that copper alloys could be 'infected' by sprinkling on small amounts of powdered copper sulphide and leaving them in an atmosphere with sulphur at 50°C and 100% relative humidity for seven weeks; a black corrosion slowly spread from these spots.

Figure 9: 'Infected' pewter (3% copper content) after being in contact with heavily corroded copper alloys at ca. 4 ppm hydrogen sulphide for appr. 8 weeks[10].

3.2 Copper alloys and pewter from marine finds

Black, sulphurous corrosion can develop on copper alloy or pewter objects in contact with marine crusts and gunpowder containing elemental sulphur. This could be confirmed by an extensive survey of marine archaeological objects from the *Mary Rose* collection in Portsmouth, UK. The investigated objects belong to the inventory on board the *Mary Rose*, a war ship of King Henry VIII, which sank off the Portsmouth coast in 1545.

After the ship was raised and artefacts were being stored in the museum from the early 1980´s, some objects made from copper alloys and pewter, developed a black corrosion. On some copper alloys, the black corrosion product had a fuzzy appearance, even visible to the naked eye, which was only loosely attached to the metal, a characteristic feature of 'black spots'. Corrosion on some pewter objects, containing copper in amounts from only 0.7%, was described as 'a black brown sooty layer over a poor powdery surface', and also as 'a brown thick tarnish, initially localised in occurrence but eventually covering the entire surface. High in sulphur and unpleasant to look at' (personal correspondence between Mary MacQueen, formerly Mary Rose Trust, and Dr. Warwick, International Tin Research Institute, Greenford, England, February 1986).

XRF analysis of the pewter corrosion carried out in the 1980´s by Ernest H. Pitt and R. C. Hollyak, of Coventry Lancaster Polytechnic (internal reports), identified copper and sulphur, often as major components. Additionally, a positive iodine-azide test (Weichert 2002) proved the presence of sulphur or other reduced sulphur compounds. It is therefore likely, that the corrosion product consisted, at least partially, of copper sulphides. In one case, the corrosion of a pewter object (a fragmented jug, MR 78 A 118 1-3) was clearly identified by XRD; it mainly consisted of covellite. The object was covered with white, marine deposits.

3.3 'Black spots' on minerals

It is known that copper minerals can, under certain circumstances, develop a black sulphurous efflorescence (Eggert, 2000). When different copper minerals are stored in the same closed display case, the interaction of single reactions can lead to the formation of reduced sulphur gases. Sulphur and reduced sulphur gases can also be directly emitted by adjacent minerals. Marcasite, for example, produces elemental sulphur during oxidation. Products resulting from the disintegration of pyrite can react with sulphide minerals, producing hydrogen sulphide (Waller et al., 2000). Discoloration of non-sulphidic copper minerals to a deep black is mainly due to the effect of sulphurous substances. Sulphurous, black corrosion products on copper sulphide minerals can also be the result of oxidation reactions which take place at an accelerated rate at a relative humidity from about 60%. The sulphur content of the sulphide is partially oxidised, i.e. a black efflorescence can develop without a pollution source (Howie, 1992).

[10] width of photo relates to ca. 7 cm of the original

4. How can affected objects be treated? – Strategies for active treatment and preventive conservation

'Black spots' can in most cases easily be removed mechanically. Removing 'black spots' using chemicals (dithiolates) does not seem appropriate, because even more damage may be caused. But just removing the 'black spots' from the object will not solve the problem – if storage conditions are not adequate, they may reappear.

Therefore, the best way to solve the problem is to take preventive measures, i.e. environmental monitoring and control, suitable storage conditions, and the detection and removal of pollutant sources. To be able to find potentially harmful material, it is important to document all aspects concerning the collection, i.e., materials used for conservation, storage and display, loans, and movement of objects within the museum.

4.1 Storage

It is best practice to store susceptible material at low temperatures and relative humidity, and keep them clean of dust and dirt. Airtight display cases can, on the one hand protect the collection from external pollutants, but on the other hand may keep in harmful substances emitted by the objects themselves.

There are different pollutant absorbers available which absorb sulphurous components. Care should be taken when using pollutant absorbers in mineral collections (see chapter 4.3).

4.2 Detecting pollutant sources

Some materials which are used for conservation, storage and display, such as plasticine (Figure 10), certain fabrics (Werner, 1972; Weichert, 2002), paper (Rubin and Rubin, 1938), rubber and vulcanised glues (Howie, 1992; Oddy, 1973; Sease, 1994) and leather (Howie, 1992), could be harmful. Wool and felt (sometimes even when sold as 'synthetic') are typical examples of materials emitting reduced sulphur compounds (Sease, 1994; Brimblecombe et al., 1992).

Figure 10: Back of the fibula shown in Figure 7; 'black spots' spread from the area where plasticine was placed onto the surface for mounting[11].

Often it is not so obvious whether certain materials might be harmful. It is therefore absolutely necessary to test and re-test all materials used in connection with museum objects to see whether they might contain sulphur or sulphidic compounds; the available test methods are both inexpensive and easy to use. The Oddy Test (Lee and Thickett, 1996) can be employed to determine the general corrosiveness of a material. Disadvantages lie in the relatively long running time of the test and in the fact, that neither the corrosion product nor the pollutant can be characterized. With the iodine-azide test, quick and easy testing for elemental sulphur and other reduced sulphur compounds is possible. A microscopic sample of the material to be tested is sufficient.

If the pollutant source cannot be traced inside the museum, it is worthwhile to take a closer look outside – are there any paper mills, swamps or sewage plants (Sherwood, 1992, quoted from Strandberg, 1997) nearby?. Even mineral springs might emit reduced sulphur gases (Daubree, 1875; Lacroix, 1909, quoted from Scott, 2002).

It is difficult to predict a critical indoor pollution level; it has been proved that even the very low vapour pressure of sulphur at room temperature (app. 1 ppb at 20 °C) is sufficient to cause black spots on copper (Eggert and Sobottka-Braun, 1999). Also, the presence of one pollutant alone, often does not explain the damage; the interaction of different reduced sulphur compounds with organic acids or hydrochloric acid for example, may multiply the harmful effect (Watts, 1999).

[11] Scale in mm.

4.3 Minerals, patinated objects and artefacts decorated with niello

Disintegration reactions of minerals caused by oxidative processes can only be prevented by storage at low relative humidity; 30% is recommended (Waller, 1992).

Some minerals themselves emit reduced sulphur compounds; it is therefore good advice to store potentially harmful minerals such as pyrite and marcasite in separate, airtight containers. Pollutant absorbents should only be used for such minerals that emit the pollutant as a result of a thermodynamic reaction, e.g. pyrite (Waller et al., 2000). They should not be employed for minerals that emit reduced sulphur gases through sublimation or evaporation, because this would accelerate their degradation. Minerals that emit a certain sulphurous gas should not be stored together with minerals that absorb the same substance; they will harm each other (Waller et al., 2000).

Oxidation processes as mentioned above, can also lead to the disintegration of copper sulphides which are part of the object. Artificially patinated surfaces or niello decoration may oxidise and change colour when storage conditions are inappropriate.

4.4 Special precautions for marine artefacts and objects with adhering sulphurous substances

Marine crusts should be removed from the object as long as they are not important for the interpretation of the object. It is crucial to remove these deposits completely, since remaining sulphurous substances could be the starting point for further corrosion. Sulphur emitted by marine crusts can also harm adjacent objects; large pieces of these crusts or thickly covered artefacts should therefore not be stored in close contact (or in the same showcase) with sensitive material.

For objects from which sulphurous material cannot be removed, such as powder ladles and containers, weapons operated with gun powder, kettles used for boiling tar, or hollow objects filled with sulphurous cement (Eggert et al., 1999), storage at low temperature and a low relative humidity, is crucial.

4.5 Protective coatings on copper alloys and on pewter

The evaluation of test plates from laboratory experiments (test conditions as in chapter 2) and artefacts of the *Mary Rose* showed the protective effect of coatings on copper alloys generally to be of limited reliability. This can partially be due to the thoroughness of application (Figure 11) .

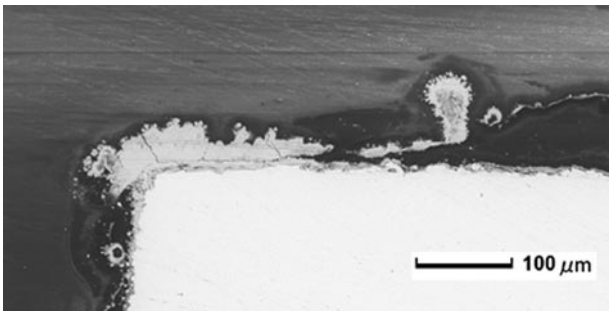

Figure 11: Copper test plate coated with microcrystalline wax (COSMOLLOID H80©, appearing black); 'black spots' grow along the edge, where the protective coating is thinned (application by immersion). The sample was exposed to hydrogen sulphide concentrations of ca. 4 ppm for three months[12].

However, the application of INCRALAC© in most cases prevented further corrosion on *Mary Rose* objects; the investigated coatings being fifteen to twenty years old. But due to the relatively small number of investigated objects, the results do not provide sufficient evidence.

A survey of 19 pewter objects from the *Mary Rose* collection, coated with silicone wax (12 objects, product name unknown), INCRALAC© (two objects), and FRIGILENE© (five objects) showed, that in most cases, further corrosion occurred, despite the protective coating. Four artefacts treated with microcrystalline wax remained stable.

[12] SEM photo by Ineke Joosten, ICN.

5. Results and Discussion

'Black spots' do not only grow on copper and copper alloys, but also on alloys containing minimal percentages of copper, such as pewter, and even on copper minerals. It is possible, that copper sulphides which are part of the object, such as artificial patination or niello, can oxidise and change colour when storage conditions are inappropriate.

The exact composition of the corrosion product could not yet be determined in all cases. However, it is proved that 'black spots' are not exclusively copper sulphides, but can as well contain other phases, such as sulphates or amorphous components which could not yet be identified.

The growth mechanism of 'black spots' depends on many parameters, such as temperature, humidity, pollution concentration, and time, but also on alloy composition and metal structure. The pollutants in this process are known, but it is rarely possible to exactly determine the circumstances that lead to the formation of black spots on museum objects. It is therefore of great importance to record the collection history of an object properly (conservation treatment, materials used for display, loans, movement within the museum etc.).

Taking preventive measures is crucial for all collections, which means storage of metal objects at low temperatures and a low relative humidity, separation of sulphur-emitting exhibits, and testing of all materials in stores and exhibition rooms.

Acknowledgements

The corresponding author wishes to thank Ernst-Ludwig Richter and Heide Härlin, State Academy of Art and Design Stuttgart, Glenn McConnachie and Peter Crossman of The Mary Rose Trust for contributing to this work. Many thanks to Ineke Joosten, Peter Hallebeek, and Henk van Keulen, ICN, for analyses. Also, David Dungworth from English Heritage, Derek Weights from Portsmouth University, Harald Euler and Bruno Barbier of the Mineralogical and Petrological Institute of the University of Bonn, all supported this work with scientific analyses. Corrosion samples of minerals courtesy to Paul Keller, University of Stuttgart, Institute of Mineralogy. Finally, the corresponding author wishes to thank Anette Klöpfer, Museum of Landshut, Bavaria, for the possibility to do a survey of the Landshut collection.

Table of registered trade items

COSMOLLOID H80©
CU ROTIN 3©, tin solder
INCRALAC©,
FRIGILENE©,
MERCKOQUANT©

References

Brimblecombe, P., Shooter, D., Kaur, A. (1992) *Wool and reduced sulphur gases in museum air*, Studies in Conservation **37**, 53-60.

Brinch-Madsen, H. (1977) *Mikrobiologisk angreb på bronzerne fra Budsene brønden*, Meddelelser om Konservering, **2** , 9, 265-270.

Eggert, G. (2000) *Die schwarzen Bronzeflecken und der „Schimmel" auf Kupfersulfid-Mineralien*, Archäometrie und Denkmalpflege – Kurzberichte, Mensch und Buch Verlag, Berlin, Germany, 149-151.

Eggert, G., Kutzke, H., Wagner, G. (1999) *The use of sulphur in hollow ancient gold objects,* Journal of Archaeological Science **26**, 1089-1092.
Eggert, G., Sobottka-Braun, U. (1999) *Black spots on bronzes and elemental sulphur*, 12th ICOM –CC Triennial Meeting Lyon 29 August - 3 September 1999, Preprints Vol. 2, James & James, London, UK, 823-827.

Eggert, G., Weichert, M., Euler, H., Barbier, B. (2004) *Some news about 'Black spots'*, this volume.

Hjelm-Hansen, N. (1984) *Cleaning and Stabilization of Sulphide-Corroded Bronzes*, Studies in Conservation **29**, 17-20.

Howie, F. M. (1992) *Sulphides and allied minerals in collections*, The Care and Conservation of Geological Material: Minerals, Rocks, Meteorites and Lunar Finds, Butterworth & Heinemann, Oxford, UK, 56-69.

Kawawata, S., Ogura, J. (1971) *Chemical tree deterioration in the insulation of plastics-insulated wires and cables*, Hitachi Review, **20**, 2, 55 - 63.

Lee, L. R., Thickett, D. (1996) *Selection of materials for the storage or display of museum objects*, Occasional Papers **111**, British Museum (ed.), London, UK.

Lie, H., Scheifler, L. (1982) *Copper sulphide growth on copper and copper alloys*, Abstracts of Poster Sessions, IIC 9th International Congress on Science and Technology in the Service of Conservation, Washington DC, 3 - 9 September 1982, Washington DC, USA.

Oddy, W. A. (1973) *An unsuspected danger in display*, Museums Journal **73,** 1, 27-28.

Rubin, M. M., Rubin W. R. (1938) *Metallic dendrites in paper*, The Paper Industry **1**, 1155 - 1162.

Scott, D. A. (2002) *Copper and Bronze in Art – Corrosion, Colorants, Conservation*, The Getty Conservation Institute, Getty Publications, Los Angeles, USA.

Sease, C. (1994) *The cases of the black fuzzies*, Preprints of the SSCR Conference in Edinburgh 1994, The Scottish Society for Conservation and Restoration, Edinburgh, UK, 125-130.

Strandberg, H. (1997) *Perspectives on bronze sculpture conservation, modelling copper and bronze corrosion*, Doctoral Dissertation, Gothenburg University, Gothenburg, Sweden.

Waller, R. (1992) *Temperature- and humidity-sensitive mineralogical and petrological specimens*, The Care and Conservation of Geological Material: Minerals, Rocks, Meteorites and Lunar Finds, Butterworth & Heinemann, Oxford, UK.

Waller, R., Andrew, K., Tétreault, J. (2000) *Survey of gaseous pollutant concentration distributions in mineral collections*, Collection Forum **14**, 1/2, 1-32.

Watts, S. (1999) *Hydrogen sulphide levels in museums: What do they mean*, Abstract of Conference Report, Indoor Air Pollution (IAP) Working Group Meeting, Amsterdam, The Netherlands.

Weichert, M. (2002) *Büschel, Bäumchen, Blumenkohl – Durch Schwefel und reduzierte Schwefelverbindungen hervorgerufene Ausblühungen auf Kupfer, kupferhaltigen Legierungen und Kupfermineralien*, Diplom Dissertation, State Academy of Art and Design, Stuttgart, Object Conservation, Stuttgart, Germany, unpublished.

Werner, A. E. (1972) *Conservation and display, environmental control*, Museums Journal **72**, 2, 58-60.

Analysis of some copper-alloy items from HMAV *Bounty* wrecked at Pitcairn Island in 1790.

A. Viduka [a], S. Ness [b]

[a] Museum of Tropical Queensland, Townsville, QLD, 4810, Australia.
[b] Advanced Analytical Centre, James Cook University, Townsville, QLD, 4811.

Abstract

The underwater site of HMAV *Bounty* and the area of the mutineer settlement at Adamstown on Pitcairn Island were investigated archaeologically during a four-month expedition in 1998 and 1999. Due to high energy environmental conditions on the maritime site and human activity associated with collecting or recovering material post the vessel's wrecking in 1790, only 147 artefacts and or concretions remained to be recovered during the maritime excavation. These artefacts consequently represent a unique collection of provenanced material from which a chemical and metallurgical investigation can be undertaken. Comparative analysis was conducted between some copper maritime and terrestrial artefacts to reveal the extent of recycling by the mutineer settlement. Further comparative analysis was conducted between copper artefacts from HMAV *Bounty* and HMS *Sirius* (1789), as both vessels were extensively refitted a year apart at Deptford dockyard on the Thames before both departed on voyages to the Pacific. Copper-iron composite objects found on the *Bounty* wreck-site were identified as Bent's pins which have not been found previously in the artefact assemblage of two contemporary RN vessels excavated in the Pacific.

Keywords: Copper alloy, chemical characterisation, metallography, HMAV *Bounty*, Bent Pins.

Corresponding author: TEL: (+617) 4726 0616 Fax (+617) 4721 2093 email: andrew@mtq.qld.gov.au

1. Introduction

Archaeological investigations of the mutineer settlement on Pitcairn Island and the shipwreck site of HMAV *Bounty* produced a variety of typologically similar copper alloy artefacts. To understand the use and extent of recycling of *Bounty* material within the mutineer settlement, chemical and metallurgical studies were undertaken on a number of copper alloy artefacts from both these sites and other local sites where material could have been acquired over the period of occupation.

Pitcairn is a small volcanic island rising abruptly out of the deep waters of the eastern South Pacific Ocean at latitude 25º 04´ south, longitude 130º 06´ west. The island is cliff-bound and open to full ocean swell, limiting access to the island to small boats capable of negotiating the surf. There is no safe anchorage and little flat land; indeed the island lacks almost every convenience conducive to settlement.

In January 1790, a small British naval vessel carrying 28 people arrived at Pitcairn. The ship was the *Bounty* and until a successful mutiny in April 1789, the vessel had been employed in an ambitious expedition to collect breadfruit in Tahiti for transport to British plantations in the West Indies (Bligh, 1937). Since the mutiny, the mutineers had suffered a number of reversals, culminating in a split between those who wished to settle at Tahiti, and those who, along with Fletcher Christian, chose to remain with the ship and search for a place secluded from the eyes of the world.

Pitcairn Island served this purpose particularly well and it was there that the mutineer's hoped to evade Royal justice. The establishment of a settlement required equipment and material and the primary source of this for the mutineers was the *Bounty*. Dissent amongst the remaining mutineers continued on Pitcairn Island, culminating in murders and the *Bounty* being burnt at anchor and the remainder sunk as a result of the fire.

The underwater site of the *Bounty* wreck lies in Bounty Bay, and the areas of the mutineer settlement at Adamstown were investigated archaeologically during a four-month expedition in 1998 and 1999. One of the primary archaeological research parameters and the initial impetus for this study was to ascertain the extent of recycling of material from the *Bounty* to the mutineer settlement. Bronze sheathing nails constituted the largest single artefact group recovered from the wreck site and they represent a significant resource with potential multiple applications within the mutineer settlement (Figure 1) (Erskine, 2000). Besides nails, copper sheathing, a keel bolt and several copper iron composite objects were discussed.

Although several copper alloy nails recovered from Adamstown sites appear to be *Bounty* nail types, a more positive identification of the nails is not possible without metallographic examination and chemical characterisation. Potentially the nails may also have originated from a number of other wrecks in the Pitcairn group: *Wildwave* (1858), *Cornwallis* (1875), *Khandeish* (1875), *Acadia* (1881), *Oregon* (1883), *Bowden* (1893) and *St James* (1918). Physically the *Bounty* maritime site sheathing nails appear curved from use, the common length is 40 mm with very slight variations and approximates to an imperial measurement of 1½ inches. The head of each nail is flat and round with a diameter of 10 mm and is conical under the head before forming a tapering, square-sectioned shank, ending in a sharp point. The physical uniformity of sheathing nails offers a potentially useful indicator of salvage and recycling of material from the *Bounty*.

Figure 1: Nails with typological features described as common to *Bounty* assemblage (Scale in mm).

Other possible distinguishing features include the fact that the other wrecks in the Pitcairn Island group all occur in the second half of the 19th Century and thus fall into a period after the widespread introduction of Yellow (or Muntz) metal. Muntz metal was an alloy formed by combining copper (60%) and zinc (40%) and, by the 1850s, was used by both British colonial and foreign shipping (Bingeman et al, 2000; Staniforth, 1985). The use of this metal represents a technological innovation that would clearly separate the artefacts by their chemical signature. Equally, *Bounty* nails were produced in a uniform way which was casting in this period. Metallurgical examination would quickly identify if any of the other more modern nails were produced by other methods, eliminating them from the study. In order to positively identify the source of copper alloy nails found at Adamstown sites, sheathing nails from the *Bounty* site and the wrecks of the *St James*, *Bowden* and *Acadia* were sent for chemical analysis to the Advanced Analytical Centre at James Cook University. Metallographic analysis was conducted at the Museum of Tropical Queensland.

A secondary focus of this research was instigated by the physical and temporal association between the refit of HMAV *Bounty* and of HMS *Sirius*, the latter wrecked at Norfolk Island (latitude 29.02 S, longitude 167.93 E). Both vessels were extensively refitted for long distance voyaging at the

Deptford works on the Thames, approximately one year apart. The *Sirius* was finally and extensively refitted in 1786 (Samuels, 1983) and the *Bounty* in 1787. The period is important as the refits happened in a time of great metallurgical experimentation and technological innovation for the British RN (Royal Navy) (Knight, 1973) The short time frame between refits potentially offers an insight into the rate of new technologies being introduced into naval vessels for the purposes of improvement to capacity and longevity, or equally it could reveal information about ship yard working practices. Copper artefacts from the *Sirius* have been reported and studied for the quality of the material and historical methods of manufacture (Samuels, 1983; MacLeod, 1991; Stanbury, 1994) Consequently chemical characterisation data collected from the *Bounty* copper based artefacts were compared with the published data associated with artefacts recovered from the *Sirius*.

2. Method

2.1 Preparation

Metal samples were cut from nails, bolts and sheathing. Samples were sectioned using a continuous rim diamond saw. Those to be studied by Scanning Electron Microscopy (SEM) and optical microscopy (OM) were mounted into Canadian Balsam and then polished on a polurethane lap to <3 micron of deformation. Samples selected for SEM were then carbon coated.

Samples selected for OM were etched with a ferric chloride ($FeCl_3$) – hydrochloric acid (HCl) solution (50 gms $FeCl_3$, 10ml HCl made up to 1litre with ethanol). Effective etching took place after immersion of the samples for approximately 5-10 seconds.

Samples selected for chemical analysis by Inductively Coupled Plasma – Mass Spectrometry (ICP-MS) were prepared as follows:

The samples were first soaked in acetone to remove any oily dirt, then the samples were air dried. The second step of cleaning is an acid mix leaching to remove any corrosion until a fresh surface was exposed, thereafter the samples were rinsed with Milli-Q water and dried.

To dissolve the samples, a mixture of 20 ml HCl and 10 ml HNO3 plus 5 ml of water was prepared for 1 g of sample, and the beaker was gently heated to speed up the dissolution process. After dissolution, the resulted solution was transferred quantitatively to a 100 ml flask and was filled up to the mark with Milli-Q water.

2.2 Instrumentation and measurement

The elements of interest were measured by a Varian UltraMass 700 Inductively Coupled Plasma Mass Spectrometer (ICPMS). A multi-element standard solution purchased from a reputable commercial source was used to externally calibrate the ICPMS. Indium (In, atomic number 49) was used as an internal standard to correct for matrix effects and the instrument drift.

The detection limits for all elements analysed are:

Element	Detection Limit in ppm
Ag	0.05
Bi, Sb, Sn, Ni	0.1
Zn, As	1
Cu, Pb	5
Fe	100

Cu, Pb, Fe have higher detection limits because of their significant concentrations in the samples. The Relative Standard Deviation for data in Tables 1, 2, 3 is < 2%.

SEM studies were performed with a JEOL 840 JXA scanning electron microprobe, operating at 15 kV accelerating voltage. Optical microscopy studies were undertaken on an Olympus PME3 microscope with a Polaroid Polapan B/W ISO 400/27^o attachment for optical photography. ICP-MS analyses were obtained from a Varian UltraMass.

3. Results

3.1 *Sheathing*

Copper sheathing a RN vessel was standard procedure by 1787, the date of the *Bounty's* refit. Sheathing from *Acadia*, *Bowden, Bounty* and several land sites on Pitcairn Island were chemically analysed (Table 1). Two samples collected from land sites (LF0037 and LF0045) were both highly corroded. The elements being analysed in this study precluded corrosion products and the significant weight % absence in the data of these samples reflects both the condition of the samples and the method of analysis. The material from the *Bowden*, *Acadia* and sample LF0045 is chemically in proportion to the composition of 'yellow metal' being two parts copper to one of zinc. The Bowden and Acadia samples have major components of: copper 61-63% and zinc 33 -37% respectively. LF0045 has major components of: copper 58.4% and zinc 24.0%. This dates this material to originating in the nineteenth century and metallurgically distinct from the *Bounty* artefact assemblage.

The main impurities in the copper sheathing recovered from the *Bounty* site, Steve Christian's Dunkan in Adamstown and sample LF0037 are; arsenic, lead and bismuth. Arsenic causes an increase in the microhardness of the metal during cold working. MacLeod in his study of the S*irius* sheathing notes that "since the maximum amount of arsenic occurs in the bulk sheathing material, it is reasonable to assume that the vessel was covered with good quality sheathing" (McLeod, 1991). This interpretation is then equally valid for the *Bounty* sheathing. The maximum amount of arsenic in the *Bounty* and *Sirius* sheathing is 0.882 % and 0.826% weight respectively. For both vessels this proportion of arsenic is at the lower end of the range for ancient alloys (McLeod, 1991; Scott, 1991)

The sheathing excavated from terrestrial sites, the Dunkan and LF0037 have a positive chemical correlation with the samples analysed from the *Bounty* wreck site and quantifiably demonstrates that there was recycling of sheathing metal from the vessel. Whilst it is not possible to positively correlate *Bounty* samples to particular production batches, it is possible to say that their major and trace metallurgical composition is indicative of methods of manufacture and refining techniques prior to the introduction of yellow metal. The samples are chemically similar in their makeup.

3.2 *Sheathing Nails*

Metallurgical and chemical analysis of copper alloy nails recovered from Pitcairn Island, and the wrecks of the *Bounty*, *St James*, *Bowden* and *Acadia* were conducted as complementary studies to typological analysis. The results were comparatively studied with the aim of identifying the source of the sheathing nails found on Pitcairn Island and quantifying the extent of recycling from the *Bounty* to the mutineer settlement on Pitcairn Island (Table 2).

Metallurgical analysis of sheathing nails recovered from the *Bounty* site revealed that all of these nails were cast. Of the seven nails sectioned, three nails have evenly distributed small, spherical porosity. The remaining four samples are very porous, with large unevenly distributed spherical voids and with two distinct phases visible.

Since all the *Bounty* site nails studied were produced by casting, the sheathing nails analysed in this study and collected from the Adamstown settlement were inspected for comparison. All the nails analysed from the mutineer settlement were made by casting.

Chemical analysis was undertaken to compare and contrast all the samples. The only element besides copper in a weight percent > 1 is tin; all other elements are present only in trace proportions. Similar proportions of arsenic appear in both the *Bounty* and *Sirius* sheathing nails, the latter described as an arsenical tin bronze (Samuels, 1983) The high tin content affords a higher level of corrosion resistance and hardness to the metal.

Significant variation does occur in the ratios of copper: tin, and tin: arsenic within the *Bounty* site samples. Of the seven nails removed from the *Bounty* site, two nails have neither significant tin nor arsenic. One nail recovered from Adamstown cemetery is 99.7 % weight copper with trace levels of tin and
0.7 % weight concentration of arsenic. Variation to this extent is explicable by the use of different ore bodies for producing the metal, the level of technology in the mid-eighteenth century and the standards of manufacturing processes.

Of the remaining trace elements, there is sufficient variation in the concentrations to negate their use as unique identifying features individually or collectively. However, when studying all the sampled material, it is readily apparent that it is the absence of zinc in significant quantities, typically <1% by weight, which separates the *Bounty* artefact assemblage from that of the *St James*, *Acadia* and

Bowden shipwrecks. Only one artefact LF37.3 , recovered from the Adamstown settlement, has a weight % concentration of zinc. This nail is cast but is typologically dissimilar to the *Bounty* site nails and chemically is significantly different from the sampled artefacts.

3.3 *Bolts*

HMAV *Bounty* was bought in by the RN in 1787 for £1900. The vessel was extensively refitted under the waterline and her bolts were changed from iron to copper with the addition of copper sheathing for the hull at the cost of approximately £2400. A keel bolt (ZA100) from the *Bounty* was chemically and metallurgically analysed. This bolt had been previously recovered from the *Bounty* site by Steve Christian in the 1970's (Christian, 2000).

The bolt is essentially pure copper with trace amounts of arsenic, lead, tin and zinc (0.390, 0.201, 0.038 and 0.013 weight % respectively). Metallurgical analysis of the keel bolt revealed the extensive work hardening required for a keel bolt which needs to combine both strength and corrosion resistance. The bolt was made and cast under reducing conditions. After casting, the metal was probably hot forged, then cold forged to give tensile strength and hardness. This cold working of cast copper, visible throughout the cross-section, is exemplified by the extensive twinning, the distribution of porosity, grain size, shape and the degeneration of the typically organised pattern of a cast metal (Figure 2).

According to Samuels, HMS *Sirius* was extensively refitted at Deptford yard in 1786 when the most technologically recent materials would have been added to the vessel (Samuels, 1983) A comparison between the chemistry of bolts from both vessels (ZA100 and SI 32C) reveals that the bolts, whilst manufactured from different ore bodies, are essentially the same product. Elements such as lead, silver and nickel are not affected through the process of manufacture and can be used in this purpose as distinguishing elements. The trace level of arsenic in the *Bounty* bolt is higher than the *Sirius's* and as elucidated, arsenic is largely beneficial because it increases the hardness of the bolt undergoing cold working (McLeod,1991). Neither ZA100 nor SI 32C has any significant level of zinc.

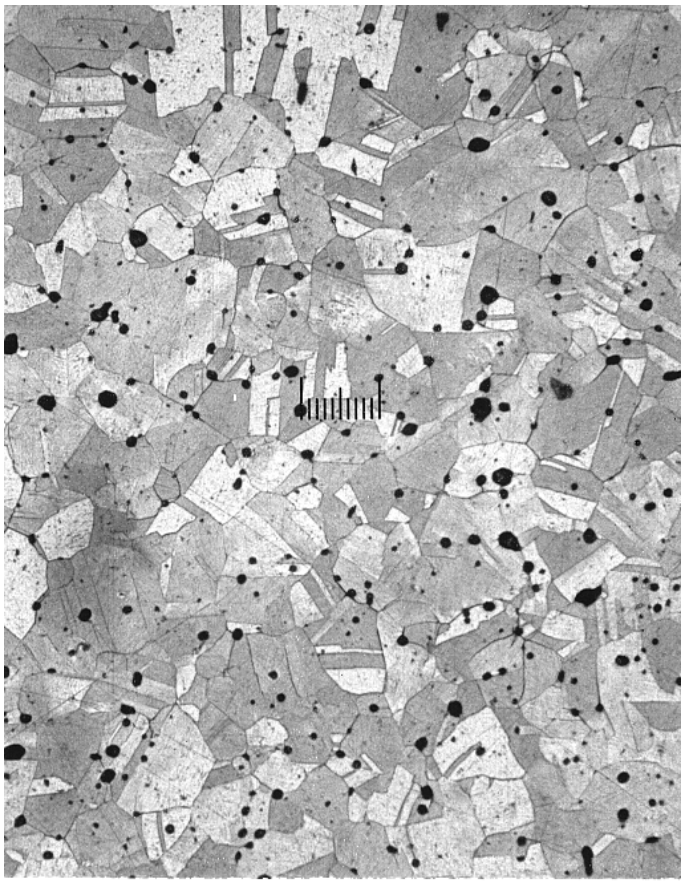

Figure 2: ZA 100 etched x 500 magnification. Cross section showing extensive twinning

3.4 *Copper – iron composite artefacts*

Copper - jacketed iron objects preliminarily identified as bolts were later identified as Bent pins (Erskine, 1999a, 1999b). In William Bent's 1778 patent, *No.1205 Ships' Blocks- A, a new kind of ships block which turn upon iron or steel pins or axels cased with metal* Bent describes the manufacturing process as follows:

> "The Invention consists chiefly in the pin bolt or axle on which the shive turns being made of steel, iron, or cast metal called cast iron, and covered or cased with copper, brass, block tin, or pewter, or a mixture of the aforesaid metals, which is done in the following manner:- The pins of the blocks are made of iron or steel, which may be prepared for covering with metal by pickling, tinning, fluxing, or otherwise, or without such preparation, though the same thought to be preferable; after which a proper quantity of metal, consisting of brass, copper, tin, pewter, lead, or other metal, or a composition of all or any of the said metals, is melted and poured or cast upon the plus, which are previously put into a flask or mould, to which the said metal adheres, and thereby the pins become free from the inconvenience of rusting, which iron pins not covered are very liable to, and such pins so covered preserve a sufficient strength; and plus cased or covered as above specified may be applied to the purpose of bolting ships. The shives of the said blocks may be made of mahogany, lignum vitae, or other wood, with or without pieces or plates of metal fixed on each side in the centres to strengthen the wood; or the whole shive may be made of metal or of cast iron. If of cast iron the holes in the middle should be lined with metal, which may be done either by casting in the same manner as above described for covering the pins. The case block may be made of elm or any other wood."

A study of the artefact catalogues from HMS *Sirius* (1789) and HMS *Pandora* (1791), both contemporaneous vessels with the *Bounty* and equally commissioned by the RN for voyages to the Southern Hemisphere, revealed no copper jacketed iron objects in the published artefact assemblages (Stanbury, 1994; Campbell and Gesner, 2000)

Figure 3: ZA 43 Sectioned pin (scale in mm)

Three of the composite objects recovered from the *Bounty* shipwreck site were sectioned for chemical and metallurgical analysis, though only two had remaining core metal (Table 3; Figure 3).

3.5 Core

The core from ZA106 was significantly corroded and weight percentage analysis was not feasible. Analysis of the iron core in the two remaining samples ZA 98 and ZA 43 suggests that the cores were cast slugs with no subsequent work hardening. Visual observation of the corrosion evident in the remaining two pins shows corrosion more typical of cast iron than wrought. Within the iron core there were isolated pools of lead and tin as well as distributed copper with melt effects (Figure 4).

Whether the elements inside the iron core came from manufacture or deterioration cannot be categorically determined without more metallurgical research. At present there are only possible scenarios;

a) the elements now present in the iron core were included in the original melt to produce the slug,

b) the elements were a contamination from a general-use crucible, or

c) the elements are present due to a preferential corrosion process where they have migrated and solidified in voids in the pin's core.

If scenario (a) were the case, then the elements would have had to have formed as discreet elements upon cooling of the melt, coming out of solid solution. Metallurgical phase diagrams should be able to resolve the potential of this scenario.

If scenario (b) were valid, then the elements are contamination of the iron melt picked up from a crucible used also to pour the copper composition. However, the possibility of contaminated elements being more evenly distributed in the slug due to the pouring process, could result in this scenario being discounted.

Scenario (c) is supported by observations detailed in Figure 4. It appears likely that there has been a migration of elements caused by preferential corrosion. At the iron/copper-alloy interface, tin has been removed preferentially from the copper-alloy composition and then distributed near the interface boundary as an element within the iron core.

3.6 Casing

Chemical analysis of the copper alloy casings revealed similarities between the samples, particularly ZA 98 and ZA 43. ZA 106 has a reduced copper wt % and significant trace iron levels in the sample possibly associated with extensive corrosion. The chemical composition of the three casings has wt % of Cu, Sn, Zn and Pb and significant trace amounts of antimony. All these elements are described in Bent's patent in what he terms a metal composition.

All the copper alloy casings are porous with an undistorted cast dendritic pattern. This is clear evidence that the copper alloy was cast in a mould directly to shape and that no cold work or work hardening was done after manufacture. Porosity associated with the last melt pool in the dendrites appears as essentially spherical bubbles throughout the cross sections of ZA 98 and ZA43. There is a visible difference in the distribution of porosity in ZA 106 as shape and number change near the copper/ iron interface.

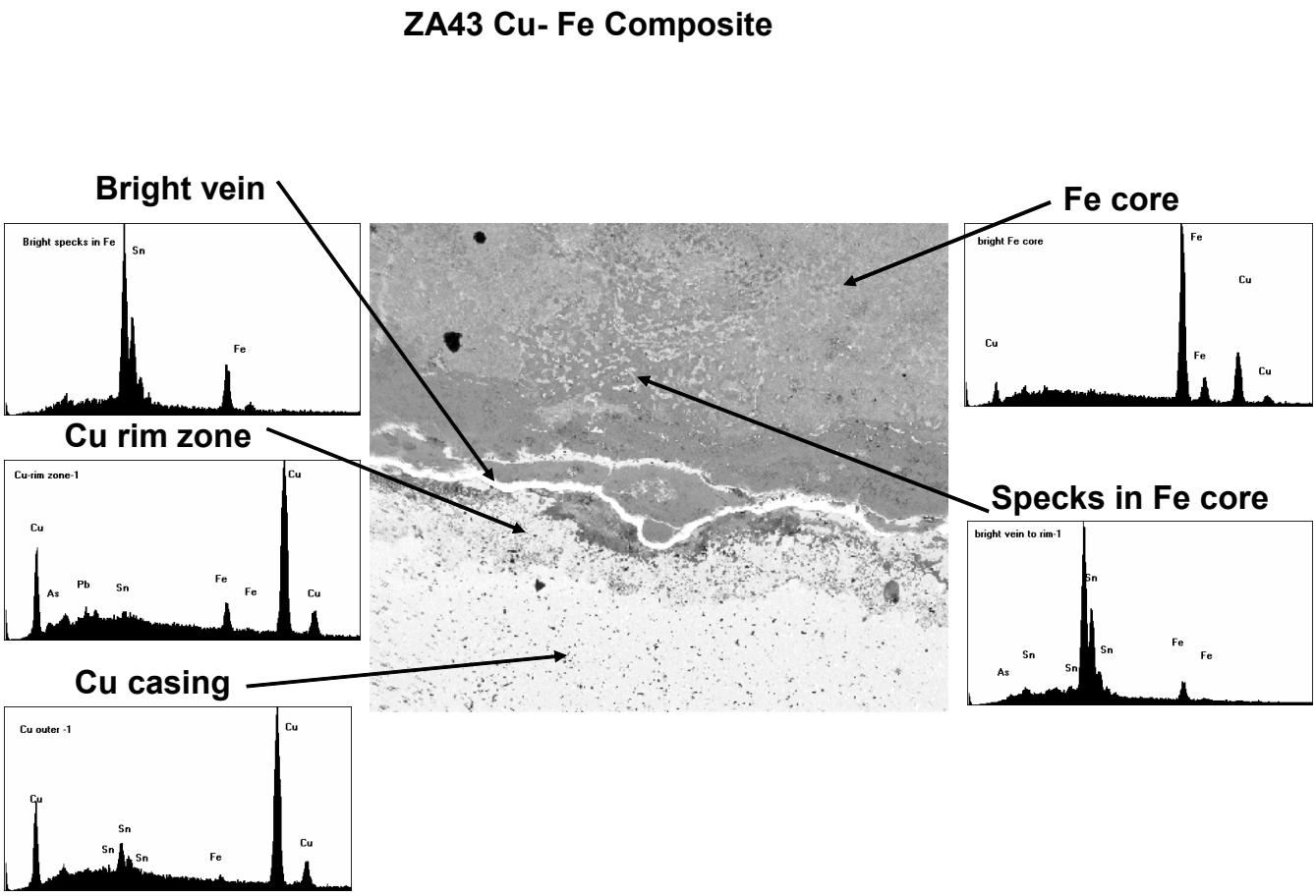

Figure 4: SEM image of Cu-Fe boundary ZA43

4. History

Typological identification and chemical analysis combine to identify the composite iron-copper alloy objects as most likely Bent pins for ships blocks. Without direct historical evidence, or knowledge of the chemistry of the ore source used by the original foundry, this identification cannot be conclusive.

Bent's pins were patented in 1778 during the American Revolutionary War, nine years prior to the *Bounty's* refit. During this period Walter Taylor was the monopoly holder of block supply to the RN and ships blocks with Bent pins were not standard issue. Research by Erskine, that he proposes to publish in the future, suggests that the Bent Pins were not standard issue to the *Bounty* but that Bligh deliberately obtained these pins specifically for the voyage (Erskine, 2004). An alternative theory for their presence has been put forward by Ron Coleman (ex Senior Curator Maritime Archaeology Queensland Museum). Coleman focuses on the practice of the dockyards at the time and suggests that since it was common in the period to reuse anything that was serviceable, it is also likely that when bought in by the Navy as the *Bethia,* the vessel was already equipped with those blocks and that they were simply re-used to alleviate further cost (Coleman, 2002). As the data is inconclusive in this matter and open for interpretation, the reason for the presence of Bent pins on the *Bounty* cannot as yet be definitely ascribed.

Regardless of the origins of the pins they were later reused by the descendants of the mutineers who sectioned them for decorative rings (Christian, 2000).

5. Conclusion

The source of copper sheathing, copper bolts, decorative jewellery and copper alloy nails found at Adamstown sites have been shown to have originated from the *Bounty*.

Chemical analysis of the material recovered during the 1999 Pitcairn Island expedition revealed that the copper artefacts associated with the *Bounty* have significantly different composition to those artefacts derived from later shipwrecks. Consequently, a picture of the mutineer settlements early utilisation of recycled *Bounty* material emerges. The one sheathing nail examined in the study that cannot be chemically matched with the *Bounty* artefact assemblage is also typologically dissimilar to the material and cannot be attributed.

Comparative studies between some *Bounty* and *Sirius* copper artefacts illustrate the similarity of the materials in their method of manufacture and metallurgical composition. The extensively cold worked copper keel bolts in both vessels' highlights the swift and uniform implementation of the Admiralty's 1786 directive to change all vessels to the 'new bolts'. A metallurgical analysis of the copper and iron composite artefacts recovered from the *Bounty* confirmed the typological identification by Erskine as Bent Pins for ships blocks, rather than bolts.

Acknowledgments

Nigel Erskine, Director, Pitcairn Project for his many comments and involvement in this paper. Janet and David Sewell for searching for patents in the U.K. Steve and Olive Christian, Ron Coleman, John Cutmore (Metallurgist, Townsville Copper Refinery), Peter Maxwell and the staff at James Cook University Advanced Analytical Centre for their comments.

References

Bligh, W. (1937). *The log of the Bounty*: *being Lieutenant William Bligh's log of the proceedings of His Majesty's armed vessel Bounty in a voyage to the South Seas, to take the breadfruit from the Society Islands to the West Indies (1792),* London, Golden Cockerel.

Erskine N.,verbal communication, Director Pitcairn Project (2000).

Bingeman, J.M., Bethell, J. P., Goodwin, P. and Mack, A. T. (2000) *Copper and other sheathing in the Royal Navy*. International Journal Nautical Archaeology, **29.**2:218-229.

Staniforth, M. (1985) *The introduction and Use of Copper Sheathing: A history*, Bulletin of the Australian Institute for Maritime Archaeology **9**:21-48

Samuels, L. E. (1983) *The Metallography of Some Copper-Alloy Relics from HMS Sirius*, Metallography **16**: 69-79.

Knight, R. J. B. (1973) *The Introduction of Copper Sheathing into the Royal Navy, 1779-1786*, The Mariner's Mirror **59**(3): 299-309.

MacLeod, I. D. (1991) *Conservation of corroded metals- a study of ships' fastenings from the wreck of HMS Sirius* (1790). Ancient and Historic metals: conservation and scientific research, Getty Conservation Institute, Getty Conservation Institute.

Stanbury, M. (1994) *HMS Sirius 1790: An illustrated catalogue of artefacts recovered from the wreck site at Norfolk Island*, Australian Institute for Maritime Archaeology. **7**.

Scott, D. A. (1991) *Metallography and Microstructure of Ancient and Historic Metals*, Archetype Books.

Erskine, N. (1999 A) *The Pitcairn project: a preliminary report of the first integrated archaeological investigation of the mutineer settlement of Pitcairn Island*, Bulletin of the Australian Institute for Maritime Archaeology **23**: 3-10.

Erskine, N. (1999 B) *Reclaiming the Bounty*, Archaeology **52**(3): 1-8.

Campbell, J. and Gesner, P. (2000) *Illustrated catalogue of artefacts from the HMS Pandora wreck site excavations 1977-1995*, Memoirs of the Queensland Museum Cultural Heritage Series. **2:** 53-159.

Erskine, N., (2004), verbal communication, Director Pitcairn Project.

Coleman, R., (2002), verbal communication, ex Senior Curator Maritime Archaeology, Queensland Museum.

Christian, S., (2000), verbal communication, direct descendant of Fletcher Christian, Pitcairn Island.

TABLE 1 COPPER ALLOY SHEATHING

Object	Object Reference	Site	Ag	Bi	Cu	Fe	Ni	Pb	Sb	Sn	Zn	As
SHEATHING	*Acadia*	wreck at Ducie Island (1881)	0.016	0.018	62.9	<0.01	0.027	0.402	0.006	0.029	33.20	0.032
	Bowden	wreck at Oeno Island (1889)	0.019	0.015	61.9	0.150	0.037	0.421	0.004	0.021	37.30	0.039
	Steve's dunkan	Bounty sheathing from Steve Christian's collection	0.009	0.039	74.3	0.137	0.018	0.283	0.017	<.005	0.091	0.620
	Bounty	Bounty wreck site (Area 7)	0.015	0.095	96.9	<0.01	0.022	0.115	0.023	<.005	0.001	0.534
	Bounty	Bounty wreck site (Area 7)	0.020	0.080	70.2	5.19	0.015	0.150	0.013	<.005	0.002	0.363
	Bounty	Bounty wreck site ZA122.3	0.025	0.131	88.6	<0.01	0.025	0.069	0.021	<.005	<.0005	0.882
	LF0037	Land site	0.00331	0.078	078.7	0.304	0.0195	0.107	<0.02	0.015	0.0299	0.466
	LF0045	Land site	0.00363	<0.015	58.4	0.0757	0.0304	0.261	<0.02	<0.015	24.0	0.0791

Table 1: Copper sheathing from HMAV *Bounty*, *Acadia*, *Bowden* and several land sites on Pitcairn Island.

TABLE 2 COPPER ALLOY NAILS

Object	Object Number	Site	Ag	Bi	Cu	Fe	Ni	Pb	Sb	Sn	Zn	As
NAIL	ZA20.1	*Bounty* site underwater	0.070	0.093	88.9	0.349	0.030	0.475	0.033	8.210	0.456	0.640
	ZA20.2	*Bounty* site underwater	<0.005	0.007	91.8	0.690	0.006	0.440	<0.005	0.102	0.450	<.150
	ZA20.3	*Bounty* site underwater	0.013	0.005	91.9	0.463	0.028	0.338	0.001	0.123	0.140	0.146
	ZA20.4	*Bounty* site underwater	0.025	0.085	90.6	1.200	0.027	0.366	0.039	5.130	0.170	0.391
	ZA20.5	*Bounty* site underwater	0.027	0.086	90.6	<0.01	0.029	0.321	0.028	3.336	0.077	0.316
	ZA20.6	*Bounty* site underwater	0.021	0.042	92.9	<0.01	0.026	0.380	0.025	2.680	0.187	0.486
	ZA20.7	*Bounty* site underwater	0.017	0.061	90.7	0.111	0.031	0.419	0.039	4.956	0.813	0.124
	LF0033.1	*Bowden* wreck at Oeno Island (1889)	0.019	0.014	80.0	0.327	0.221	0.473	0.020	0.573	17.00	0.156
	LF0033.2	*Bowden* wreck at OenoIsland (1889)	0.017	0.036	81.7	0.129	0.128	0.500	0.044	2.530	17.13	0.123
	LF0034	*St James* wreck at Oeno Island (1918)	0.019	0.004	56.9	<0.01	0.022	0.464	0.032	0.385	32.80	<.002
	LF0037	Field #37.73	0.033	0.015	88.1	<0.01	0.008	0.247	0.003	0.015	0.005	<.002
	LF0037.3	Field # 37.3 characteristics of *Bounty* nail	0.012	0.017	83.0	0.043	0.037	0.512	0.044	0.574	10.40	0.207
	LF0037 (5.2)	Field # 37.3 Cu alloy nail	0.016	0.079	88.7	0.160	0.025	0.421	0.041	5.480	0.837	0.125
	LF0042.1	Cemetery Adamstown	0.017	0.157	92.0	<0.01	0.027	0.318	0.035	4.400	0.134	0.272
	LF0042.2	Cemetery Adamstown	0.035	0.082	89.7	0.048	0.022	0.381	0.050	5.250	0.268	0.188
	LF0042.3	Cemetery Adamstown	0.017	0.121	99.7	<0.01	0.022	0.053	0.021	0.047	0.026	0.732
	18	*Acadia* (1881) wrecked at Ducie Island.	0.015	0.026	79.3	0.081	0.063	0.372	0.014	1.556	11.20	0.026
	19	*Acadia* (1881) wrecked at Ducie Island.	0.018	0.012	74.3	0.064	0.057	0.421	0.018	1.298	10.00	<.002
	20	Steve's Duncan	0.018	0.091	86.6	0.430	0.022	0.324	0.056	5.260	0.171	0.551

Table 2: Nails recovered from Pitcairn Island, and the wrecks of the *Bounty*, *St James*, *Bowden* and *Acadia*.

TABLE 3 COMPOSITE IRON - COPPER ALLOY PINS

Object	Object Number	Site	Ag	Bi	Cu	Fe	Ni	Pb	Sb	Sn	Zn	As
Pin Fe core	ZA43	*Bounty*	0.000	0.003	0.2	96.2	0.104	0.029	0.001	0.014	0.019	<.002
Pin Cu casing	ZA43	*Bounty*	0.037	0.078	82.2	0.596	0.078	7.460	0.426	2.120	2.410	0.302
Pin Fe core	ZA106	*Bounty*	0.004	0.011	4.1	57.1	0.005	1.240	0.005	0.753	0.124	<.002
Pin Cu casing	ZA106	*Bounty*	0.030	0.070	62.8	16.1	0.047	5.200	0.205	3.834	0.944	0.248
Pin Cu casing	ZA98	*Bounty*	0.081	0.075	86.4	0.177	0.090	6.600	0.622	2.177	1.352	0.687
Bolt Cu	ZA100	*Bounty*	0.022	0.087	96.6	0.187	0.021	0.201	0.013	0.038	0.013	0.390
Bolt Cu	SI 32C*	*Sirius*	0.236	nd	98.35	0.0093	0.094	0.22	0.162	0.47	0.029	0.06

Table 3: Composite objects recovered from the HMAV *Bounty* shipwreck site.

* MacLeod, (1985): 54-5; 59; Stanbury, (1994), Appendix 2.1

Objects from the ancient site of Qalat Rabah (Calatrava la Vieja): a case study on the characterization and conservation of Islamic gilded bronzes from Spain

J. Barrio [a], L. Campanella [b], M. Ferretti [c*], A. I. Pardo [a], M. Retuerce [d]

[a] Departamento de Prehistoria y Arqueología, Universidad Autónoma de Madrid, Spain
[b] Dipartimento di Chimica, Università di Roma "La Sapienza", Italy
[c] CNR – Istituto per le Tecnologie Applicate ai Beni Culturali, Monterotondo St. (Roma), Italy
[d] Facultad de Ciencias Humanas, Universidad SEK de Segovia, Spain

Abstract

The recent archaeological excavations at Qalat Rabah (Calatrava la Vieja, Spain) brought to light a number of gilded pieces – harness and personal ornaments – of very high aesthetic and technological quality. These artefacts are being studied from different points of view, as they unquestionably represented the state of the art in the Mediterranean Europe of the Middle Ages. Selected pieces were investigated, mainly by scanning electron microscopy (SEM-EDXA), with regard to the corrosion structures and the gilding technique. The identification of the corrosion products and their distribution provided information for the conservation treatments, whereas the simultaneous presence of gold leaf and mercury lead to hypothesize either a gilding technique known as "cold mercury gilding" or a traditional leaf gilding in which mercury is already contained in the gold.

Resumen

Las últimas excavaciones en Qalat Rabah (Calatrava La Vieja, España) han sacado a la luz numerosas piezas sobredoradas (adornos personales, apliques para muebles e indumentaria, etc.) de gran calidad estética y tecnológica. Estos objetos ha sido estudiados desde distintos puntos de vista ya que constituyen una incuestionable representación del arte en el Mediterráneo europeo en la Edad Media. Se han seleccionado algunos de ellos para, mediante microscopio electrónico de barrido (SEM-EDXA), realizar un estudio de la estructura de la corrosión y la posible técnica utilizada en el dorado. La identificación de los productos de corrosión y su distribución aporta una valiosa información para la conservación y la restauración de piezas de estas características. Además, la presencia conjunta de una lámina de oro y de mercurio nos ha llevado a dos hipótesis distintas: una, que se trate de una técnica de dorado conocida como "cold mercury gilding"; y la otra, que sea una técnica de dorado con lámina de oro de tipo tradicional y que el mercurio ya estuviese presente en el oro desde el inicio.

Keywords: gilded bronzes, gilding techniques, conservation, Islamic artefacts, corrosion processes, SEM-EDXA

1. Introduction

Archaeological excavations started in 1984 in the Islamic city of Qalat Rabah (Calatrava la Vieja) in Upper Guadiana, Spain. The city played a starring role during the Middle Ages; being founded during the 8th century A.D. by the Omeyad Dynasty as a strategic point to protect Cordoba from the rebellious Toledo. It became the capital of the region during the three centuries of Omeyad domination of Al-Andalus. The city was annexed by the Christian kingdom of Castilla shortly before the battle of Las Navas de Tolosa, in 1212. Then Calatrava underwent an irreversible decay, ending with the final abandonment of the city at the beginning of the 15th

* Corresponding author: tel +39 06 9067 2690; fax +39 06 9067 2373; email: marco.ferretti@itabc.cnr.it

century. The archaeological evidence points out the existence of a bronze workshop – which specialized in gilding techniques – placed in the Islamic part of the city.

So far a number of metallic objects has been recovered from the site, including a set of gilded bronze objects, outstanding for the high aesthetic and technological quality (Figure 1). They are small decorative elements, appliqués for clothes and furniture, buttons, etc.; with a few exceptions, they present poor conservation conditions and loss of the gilding.

Our research was designed with the aims of investigating the ancient gilding techniques, going deeper into the mechanisms of deterioration – including those of the gilding – and identifying optimum cleaning and conservation treatments. Following a previous study (Barrio et al., 2003) on a first group of objects, we continued and investigated a second group of recently excavated pieces.

Figure 1. Objects excavated at Qalat Rabah, significant for the high artistic and technological level.

2. Background on the gilding techniques

The high artistic and technical level achieved by the Islamic metal ateliers in the Mediterranean regions where this culture flourished in the Middle Ages (Allan, 1979, 1986), is clearly demonstrated by the wonderful gilded objects remaining from that period. The fact that even small ornamental objects were gilded, such as those from Calatrava la Vieja, points out the widespread use of this technique in Medieval Spain. Furthermore, the production of small gilded objects used as personal ornaments or harness appliqués became a specialization in the atelier of Qalat Rabat.

As regards the gilding techniques concerned with the objects discussed here, those involving cold hammering of gold sheets – documented in very few Islamic coins – can be excluded, as mercury was detected. Rather we had to focus on those artefacts involving this element that is, cold mercury gilding and fire gilding. The techniques can be shortly described as follows (Oddy, 1993):

- cold mercury gilding: the mercury is spread over the object's surface, then gold leaf is applied so that the amalgam is formed *in situ* at the interface between the leaf and the object; mercury is allowed to evaporate at room temperature;
- fire gilding: the gold-mercury amalgam is prepared separately and applied to the object's surface; subsequently the object is heated to allow for mercury evaporation.

Though the former technique has been mentioned since Pliny the Elder (Natural history, XXIII, 64-65, 100), replication experiments carried out by Anheuser (Anheuser, 1996) show that Oddy's description of the process may be oversimplified; in particular the word "cold" is questioned, as Anheuser could not avoid the complete amalgamation of the gold leaf. Consequently heating followed by burnishing was necessary to remove excess mercury and obtain a good quality golden aspect. As regards the latter technique, we have references in ancient sources from the 4th century A.D. Fire gilding seems to be the most frequently used method during the Middle Ages (Oddy, 1993). It was early in history mastered by the Islamic metal workers – it is mentioned in the texts of Al-Hamdani (A.D. 942) – although gilding methods were probably known in Al-Andalus even earlier. This is demonstrated by a fake dinar coin from the conquest period (A.D. 711-755) that shows a gilded layer of about 5 microns (Paredes, 1998), which is not too far from the 2-4 microns measured on the first group of Calatrava

objects (Barrio et al., 2003). A later text, *Al-Muqaddimah* by the Sevillan historian Ibn Khaldoum (1332-1402) (Ibn Jaldún, 1977), sheds light on the methods that contemporary alchemists used to produce fake coins: among them it includes amalgam silver plating, which is identical to the technique used for gilding; numerous material evidences are available concerning the use of this method.

Analytical methods simply based on the detection of mercury do not help much to distinguish the two techniques, as mercury is present in both cases (Oddy, 1993, 2000). To obtain significant information one has to go further and consider the microstructure of the gilded layers and their immediate environments.

3. Description and preservation state of the objects

As gilding is usually hidden by the corrosion products of copper, we carried out a preliminary selection of those objects or fragments that, for their morphology, could be supposed to have gilding. Finally the following five objects were chosen by also taking into account the conservation conditions, in order to provide different corrosion situations.

Object A (Figure 2): fretted ornament, gilded on the obverse, measuring 70mm (length), 24mm (width), 1mm (thickness). The decoration repeats a geometrical pattern based on the square as a main figure. The reverse, which is not shown, is not gilded. A punched decoration goes across the whole decorative scheme. The samples were taken after restoration, to be more significant to the gilding technique. The preservation state is excellent with a sound metallic core and an almost complete gold layer.

Figure 2. Object A: fretted ornament.

Object B (Figure 3): Similar to object A, with a geometrical pattern, measuring about 46mm (length), 24mm (width), 3mm (thickness). It differs greatly from object A as regards the preservation state: it is completely mineralized – and therefore extremely fragile – and no remains of gilding were visible in the preliminary optical examination. Samples were taken from loose fragments prior to treatment. Analytical investigations proved that it was gilded.

Figure 3. Object B: fretted ornament.

The different preservation states of the two objects allowed us to comparatively evaluate the corrosion processes and the fabrication technology. No remains of gilding were observed on the other three (C,D and E) objects prior to restoration. Only Object E, further investigated by optical microscopy after restoration, showed the presence of gold.

Object C (Figure 4 left): buckle in very poor preservation state, fragmented and incomplete, measuring about 41mm (length), 28mm (width), 2mm (thickness).

Object D (Figure 4 centre): disc-shaped button or appliqué with a central rounded protuberance, fragmented and incomplete, measuring about 45mm (diameter), 1mm (thickness).

Object E (Figure 4 right): unidentified object with a flattened conic shape, measuring 60mm (length), 29mm (maximum width), 15mm (minimum width) and 9mm (thickness).

Figure 4. Objects C, D and E: buckle (left), button or applique (centre), unidentified object (right).

The initial preservation state of these objects is generally poor and the surface is severely deteriorated. Preliminary optical examination showed, above the gilding, a layer of corrosion products hiding completely the original surface. As the cleaning progressed, we could characterize the corrosion products and go deeper into the deterioration processes.

The corrosion layer was formed by a heterogeneous mixture of soil, calcium carbonate, chlorides, copper oxide and copper carbonate. This is quite a frequent combination in archaeological copper or copper based alloys. The original gilding appeared during the cleaning underneath these products. The gilding was in different preservation conditions depending on the progress of the core corrosion.

For gilded objects much of the corrosion is due to the galvanic cells that are produced in the presence of humidity, between metals with different electrochemical potentials - namely copper and gold. During this process gold is cathodically protected and causes the progressive corrosion of copper (Selwyn, 2000). The gilding deterioration is due to the volume increase of the corrosion products – mainly basic copper chlorides (atacamite) – at the interface with gold. This produces a progressive swelling that finally results in the gilding detachment. This is not the case for Object A: the minimum chloride attack has kept the metallic core almost uncorroded and the gilding continuous. However, Object B has suffered a complete mineralization, so that remains of the gilding can only be observed by scanning electron microscope and microanalysis.

4. Cleaning and conservation techniques

Our restoration criterion had two clear objectives:

1. recovering the intact gilded areas so as to read adequately the original surfaces; and
2. achieving a good metallic stability to provide for the future integrity of the pieces.

The initial decay state of each of the objects called for individualized interventions, although all of them were carried out along common lines. The working protocol has varied for each object depending on the mineralization conditions and the presence or absence of a sound metal core. A combination of mechanical cleaning and physical-chemical cleaning (organic solvents – Acetone 50%/Xylene 50% – plus ultrasonic bath), already used in the restoring of great golden bronzes such as the statue of Marcus Aurelius (Fiorentino, 1994), has also proved itself effective on these Islamic bronzes.

The use of optical instruments such as binocular microscopes is a must when working on these small objects, where intact gilding might appear underneath the visible surface any time during the cleaning process. Mechanical cleaning methods, complemented with the advance of optical instruments, are today considered a very suitable solution for the cleaning of copper-based objects (Scott, 2002). The aim of the cleaning methods is to detect and recover all the gilding remains which can not be seen due to the corrosion of surfaces, as was the case in the analysed and restored sample objects from Calatrava. They are highly safe methods as they allow effective and constant control of the process, a specially desirable characteristic when working with deeply mineralized pieces.

Prior to mechanical cleaning, an optical examination was made and some cleaning probes were done. After establishing a gilding zone mechanical cleaning was performed under the microscope lens. The mechanical cleaning was totally manual using surgical scalpel blades and an organic brush. After finishing mechanical cleaning the objects were prepared for analysis in order not to disturb the results with the chemical products used in stabilization. The process ended with a stabilization and inhibition treatment with BTA in a 3% ethanol solution. Afterwards the pieces were stove-dried at 105ºC and covered in a protective double coating of Paraloid B-72 in a 5% xylene solution and micro-crystalline wax in W.S. at 5%, 60°C. Both Paraloid and the wax were vacuum-applied to guarantee an adequate penetration. The use of a double protective layer of acrylic resins and micro-crystalline mineral waxes has proved itself effective to protect copper-based metals from different aggressive atmospheres (Mourey, 1997; Díaz, 1997).

4.1 Microstructural investigations

Samples from the objects were investigated at the scanning electron microscope (SEM) to study the gilding technique and collect more information on materials and corrosion products. In one case (Object E) it was also possible to identify the remains of textiles fibres.

Sample CV-01 26-64 (Object A): This is the most significant sample as regards the gilding technique; in a previous publication (Barrio et al., 2003) the investigation of other samples lead to the hypothesis of a technique similar to the so-called “cold mercury gilding” (Oddy, 1993); here we have the same experimental evidence, but the discussion tries to discern greater knowledge.

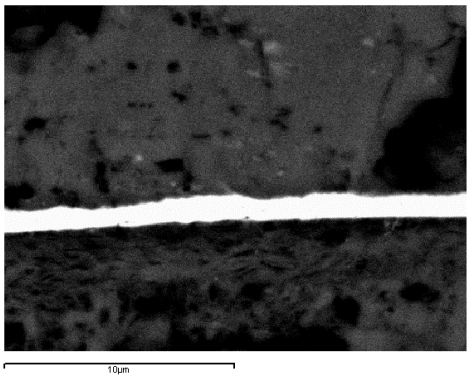

Figure 5. Sample CV-01 26-64 (object A), back-scattered electrons image of the gold layer.

Figure 5 shows a detail of the gold layer: it is approximately one micron thick and contains Hg. The thinness as well as the absence of any apparent granular structure seem to exclude proper fire gilding (Cowell et al., 1991; Jett, 1993). The use of gold leaf also seems to be confirmed by Figure 6 that shows the leaves overlapping in different parts of the sample. Hg is homogeneously distributed over the leaf thickness with a concentration ratio Au/Hg between 10 and 12. Given these facts one can propose different hypotheses, all in need of further investigation:

a) it is a leaf gilding in which the adhesion was obtained by mercury; the latter was applied to the surface in such small amounts to avoid the complete amalgamation of the leaf described by Anheuser. The homogeneous distribution of Hg over the leaf thickness may be due to the spontaneous diffusion of this element, possibly enhanced by a thermal treatment; or

b) it is a traditional leaf gilding; mercury took no part in the gilding process, as it was already present in the gold before the leaf application.

It has to be remarked that, given the sound aspect of the Au layer and the leaves overlapping, no complete amalgamation seems to have occurred here. The composition of the object's body metal is: Cu 92%, Pb 6%, Sb 2%; the latter seems related to Pb, as it has the same distribution. The presence of Pb is quite unusual and contradicts the practice, common to several cultures and periods, that avoids significant amounts of this element in alloys suitable for mercury gilding. This would confirm the latter hypothesis ie, that we are in the presence of a traditional leaf gilding, for which it is irrelevant whether the bronze is leaded or not.

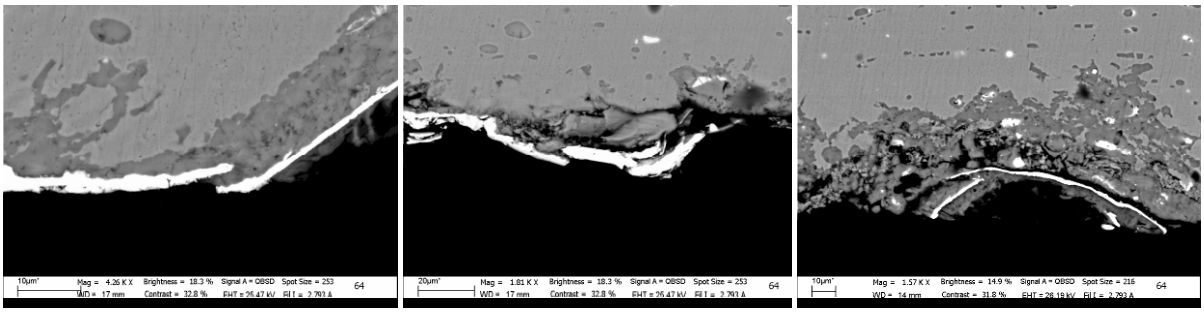

Figure 6. Sample CV-01 26-64 (object A), back-scattered electrons images showing partial overlapping of the gold leaves in different parts of the sample.

Sample CV-03 15-461 (Object B): the sample (Figure 7) shows a corrosion pattern typical of wires, actually two wires of 1.5-2 mm in diameter, possibly twisted and hammered. The gilding is visible in the lower

part of the cross-section: it is 2-4 microns thick (see detail) and contains Hg in higher concentration with respect to the previous sample, the ratio Au/Hg being around six.

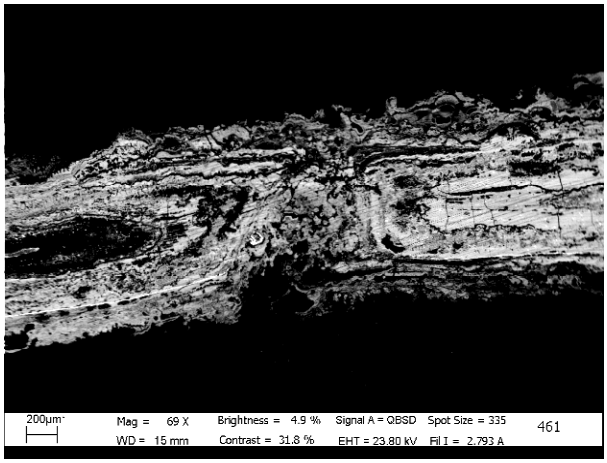

Figure 7. Sample CV-03 15-461 (object B), back-scattered electrons image showing two contiguous elements (possibly wires) with concentric corrosion structures

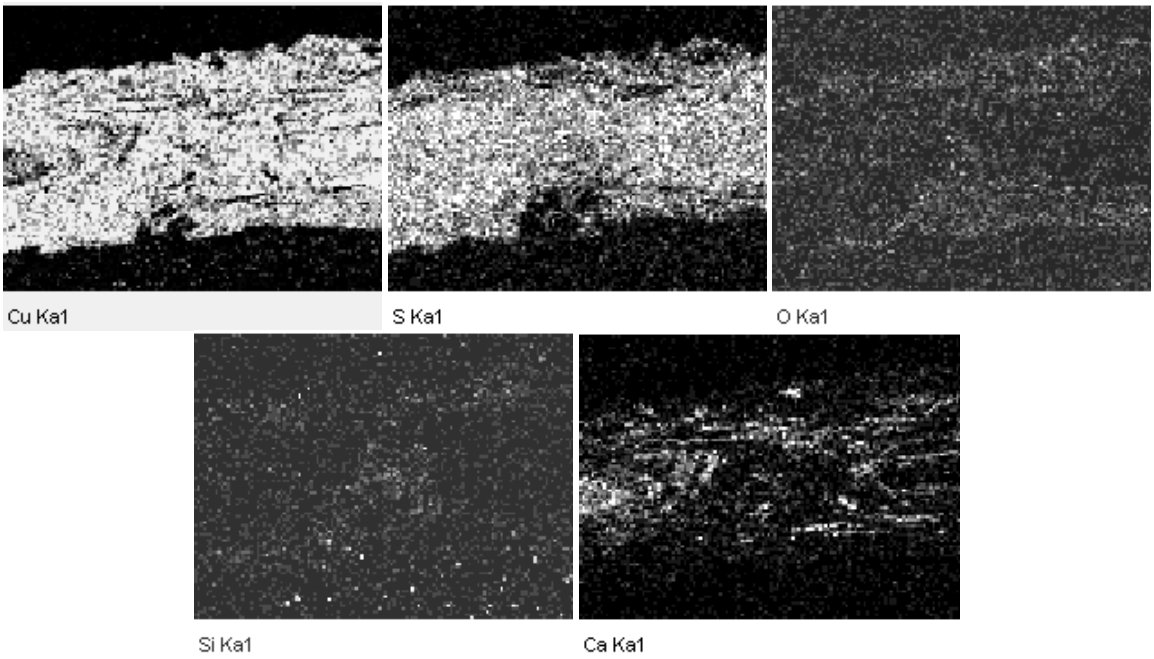

Figure 8. Sample CV-03 15-461 (object B), elemental maps concerning the area of Figure 7.

`The elemental maps (Figure 8) show that S and Cu are more or less homogeneously distributed all over the sample, whereas O is detected in the outer layers of the wires. Figure 9 shows the gold leaf and its surroundings; it is worth noting that among all the Calatrava samples, only this one has S above detection limits. The supposed copper sulphide appears both below and above the gilded surface, but it seems remarkably more solid in the interior parts (upper part of the image). Furthermore, the microanalysis shows 4-5% Au homogeneously distributed on the cross-section. No other elements, except those from soil contamination, are detected in significant amounts.

The interpretation of these data is not straightforward, as they are not completely consistent with the present knowledge of either niello or black-patinated bronze (Craddock et al., 1993), however the same reference, at p.120, reports a recipe, included in the Islamic texts of Zosimos, that involves the use of sulphur to produce a black-coloured copper. At present the experimental evidence only suggests the possible pertinence of the sample to a gilded decoration.

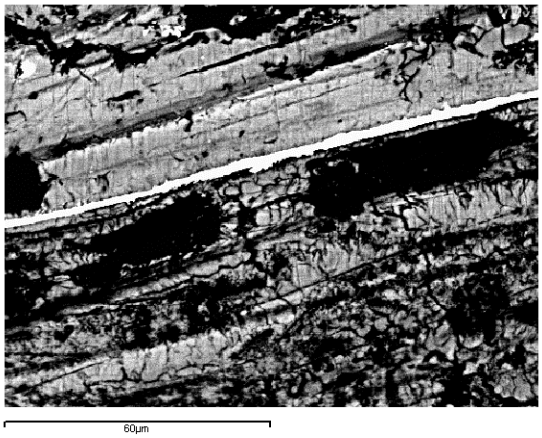

Figure 9. Sample CV-03 15-461 (object B), back-scattered electrons image of the gold leaf.

Sample CV-03 28-133 (Object C): the sample is deeply corroded (Figure 10); the alloy is a brass showing – in its uncorroded parts – the composition: Cu 87%, Zn 12%, Sn 1%. The most abundant corrosion products are copper chlorides, incorporating a few uncorroded grains; the maps in Figure 11 show a surface layer, probably made of redeposited metallic Cu and, above it an apparent Pb enrichment. The thinness of the latter layer suggests a deposition of Pb corrosion products (possibly carbonate) from the burial context, as the alloy does not contain significant amounts of Pb.

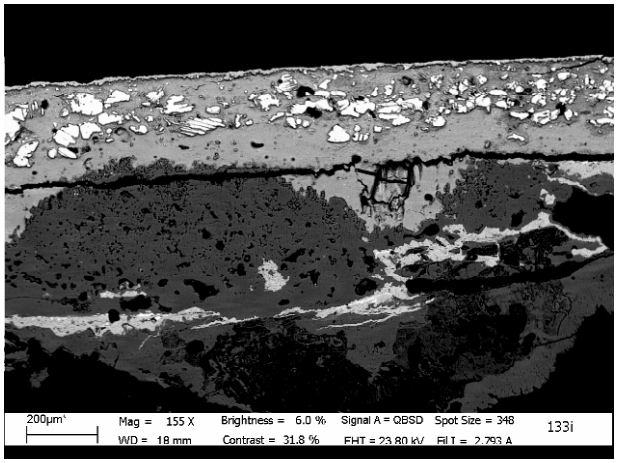

Figure 10. Sample CV-03 28-133 (object C), back-scattered electrons image of the sample's corrosion pattern.

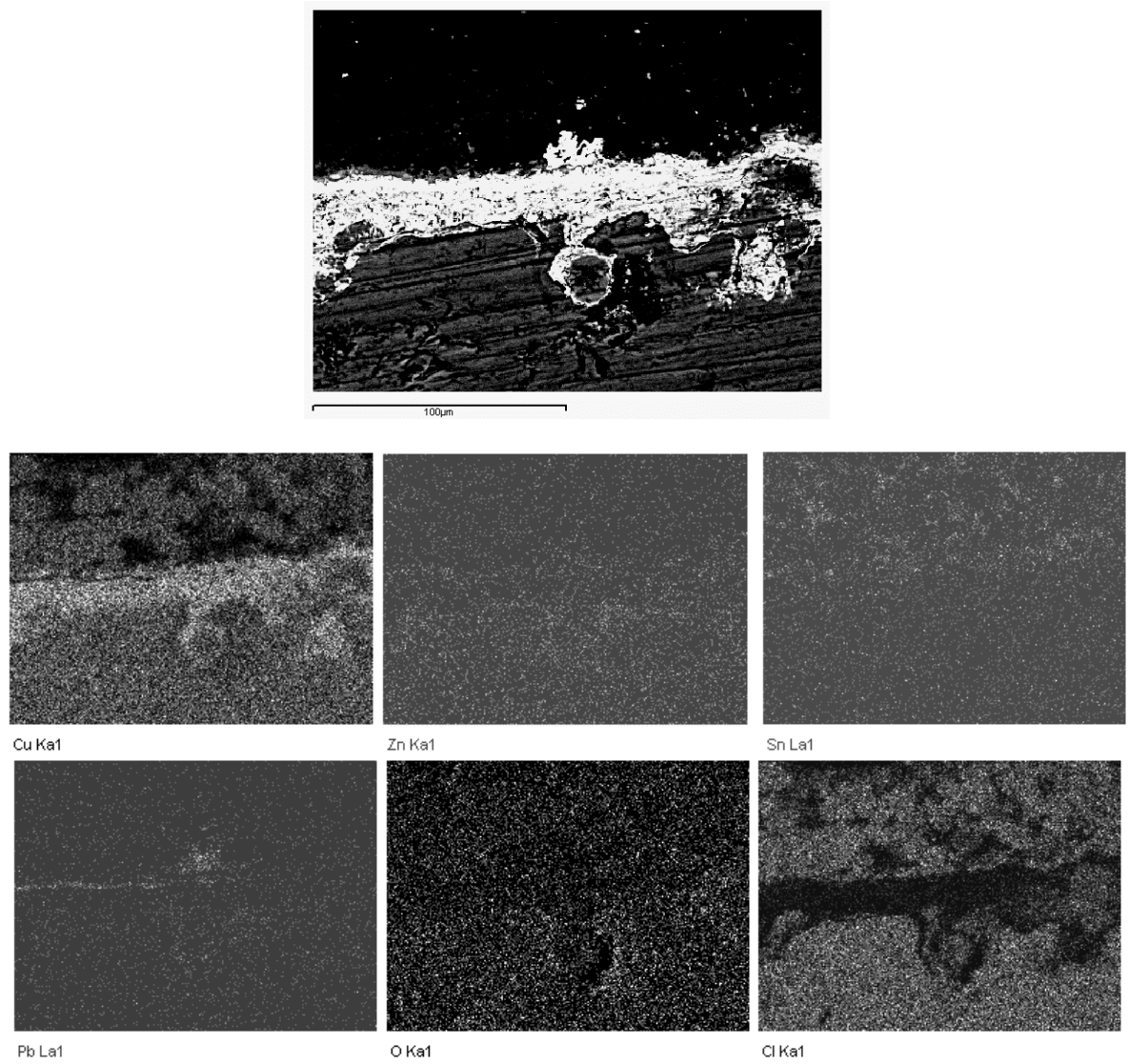

Figure 11. Sample CV-03 28-133 (object C), back-scattered electrons image and elemental maps showing form top to bottom: copper chlorides, a thin lead-enriched layer, a thicker layer of redeposited metallic copper, copper chlorides.

Sample CV-03 26-248 (Object D): this sample is deeply corroded (Figure 12); the alloy is a brass very similar to the previous one; its uncorroded parts show the composition: Cu: 86%, Zn 13%, Sn 1% with Pb just above the detection limits.

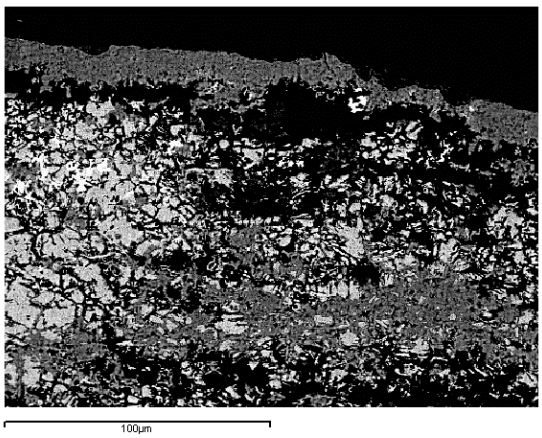

Figure 12. Sample CV-03 26-248 (object D), back-scattered electrons image showing the deep sample corrosion.

Sample CV-03 28-127 (Object E): the alloy (Figure 13) is a brass with composition: Cu 76%, Zn 18%, Sn 2%, Pb 4%. Before embedding the sample in the resin, it was also possible to observe the remains of fibres on the surface: these were identified as cotton (Figure 14).

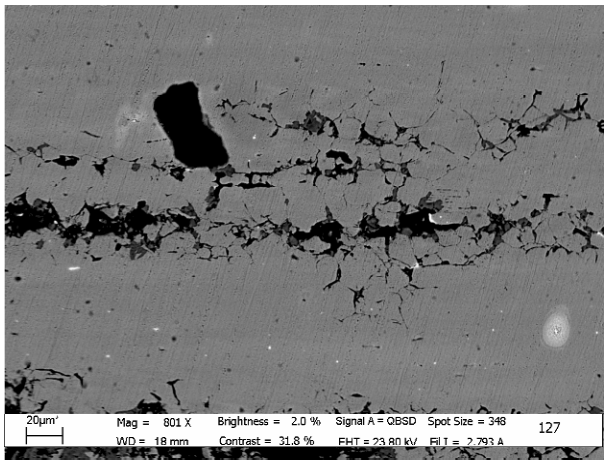

Figure 13. Sample CV-03 28-127 (object E), back-scattered electrons image of the cross-section.

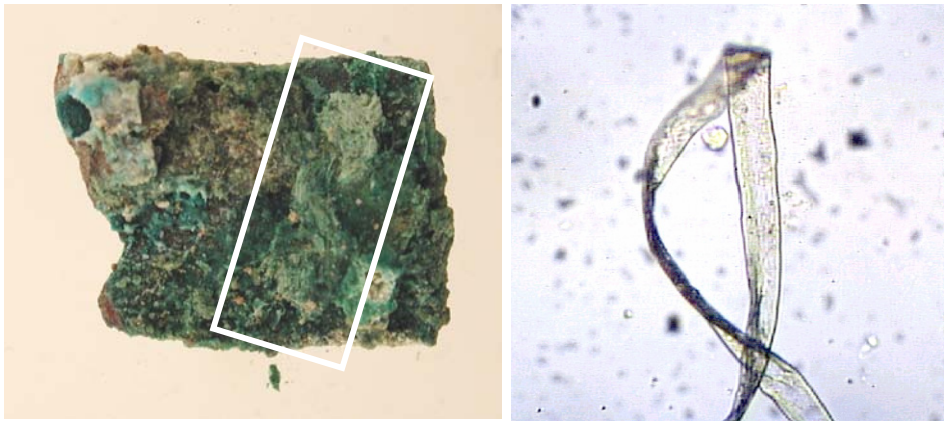

Figure 14. Sample CV-03 28-127 (object E), remains of textile fibres and (right) image of a single fibre (optical microscope, courtesy of A. Lentini, CNR-ITABC), identified as cotton.

5. Conclusions

The restoration of a second group of objects from the ancient city of Qalat Rabah (Calatrava la Vieja, Spain) was undertaken with the objectives of: first, recovering the intact gilded areas so as to read adequately the original surfaces; second, achieving a good metallic stability to provide for the future integrity of the pieces. The working protocol involved a combination of mechanical cleaning and physical-chemical cleaning and a final stabilization and inhibition treatment.

A further goal was to investigate the gilding technique, the alloys composition and the corrosion products. The presence of mercury and the partial overlapping of gold layers were observed; furthermore the gildings appeared solid, with no granular structure, and thinner than proper fire gildings. Such an experimental evidence is similar to that described in a previous work (Barrio *et al.*, 2003), however its interpretation needs to be someway revised. In the light of Anheuser's replication experiments, Oddy's theory of "cold mercury gilding" can be retained only if one assumes that mercury was spread in much lower amounts than Anheuser could achieve, which obviously opens the problem of how this was done. A second and opposing hypothesis is that of a traditional leaf gilding: where mercury has nothing to do with the gilding technique, it is already in the gold leaf and is possibly related to the techniques used to refine the gold or recover it from scrap materials. This hypothesis is also consistent with the fact that one of the gilded objects is made of leaded bronze (6% Pb), that in principle would be unsuitable for mercury gilding.

The sample (CV-03 15-461) from one of the two gilded objects is suspected to be a fragment of decoration: it seems to consist of two wires, twisted and hammered, with local gildings; the presence of gold and sulphur – this is the only sample from Calatrava in which sulphur was found. It evokes the Islamic texts of Zosimos and his recipe for the production of a black-coloured copper. As regards the composition of non-gilded objects, they are all made of brass; two (C and D) are compositionally similar; Object E provided the remains of textile fibres that were identified as cotton.

If one excludes the sample with sulphur, whose nature is not completely understood at the moment, quite common corrosion patterns were found; a peculiar structure was observed in one of the samples, consisting – from the surface inwards – in: a thin layer of lead corrosion products from the burial context, a thicker layer of redeposited metallic copper and, finally, copper chlorides resulting from the almost complete corrosion of the metal.

Acknowledgements

We are grateful to those who contributed to the progress of the research; in particular to:

- Dr. Giuseppe Caruso, Dipartimento di Chimica, Università di Roma "La Sapienza", for having carried out the SEM measurements in Roma;
- Dr. Esperanza Salvador, SIDI, Universidad Autónoma de Madrid, for having carried out the SEM measurements in Madrid;
- Mr. Alessandro Lentini, CNR Istituto per le Tecnologie Applicate ai Beni Culturali, Roma, for the identification of the textile fibres;
- Dr. Cecilia Bartuli, Mr. Mauro Spinosi and Mr. Carmine Panzironi, Dipartimento di Ingegneria Chimica e dei Materiali, Università di Roma "La Sapienza", for the support in sample preparation;
- Mrs. Olimpia Colacicchi, Soprintendenza Archeologica di Roma, for the photographic documentation of the samples and for the invaluable discussions.

References

Allan, J.W. (1979) *Persian metal technology (700-1300 A.D.)* Oxford Oriental Monographs n°2, Ithica Press, London.

Allan, J.W. (1986) *Metalwork of the Islamic World, The Aron Collection.* Sotheby´s, London.

Anheuser, K. (1996) *An investigation of amalgam gilding and silvering on metalwork*, doctorate thesis, Oxford, 34-41, 50-56, 69-71.

Barrio, J., Ferretti, M. (2003) *Archaeometry and conservation of gilded bronzes from the city of Qalat Rabah (Calatrava La Vieja) Spain*, in Proc. Archaeometallurgy in Europe, Associazione Italiana di Metallurgia, Milano, 391-400.

Cowell, M., La Niece, S. (1991) *Metalwork: Artifice and artistry*, in Science and the Past, Bowman, S. (ed.), The Trustees of the British Museum, London, 74-98.

Craddock, P., Giumlia-Mair, A. (1993) *Hsmn-Km, Corinthian bronze, shakudo: black-patinated bronze in the ancient world*, in Metal Plating & Patination, La Niece, S., Craddock, P. (eds.), Butterworth-Heinemann Ltd, Oxford, 101-127.

Diaz, S. (1997) *Traitement de Resatauration appliqué à une statue d´Apollon en Bronze trouvée au fond de la mer*, in Macleod, I., Pennec, S., Robbiola, L. (Eds.) Proc. Int. Conference on Metals Conservation, Metal 95, Semur en Auxois, sept.1995, James & James, London, 178-182.

Fiorentino, P. (1994) *Restoration of the monuments of Marcus Aurelius: Facts and Comments,* in Scott/Podany/Considine (Eds.), Ancient & Historic Metals. Conservation ans Scientific Research, The Getty Conservation Institute, 21-23.

Ibn Jaldún (1977) *Al- Muqaddimah*, Edt. Fondo de Cultura Económica, México.

Jett, P. (1993) *A study of the gilding of Chinese Buddhist bronzes*, in Metal Plating & Patination, La Niece, S., Craddock, P. (eds.), Butterworth-Heinemann Ltd, Oxford, 193-200.

Mourey, W. (1997) *Synthèse des essais sur les rêvetements de protection des Métaux (1986-1995)*, in Macleod, I., Pennec, S., Robbiola, L. (Eds.) Proc. Int. Conference on Metals Conservation, Metal 95, Semur en Auxois, sept.1995, James & James, London, 225-227.

Oddy, A. (1993) *Gilding of metals in the Old World*, in Metal Plating & Patination, La Niece, S., Craddock, P. (eds.), Butterworth-Heinemann Ltd, Oxford, 171-181.

Oddy, A. (2000) *A History of gilding with particular reference to statuary,* in Drayman-Weiser, T. (Ed*.)*, Gilded Metals. History, Technology and Conservation*.* Archetype Publications, London.

Paredes, N. (1998) *Técnicas de falsificación de monedas en Al-Andalus: Testimonios materiales.* Memoria de Licenciatura, Universidad Autónoma de Madrid, unpublished.

Pliny, *Natural History XIII*, 64-65, 100.

Scott, D. (2002), *Cooper and bronze in art: corrosion, colorants, conservation*, Getty Publications, Los Angeles.

Selwyn, L. (2000) *Corrosion Chemistry of Gilded Silver and Copper* in Drayman-Weiser, T. (Ed.), Gilded Metals. History, Technology and Conservation. Archetype Publications, London, 21-47.

Proceedings of Metal 2004 National Museum of Australia Canberra ACT 4–8 October 2004
ABN 70 592 297 967

Electrochemical characterisation of patina protectiveness evolution on outdoor bronze sculptures

M. A. Crespo [a], G. P. Cicileo [b], B. M. Rosales [c]

[a] Area de Conservación-Restauración, Secretaría de Cultura G.C.B.A.
Av. de Mayo 575 6º Piso, Buenos Aires, Argentina. cloclo@infovia.com.ar

[b] CITEFA-DEICOR, Juan Bautista de Lasalle 4397, (B1603ALO) Villa Martelli, Argentina.

[c] CIDEPINT, Av.52 entre 121 y 122, (B1900AYB) La Plata, Argentina.

Abstract

A modern aesthetic criterion focuses on the visual effect produced by the original patinas colour transformations. The La Recoleta cemetery is one of the sites where numerous bronze sculptures, recognised by their aesthetic and historical value, can be found. Three works in this cemetery were selected for this study. The aim of this work was to elaborate an intervention criterion based on the present state of patinas by means of non-destructive in situ analyses. On different coloured areas the electrochemical behaviour and chemical composition of patinas were determined. Our interdisciplinary intervention policy considers the aesthetic intention of the sculptor and the transformation of the original patina since the sculpture installation to its present reading, in the frame of a scientific and historical study.

Keywords: patina, electrochemical potential, protectiveness, in situ, bronze, monuments.

1. Introduction

The public space of Buenos Aires City has numerous sculpture repositories made by European and Argentine sculptors, cemeteries among them. That of La Recoleta is recognised by its aesthetic and historical value. The selection of this material is based on its expressive potential and conceptions around temporality (Crespo, 2002). Time and its effects are part of the expectations of the authors either in the maintenance of a uniform colour or in the chromatic heterogeneity achieved since the beginning of the work and accentuated in the course of time by its outdoor exposure (Crespo, 2001).

Both reasons, taking part in the aesthetics of the sculptures are observed in the studied art works: the sculptures "El Karma", by Troiano-Troiani, the two metallic pieces of the group Mausoleum to Adolfo Alsina, by Margarita Bonnet, and “El Cristo Central” by Zonza Briano.

In the first and third, “El Karma” and “El Cristo Central” respectively, the artists intention with the artificial patina developed was to create an heterogeneity associated with

Corresponding author: cloclo@infovia.com.ar

colour (green bluish, green yellowish) emphasising the concave and convex areas in the formal interpretation of the work (Crespo et al, 2000). Conversely, in the metallic sculptures of Monument Tribute to A. Alsina, the intention was to create an homogeneous artificial green patina whose harmonic relationship with the rest of the materials (red granite stone and white marble of the exalted figure) determining the reading rhythm of the monument (Tribute commission, 1915). To define the instance in the piece time circuit during the work diagnosis, we refer to the Restoration theory of Cesari Brandi: "Time, however it may structure the rhythm, is present in the work in three moments, not yet under the formal aspect but in its phenomenology, whatever the masterpiece it concerns. First as duration of the piece while it is being conceived by the artist; secondly as the interval since the end of the creative process to the moment in which our consciousness updates the masterpiece and thirdly as the instant of the art work irruption in the consciousness" (Brandi C., 1988).

In this diagnostic work we will focus on the span of time starting from the creative process to the present moment, when the patinas transformations are altered with the purpose to establish the moment of the piece in which intervention occurs in each case.

Nevertheless it is during this exposure (by the atmospheric pollutant causing alterations) and due to the uneven quality from smelting (as far as heterogeneity of the alloy and patches made with different alloys further to the original cast) that patina transformations change from their positive chromatic and protective characteristics to a negative sense (unpleasant aspect and protectiveness decrease).

Atmospheric corrosion, the most frequent cause of destruction of different metals and alloys, has increased in the last years, especially in urban atmospheres, due to the action of different environmental polluting agents and acid rain. This type of corrosion is electrochemical and is favoured in atmospheres with high relative humidity, since the electrolyte is a liquid water layer originated from rain, dew or condensation. The magnitude of the attack depends on the time during which this water layer remains on the metallic surface and it is influenced by a series of factors like humidity, temperature, rain, solar radiation, atmospheric pollution, etc. (Arroyave et al. 1995, Oescht et al, 1997). Hence, it depends strongly on the climatic conditions where the metal is exposed (Masamitsu, 2003). Humidity, temperature and atmospheric polluting agents of a certain region constitute its "macroclimate" whereas the "microclimate" is the specific condition surrounding the object and in areas of the work, depending on the sculpture morphology. It is defined by factors like the time of wetness (TOW) of the surface or dew condensation, heating of the object by the solar radiation, hygroscope deposits and the ion accumulation of the acidic nature (SO_2^-, NO_2^-, Cl^-) of the surface water film.

When copper is exposed to natural atmospheres it begins to lose its characteristic brightness to develop a dark coloured film adhered to the base metal. It tends to turn brownish green first, then bluish green and finally green. That film is called patina, the name derived from that given by the ancient Romans to green deposit on plates of copper, bronze or brass (Almeida 1997).

The colour, morphology and texture of the patinas depend on the nature and proportion of their chemical components, which are determined by several factors. These are the compounds present in the atmospheres and their concentration, time of exposure of the sample, etc. The first corrosion product that forms on the copper based alloy surface is cuprite (Cu_2O). Later the cuprite reacts slowly with the components (O_2) and polluting agents of the atmosphere (SO_2, Cl^-, CO_2) forming alkaline salts. The copper patinas are chemical and structurally complex compounds and their components are related to the species found in the atmosphere (Graedel, 1987, Fitzgerald, 1998, Strandberg, 1998). The more common products are the copper oxides (CuO and Cu_2O) and the alkaline copper sulphates, carbonates and chlorides, all of them very insoluble water compounds. These patinas are heterogeneous; the inner layers are copper oxide whereas the outer layers are alkaline salts of copper sulphate.

Their protective characteristics depend on their chemical composition, adhesion to the base metal, thickness, porosity, crystalline structure, etc (Rosales et al., 1999).

The in situ Pourbaix technique is a non-destructive method that allows evaluating the protectiveness of a patina through measurement of its electrochemical potential (Pourbaix, 1969, 1978, 1982, Van Muylder et al, 1976). With the object of analysing the evolution of the patina protectiveness by means of this technique the variation of the electrochemical potential with time was determined.

2. Methods

Measurements were made on different coloured zones of metallic sculptures belonging to the historical patrimony of La Recoleta Cemetery, which has been exposed to the atmosphere for almost a century:

- The El Karma sculpture (Figure 1) by Troiano Troiani was artificially patinated prior to exposition in 1927 (Cicileo et al 2004). On this statue measurements have been monitored at two years' intervals from 2000 to 2004, as a diagnostic method of the sculpture conservation state.
- The Mausoleum to Adolfo Alsina, by Margarita Bonnet, erected in 1915 (Figure 2). On this monument the sculptures La Ciencia and El Trabajo have been selected for measurements, in order to compare protectiveness of the different coloured areas and determine the best criterion and intervention procedures. Micro-cleaning tests were made removing particle deposits and incrustations. Detergent was used to eliminate surface dirt and xylol to degrease, whereas the black crusts were carefully picked with scalpels (Cicileo et al 2002). Monitoring of E_{sce} values have been performed at two years intervals from 2002 to 2004.
- El Cristo Central, by Zonza Briazo (1914) (Figure 3). Measurements of E_{sce} values have been started in 2004.

The selection criterion was based on the characteristic pathologies determined for each material in the sculpture set of the La Recoleta Cemetery (a Historic Protected Area of Buenos Aires City). The research work was initiated with El Karma and further the Mausoleum to Adolfo Alsina was added to compare two different aesthetic intentions previously described, on the same material. This year El Cristo was included to study the same material and aesthetic intention but in another microclimate. The different colour of the patinas formed on La Ciencia and El Trabajo for the same material depend from slight differences in microclimate parameters. These involve more or less sheltered surfaces with distinct access to the atmospheric pollutants, with the same orientation in respect to the cardinal points (resulting in almost the same temperature, time of wetness by rain, dew or water condensation, etc). However, the effect of the various inclinations, amount of open exposure on convex areas, the occlusion of pollutant from washing by rains in concave regions, all create a set of diverse conditions giving as a result different patina colours and electrochemical potentials that can be seen comparing Tables 2 and 3 (Vera et al. 2003).

The Pourbaix's technique of electrochemical potential measurement was extensively applied for patinas on steel development and protectiveness evaluation. We compared the protectiveness of various coloured patinas on bronze measuring their electrochemical potential evolution in time, providing a figure to help decide the best procedure for the conservation treatments. The main points are:

- the more stable and protective the patina is, the more stable is E_{sce} during the 90 s used for measurements;
- more stable/protecting patinas produce the higher values for E_{sce};
- a stable patina on copper base alloy could be defined when E_{sce} change no more than 30 mV in two yearly consecutive measurements (Cicileo et al 2004)

The portable arrangement used for in situ potential measurements consists of a glass tube fitted with a reference saturated calomel electrode (Esce = 242 mV/SHE) in one end. The other end, closed with a cotton piece soaked in distilled water, is applied to the zone whose potential is to be measured, through a saturated NaCl solution bridge. A voltameter connected the reference electrode to a small bare metal area, (locally cleaned from its corrosion layers in only one point), to establish the electrical contact for the many potential measurements throughout the whole structure.

After testing the measurement time needed to get stationary values we chose to perform them at 30, 60 and 90s. An initial value at t = 0 s gave values almost always decreasing with time, because not all the available diffusion ways through the patina have been flushed with water. This can be seen in the first row of Table 4, only included for comparison purposes. Further readings up to 90 seconds showed almost stable potential values for most patinas on Cu base alloys. Moreover, from 30 to 90s the direction of the change trend gave us valuable information about the patina behaviour as a good or bad protective barrier. According to our experience, not only with copper base alloys (of less than 100 μm thickness patinas) but also on weathering steels after three years outdoor exposure, the patinas of which were thicker than 200 μm, further measurements to 90s up to 1 h did not show a significant change with time because during the long rainy period all diffusion ways were flushed with water.

Protection corresponds to stable or increasing values associated with more noble potentials, while potential decreases or fluctuations indicate the passive film rupture allowing environmental attack on the metal. As an example of the two variations with time and the respective meaning, (see the last zone in Table 1), where the potential measured on the 'thigh' show a decrease during the measurement time, indicating that the patina is unstable, while its potential decrease from Year 2000 to 2004 demonstrates a passive effect decrease.

In a previous paper (Rosales et al, 1999), protectiveness was attributed rather to the morphology or barrier effect of the patina protecting the structure than to its chemical composition. For that reason no point to point comparison was performed between electrochemical potential measured and available X-ray information. Only few data could be compared in this non-destructive evaluation.

The chemical composition of different coloured areas of the sculptures was already determined in a previous work (Cicileo et al., 2004) by means of EDX and x-ray diffraction analyses. Black areas, yellowish green areas partially exposed to rainwater and light green areas directly exposed to rainwater were analysed.

Figure 1. El Karma

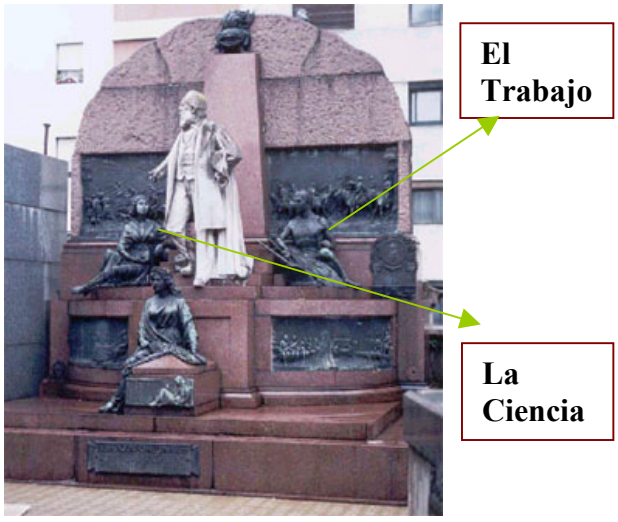

Figure 2. Alsina Monument

Fig 3. Cristo Central

3. Results and Discussion

The results of three series of *in situ* potential measurements with two years' intervals on different coloured areas of the El Karma sculpture are presented in Table 1. In the black zones higher potentials were observed, especially compared with those of the green zones completely exposed to the action of atmospheric agents, for example the area of the left thigh. After the two years' interval a general potential decrease was observed, especially in the exposed green areas. Differences amongst distinct areas of various stability potential were found in zones in contact with other metals, as on aluminium rivets and casting heterogeneities. On these latter areas it was meaningless to perform the mentioned measurements, because of the lack of a comparable patina formed on distinct metallic substrata, as verified on the left thigh area in Table 1.

Table 1. Three series of *in situ* potential measurements (E_{sce} (mV)) with 2 years' intervals on the El Karma sculpture.

Zone	Colour	Year	E(mV) 30 s	E(mV) 60 s	E (mv) 90 s
Ear interior	Black	2000	208	213	215
		2002	160	162	162
		2004	165	164	164
Forehead	Greyish green	2000	175	174	172
		2002	163	162	162
		2004	77	83	91
Chin	Green	2000	165	160	156
		2002	145	143	141
		2004	159	155	153
Left hand palm	Black crust	2000	153	150	147
		2002	165	164	163
		2004	182	179	179
Right hand (Al rivet)	White	2000	020	009	005
Left thigh	Yellowish green	2000	164	158	156
		2002	107	100	90
		2004	24	24	37

The Pourbaix technique was used as a diagnosis and monitoring test with time for El Karma sculpture whereas for La Ciencia and El Trabajo the objective was to determine the best criterion for intervention procedures. The highest potential decrease with time observed for La Ciencia as compared to El Trabajo (Tables 2 and 3), is a consequence of the least

exposure to pollutant and atmospheric factors of El Trabajo, due to its more protected microclimate than La Ciencia. In the two latter sculptures micro-cleaning tests removed particle deposits and incrustations. In some zones a bluish green patina was found underneath the black crust after chemical cleaning and mechanical detachment. The characteristics of that patina corresponded, according to the historical testimony documents of the monument, to the original patina. Also the same potential measured confirms that green patinas of the same electrochemical behaviour are found in both cases. However, it is not always clear if a black surface product is a patina or a crust, unless there is the possibility of having enough material to undergo X-ray diffraction.

Table 2. Two series of *in situ* potential measurements (E_{sce} (mV)) on Alsina Monument, El Trabajo sculpture.

Zone	Colour	Year	E (mV) 30 s	E (mV) 60 s	E (mV) 90 s
Knee	Green (not cleaned)	2002	173	173	170
		2004	99	98	98
Abdomen	Black	2002	236	236	236
		2004	165	166	165
Abdomen	Green (after scalpel elimination of black crust)	2002	134	126	119
		2004	115	116	117
Right pectoral	Black	2002	214	215	215
		2004	130	127	126
Right pectoral	Bluish green (after scalpel elimination of black crust)	2002	154	154	153
		2004	116	114	113
Head	Black	2002	180	180	180
		2004	114	113	112
Head	Black (after scalpel elimination of black crust)	2002	142	140	139
		2004	91	92	91

Table 3. Two series of *in situ* potential measurements (E_{sce} (mV)) on Alsina Monument, La Ciencia sculpture, at 2 years' intervals.

Zone	Colour	Year	E (mV) 30 s	E (mV) 60 s	E (mV) 90 s
Forehead	Grey	2002	140	131	125
		2004	87	91	94
Right side of the book	Black	2002	222	224	227
		2004	236	241	250
Left shoulder	Black (not cleaned)	2002	203	202	202
		2004	168	170	180
Left shoulder	Green (after scalpel elimination)	2002	147	146	145
		2004	133	133	133
Feet	Green	2002	163	168	175
		2004	117	118	120
Arch of the foot	Olive green	2002	155	156	156
		2004	107	110	115

After mechanical removal the black crusts gave higher stable potentials within the 90s measurement than those in the underlying patina. In the left shoulder of “La Ciencia”, for example, the underlying green patina gave stable potentials near 150 mV, whereas the potentials on the black crusts were around 200 mV, as shown in Table 3. After the two years' interval the high potentials of the black crusts remained, whereas the potentials of the green

patinas decreased, mainly on the greyish green areas exposed to rain, like the zone of the forehead of "La Ciencia" allegory (Table 3).

In "El Cristo Central", not all the black areas correspond to black crusts. They are limited to the areas sheltered from the rain. Measurements shown in Table 4 demonstrate that not only green but also black areas show a patina behaviour with similar electrochemical potentials.

Table 4. First series of *in situ* potential measurements (E_{sce} (mV)) on "El Cristo Central" sculpture, June 2004.

Zone	**Colour**	**E (mV) 0 s**	**E (mV) 30 s**	**E (mV) 60 s**	**E (mV) 90 s**
1Base front mantle	Black	156	153	152	151
3Right hand, running off	Green-greyish	112	120	122	120
7 Left hand, running off	Shiny black	134	122	125	128
10 Back, thin film, intense running off	Light green	80	70	56	58
12 Under green area, near basis (with wax)	Ochre area	129	125	123	120
14 Ear, running off	Green	102	100	99	98
15 Front	Shiny black	95	86	92	91
16 Left chest	Black area	129	127	128	127
17 Previous area after cleaning	Green area	122	120	120	119
22 Left shoulder, thin layer	Green-greyish	64	65	71	72

Measurements on areas of rain running off show low protectiveness, as in zones Nº 10 and 22. As opposed to what was observed in the three previous sculptures the measurements performed on black areas of El Cristo show a patina behaviour resulting from the similitude of their readings in respect to green areas. This is also similar to the author's aesthetic intent. Green-black running off was artificially performed in the origin, as can be seen in zones Nº 1/12, Nº 3/7 and Nº 14/15. After cleaning the black areas the measurements show a potential decrease, as shown in zones Nº 16/17.

EDX and x-ray diffraction analyses showed that the black areas of the different monuments have similar composition. They revealed a high proportion of Si and Al, from particulate material, mainly composed of Al silicates. EDX analyses of particulate material have been reported (Bogo et al. 2003) showing the presence of Cl and Fe elements involved in black crusts. The green exposed areas also presented large Cl content because of the atmospheric pollutants incidence. X-ray diffraction analyses revealed that these areas were mainly composed of brochantite ($Cu_4(SO_4)(OH)_6$), atacamite ($Cu_2Cl(OH)_3$) being also present. Cuprite and other copper oxides presence was detected in the yellowish green areas.

4. Summary of the intervention proposals

In all the work the black areas should be analysed to separate the crust from black patinas, to allow treatment in different ways, according to their potentials. From Tables 1 to 4 the increased protectiveness of the crusts, characterised by almost stationary values during the 90s measurements and decrease after their elimination, can be observed. However, the

underlying patina potential drops to the same value on different areas. This seems to be characteristic of the original patina formulated by the sculptor. It also evidences a similar protectiveness along the almost constant readings during measurements from 30 to 90s.

A clear difference appears between black areas in more protected zones with respect to more exposed zones to rain, sun, pollutants, etc. (higher and lower potentials respectively). Their cleaning results in an underlying patina with high to low protectiveness (more or less noble potential value), evidence of the negative effect of the atmospheric agents.

1. For the case of "El Karma" and "El Cristo Central" sectored treatments are proposed: black areas removal to recover the original underlying colour, as well as patina restoration on grey areas through use of the artist's original formulation. In this way the patina quality would be recovered in the differently affected areas (air quality, surface morphology and orientation, exposition angle with respect to atmospheric agents and pollutants, etc.) from past decades; differentiating sheltered from exposed regions. The intervention would recover the aesthetics of the work at the moment of its outdoor installation. The potential unit of the work would be established respecting the underlying patina below the black areas as witness of the passage of time.
2. For the metallic sculptures of the Mausoleum A. Alsina, also a sectored treatment is proposed according to the exposition type of areas. Thus, the suggestion involves black area elimination maintaining the underlying patina in sheltered areas, and patina restoration on most exposed regions. The patina would then maintain the sculptor's proposal and the transformations that have occurred since the creation of the piece up to our conscientious updating.

5. Conclusions

Each work requires a particular intervention according to the aesthetic perception designed by the sculptor.

Black crusts preserved historical dating of the surface treatments until the 1970s.

The *in situ* Pourbaix technique provides a useful tool for comparative evaluation of patina protectiveness from the environment and time impact. It also allowed us to design the best procedure for patina repair and its further protectiveness control.

The different coloured areas (green- black- grey) in the same work and their behaviour, including the post-cleaning time, determined a differentiated restoration and further protection for each case.

The intervention policies in La Recoleta cemetery for metallic sculptural heritage must consider the work as a *potential unit* from the artistic *aesthetic-temporal* proposals to the *physical reality* of the material and its environment.

References

Almeida, E., Ferreira, M. (1997) *Corrosão Amosférica- Mapas de Portugal*- INETI.

Arroyave, C., Morcillo M. (1995) *The effect of nitrogen oxides in atmospheric corrosion of metals*, Corros. Sci., 37, 2, pp 293-305.

Bogo, H., Otero, M., Castro, P., Ozafrán, M.J., Kreiner, A., Calvo, E.J., Martín Negri, R., (2003) *Study of atmospheric particulate matter in Buenos Aires city*, Atmospheric Environment, 37, pp 1135-1147.

Brandi, C., (1988) *Teoría de la restauración*, Alianza Forma. Madrid. Pág 29-34.

Cicileo, G., Rosales, B. and Crespo, M. (2002) *Análisis in situ de pátinas formadas sobre monumentos de bronce expuestos a la intemperie*, LATINCORR 2003, Santiago, Chile, October 20-24, pp 735-741.

Cicileo, G., Crespo, M. and Rosales, B. (2004) *Comparative study of patinas formed on statuary alloys by means of electrochemical and surface analysis techniques*, Corros. Sci., 46, 4, pp 929-953.

Crespo, M; Orsetti, A; Rosales, B; De Maio, B.; Ronco, A. (2000*) El deterioro del patrimonio escultórico* Rev. Gerencia Ambiental Año 7, Nº 66, 456 - 465. Buenos Aires. Argentina.

Crespo, M., (2002) *Lecturas de una transformación - Diagnóstico Histórico*"II Seminario Forum-UNESCO Universidad y Patrimonio. El Rol de La Universidad en La Formación, difusión y Conservación del Patrimonio. Buenos Aires Argentina. pp 10. In press
.
Crespo, M., (2001) *Deterioro del patrimonio escultórico y su relación con el receptor*. Encuentro Nacional de Investigación en Arte y Diseño. CD-ROM 3pp. La Plata. Argentina. pp 35
.
Fitzgerald, K. P., Nairn, J. and Atrens, A., (1998) *The chemistry of copper patination*. Corros. Sci., 40, 12, pp 2029-2050.

Graedel, T.E., Nassau, K., Franey, J. P., (1987) Corros. Sci., 27, 7, pp 639-657
.
Masamitsu, W., Yashiuro, H., Tohru, T., (2003) *Differences between corrosion products formed on copper exposed in Tokio in summer and winter*, Corros. Sci., 45, pp 1439-1453.

Oescht, S., Faller, M.,. (1997) *Environmental effects on materials: the effect of the air pollutants SO2, No2, NO and O3 on the corrosion of copper, zinc and aluminium*. A short literature survey and results of laboratory exposures, Corros. Sci., 39, pp 1505-1530.

Pourbaix, M. (1969) *Une Methode Electrochimique Rapide de Predetermination de la Corrosion Atmospherique*, Rapport Technique CEBELCOR 109, R. T. 160.

Pourbaix, M. (1969) Rapport Technique CEBELCOR N° 160.

Pourbaix, M. (1978) Proc.7th. International Congress on Metallic Corrosion, Rio de Janeiro, 3, 1181.

Pourbaix, M., Van Muylder, J., Porubaix, A. and Kissel, J. (1982) *Atmospheric Corrosion*, Hollywood, Fla., 1980. John Wiley & Sons, Inc., 167-177.

Rosales, B., Vera, R., Moriena, G., (1999) *Evaluation of the protective properties of natural and artificial patinas on copper*. Part I. Patinas formed by immersion, Corros. Sci., 41, pp 625-651.

Strandberg, H., (1998) *Reactions of copper patina compounds*- I Influence of some air pollutants. II. Influence of sodium chloride in the presence of some air pollutants. Atmospheric. Environment., 32, 20, pp 3511-3526.

Tribute Commision to the Memory of Dr. A Alsina. Archivos Mausoleo al Dr A. Alsina de Monumento Biblioteca del Senado de la Nación. 1915.

Van Muylder, J. and Pourbaix, M. (1976) Rapport technique CEBELCOR, N° 72.

Vera, R., Rosales, B.M. and Tapia, C.(2003) *Effect of the exposition angle in the corrosion rate of plain carbon steel in a marine atmosphere*. Corr. Sci. 45, 321-337.

ABN 70 592 297 967

Corrosion rate study of cannon at the Prince of Wales' fort

H.L. Croome

Parks Canada, Western Canada Service Centre, 145 McDermot Avenue, Winnipeg, Manitoba, R3B 0R9, Canada

Abstract

Prince of Wales' Fort near Churchill, Manitoba, Canada, has forty 18th century cast iron cannon set on its ramparts and exposed to the elements. Two hundred and fifty years of corrosion has removed historical detail. Although there is minimal pollution, (the neighbouring ocean has a low saline content and is frozen for much of the year), relative humidity is very high and windborne particles continually expose new material to corrosion processes. With the failure of numerous protective coating regimes, a fundamental re-examination of the problem of "preserving the cannons' fabric for future understanding, appreciation, and study" was initiated in 1996. Since no corrosion data for grey cast iron in a sub-arctic, marine environment was available to provide a scientific basis for resource management decisions, a thirty year corrosion rate study using coupons of like alloy has been instituted. Two questions have been posed in the study: what is the corrosion rate; and how long will it take at that rate to obliterate remaining surface detail? This paper presents the corrosion rate results for the first five years of the study. Also offered for discussion will be the question: what is an "acceptable" rate of material loss for cultural resources in an uncontrolled environment where access is difficult and visitation low?

Key Words: grey cast iron, cannon, atmospheric corrosion, sub-arctic marine environment

Corresponding author: TEL:011 204 984 5814, FAX: 011 204 984 3726, email: liz.croome@pc.gc.ca

Introduction

Prince of Wales' Fort is a large stone fortification constructed by the British between 1731 and 1772. It is located on a peninsula at the mouth of the Churchill River on Hudson Bay in Northern Canada. On the ramparts are forty, grey cast iron cannon manufactured between 1702 and 1760. These 6, 12, and 24-pounders still exhibit the royal cyphers, proof marks, weight marks, and astragals which anchor them in history. When the French captured the Fort in 1782, they disabled the cannon by spiking touch holes, blowing off muzzles, or knocking off trunnions. As a National Historic Site of Canada, the Fort commemorates the French-English rivalry in North America and the disabled cannon are valuable evidence of that rivalry.

Figure 1: One of forty cannon on Prince of Wales' Fort Ramparts

By the mid-1980's, the cannon exhibited an overall layer of corrosion with localized spalling. The edges of the markings were rounded from loss of material and the process was apparently continuing, albeit at a slow rate. As valued cultural resources, periodic attempts have been made to protect the cannon from corrosion. These were limited experimental treatments which it was hoped would lead to a conservation treatment strategy for long-term preservation of the collection. The various treatments included corrosion stabilization with ethylene diamine and coating with Tremclad® paint, coating with an aluminium mastic epoxy primer and an aliphatic catalysed polyurethane top coat, coating with an orthophosphoric acid metal conditioner, epoxy primer, and urethane acrylic enamel top coat, and finally coating with Conquest®, a tannic acid based solution with polymeric coating. Unfortunately, most of these coating systems have failed in large part due to the Fort's location. (Busse, 1997). The sub-arctic climate with relatively cold temperatures and high humidity year round means that most standard protective coatings developed for use in southern Canada are not appropriate.

The cannon are large artefacts with thick cross-sections of sound metal. They have survived over 200 years in their current environment with only minimal loss of surface metal and the markings are still legible. Considering this observation and the difficulty and expense of applying a protective coating to the cannon, questions were raised about the validity of the assumptions upon which the conservation treatment decisions were based. Perhaps the corrosion rate was so low as to be insignificant making expensive on-site treatments unnecessary. Was the rate of corrosion going to result in the future loss of information contained in the relatively shallow markings?

How far into the future would we have to consider: 100 years, 200 years, a 1000 years? In the next 100 years, would a conservator or conservation scientist develop a new protection plan which would effectively reduce any chance of further deterioration? Situated on a rocky, treeless coast without fresh water or electricity and only accessible by boat at high tide during the summer, all work at the fort is logistically challenging and expensive; and with shrinking financial resources, can the conservation of artefacts which appear to be barely deteriorating be justified? In addition, every time a new coating regime is tried, there is a risk of increasing the corrosion rate if the coating fails.

The cannon have been exposed to the elements since 1782 without a significant loss of material, particularly around the markings leading to the assumption that grey cast iron was relatively corrosion resistant in the environment of Prince of Wales' Fort. To confirm this assumption, a method of investigation had to be found which would not damage the cannon yet provide useful information. Corrosion rate data could provide this information, but no one has ever established a corrosion testing station at or near Prince of Wales' Fort. Data from Southern Ontario with its pollution and warm temperatures or Halifax with its marine conditions and pollution would not apply to Prince of Wales' Fort. In addition, the cannon are made of a grey cast iron alloy which has no modern industrial applications; and industrial scientists are not studying this alloy. In August 1989, Henry Unglik, Parks Canada Metallurgist, and Alex Barbour, then Chief of Marine and Industrial Conservation, Public Works Canada, visited the fort to study the cannon and obtain metal samples from broken trunnions. (Unglik and Barbour, 1992) One of their recommendations was to determine the corrosion rate of the untreated metal by establishing a corrosion testing station at the Fort using an alloy as close as possible to the cannon's grey cast iron. In 1996, a corrosion rate study was implemented.

The first step of the project was to define the objectives. Two questions were posed:

- What is the rate of corrosion for grey cast iron at Prince of Wale's Fort?; and

- Is the rate of corrosion for grey cast iron at Prince of Wale's Fort great enough to necessitate conservation intervention on the cannon?

The answers to these questions would be the foundation of future decisions concerning conservation treatments.

2. Method

This study determined the corrosion rates of grey cast iron test coupons by weight loss. Establishing a corrosion rate study is not normally part of a typical conservator's work in Canada. Fortunately, corrosion scientists have developed standard procedures. The test was based on the American Society for Testing and Materials (ASTM) G50-76, Standard Practice for Conducting Atmospheric Corrosion Tests on Metals (ASTM G50), and ASTM G92-86, Standard Practice for Characterization of Atmospheric Test Sites. (ASTM G92) The exposure times for the study were selected to find two corrosion rates – short-term (less than five years) and

long-term (more than five years). The coupons were scheduled for retrieval after 1,2, 3, 4, 5, 10, 15, 20, 25, and 30 years.

The test coupons were made from a grey cast iron as close as possible to the cannon alloys. Unglik determined that the alloy was " typical of a phosphoric grey iron. It had a pearlite matrix with ferrite, a large quantity of graphite flakes and a considerable amount of iron phosphate eutectic" (Unglik, 1995) The closest modern alloy that could be poured in a small batch was "typical for grey cast iron. The structure consists of pearlite matrix with some free ferrite associated with graphite flakes and a small amount of iron phosphide particles evenly distributed." (Unglik, 1999) It was produced by McLean Foundry Ltd. of Brantford. Table 1 has a comparison of the alloying additions in both the cannon and the modern ingot. The higher silicon and lower phosphorus contents in the coupons will have them resist corrosion better than the cannon. On the other hand, the higher sulphur content will make the coupons more susceptible to corrosion. (Unglik, 1999)

Table 1: Analysis of cast iron coupons (Unglik, 1999)

Element	**Test Coupon Average of four coupons (wt. %)**	**Prince of Wales' Fort Cannon Samples (wt. %)**
carbon	3.1	3.7
silicon	2.0	0.7
magnesium	0.5	0.7
phosphorus	0.05	0.4
sulphur	0.17	0.05

The forty, rectangular test coupons are on average 105 mm wide, 152 mm long, and 6.7 mm thick. A thick coupon better simulates the thermal effects on the metal. Each coupon had an 18.5 mm hole drilled in each corner for mounting. An identifying number was stamped in the upper left corner of the skyward side. Each coupon was prepared to bright metal by air abrading with walnut shells at 60 psi. The surface was cleaned and de-greased using acetone. Several extra coupons were also prepared for use as controls for the mass loss analysis. Each coupon was weighed and then placed in Marvelseal 360 (aluminium foil and polyethylene laminate) pouches sealed with aluminium duct tape. Pieces of blotting paper were used to interleave the coupons. Each pouch also contained a sachet of dried, non-indicating silica gel.

The testing station frame is constructed of aluminium to which the coupons are attached with black nylon cable ties. The rack is angled at approximately 30 degrees above horizontal instead of the 59 degrees prescribed in the standard. It also faces 290 degrees NW instead of 180 degrees S (ASTM G50). Deviations from the standards could not be avoided due to location constraints. The skyward and groundward sides will have varying corrosion rates much like the cannon on the ramparts.

The coupon rack was installed on a modern, one-story service building located approximately ¼ km from the Fort. The rack sits on the roof, out of sight of visitors and passing marksmen. Figure 2 shows the rack installed. The ideal test site for the study was on the Fort's ramparts along side one of the cannon. However, the Fort is an interpreted historic site and site staff did not want a modern coupon rack situated beside the historic cannon.

The coupons were installed on August 9, 1996. The weather was 8º C with a light wind and a brief rain squall passed through leaving isolated raindrops on the bright metal. Spots of flash rusting quickly occurred.

Figure 2: Coupon rack installed on roof of modern building.

Climatic data is obtained from the local Environment Canada weather station located on the east side of the river. Unfortunately, there are limitations to using an unmanned weather station. The equipment tends to quit working during extremes in weather, particularly wind. Without a human on site, there is no data for these days. The station provides daily maximum and minimum temperatures, relative humidity, and precipitation. The severe climate makes it difficult to set up a weather station beside the test station. There is no electricity and it's too cold for long-term battery use. The inaccessible nature of the site means that batteries and sulphonation discs or candles cannot be changed on a regular basis. As a consequence, there is no time-of-wetness data because of these difficulties with maintaining equipment.

At each retrieval, four coupons are removed. They are immediately sealed in Marvelseal pouches with blotting paper dividers and a silica gel sachet. The exposed coupons and some control coupons are then shipped to the Analytical Laboratory at Parks Canada's Ontario Service Centre. The coupons from the first two years of the test were stripped of corrosion using the sodium hydroxide and zinc powder procedure from ASTM Designation G1-81, Standard Practice for Preparing, Cleaning and Evaluation Corrosion Test Specimens (ASTM G1). The method conformed to those proposed by D.H. Thomson (Thomson 1971). The coupons were suspending in a boiling aqueous solution of 20% w/v sodium hydroxide with zinc for five minutes. This method was found to be harmful to the laboratory equipment and dangerous for staff. For coupons from years three, four, and five, the safer electrolytic method, also described by ASTM Designation G1-81 and D.H. Thomson, was used. The electrolyte was a 5% w/v aqueous solution of sulphuric acid inhibited with Hostacor IT® and heated to 75 C. The coupons were exposed to a current of 24 amps at 4 - 6 volts for 3 minutes. For both procedures, control coupons were stripped at the same time to determine a correction value to allow for any metal lost during the stripping process.

3. Results

The climatic data was as expected for a sub-arctic location. The only months with average temperatures above 0º C, were June, July, August, and September for an average total of 112 days per year. The bay was frozen for approximately eight months every year. There were an average of 67 days with more than 0.2 mm of rainfall and an average relative humidity above 70%. (Environment Canada, 2004) The concentration of chlorides and sulphates found at the fort was low. According to Unglik (Unglik, 1995), the water trapped in the cannon bore contained <3 parts per million (ppm) chloride ions and < 30 ppm sulphate ions. The rainfall captured around the fort area contained < 0.1 ppm chloride ions and < 1 ppm sulphate ions. The Churchill River introduces fresh water into Hudson Bay, reducing the salinity of the bay water. The waters surrounding the peninsula had salinity of less than 20 parts per thousand (Green, Singh, Hicks, and McCuaig, 1983). For an outdoor display of metal artifacts, Prince of Wales' Fort has a relatively benign environment.

To date, the first five years, or short term, coupons have been retrieved. They were visually examined and photographed to note the surface condition before stripping. The coupons from years one and two had a uniform distribution of corrosion without any pitting. The skyward sides had a mottled appearance – dark brown with light brown spots. The groundward sides were mostly dark brown.(Stewart, Sergeant, and Unglik, 1998) For years three, four, and five, both sides were mostly dark brown with a uniform distribution of corrosion and some pitting. The amount of corrosion products was similar on both sides. (Sergeant and Stewart, 2001) The appearance of the skyward and groundward sides of coupon #5 both before installation and after five years exposure is shown in figures 3 and 4. After stripping, there was some pitting due to aggressive nature of the electrolytic solution and the insufficient protective action of the Hostacor IT inhibitor.

Figure 3a

Figure 3b

Figure 3: Skyward view of coupon #5 before installation and after five years on the rack.

Figure 4a

Figure 4b

Figure 4: Groundward view of coupon #5 before installation and after five years on the rack.

The results of the mass loss analysis and corrosion rate ± one standard deviation are shown in Table 2. The mass loss was calculated using:

mass loss (g) = initial mass (g) - final mass (g) - correction (g)

The corrosion rate was calculated using:

$$\text{corrosion rate} = \frac{K \times W}{A \times T \times D}$$

where K = constant = 8.76×10^7 ☞m/year
W = mass loss (g)
A = Area (cm^2) based on the top, bottom, and sides minus the holes
T = exposure time (hours)
D = metal density of 7.17 g/cm^3

Over the five years of the study, the corrosion rate has dropped from an average of 14.5 ± 0.5 µm/yr in year one to 8.6 ± 0.4 µm/yr in year five. Figure 5 shows a graph of the corrosion rate vs. time. The rate is dropping , but has not flattened out into a consistent rate. The extrapolated long-term corrosion rate suggests a rate of 6 – 7 µm/yr which will need to be verified by the long-term results.

Table 2: Mass loss data and corrosion rates ± one standard deviation

No.	Exposure Period (hours)	Initial Mass (g)	Final Mass (g)	Mass Loss (g)	Corrosion Rate (☛m/yr)	Mean Corrosion Rate (☛m/yr)
01	8684	702.15	698.65*	3.50	13.94	14.5 ± 0.5
11		696.08	692.22*	3.86	15.48	
21		684.77	681.26*	3.51	13.96	
31		715.69	712.33*	3.36	13.34	
02	17.107	701.15	695.46*	5.69	11.74	12.3 ± 0.3
12		711.26	704.92*	6.34	12.78	
22		708.67	702.59*	6.08	12.24	
32		705.21	698.99*	6.22	12.53	
03	25,485	697.38	690.60**	6.78	9.13	9.5 ± 0.8
13		676.70	668.24**	8.46	11.46	
23		697.79	691.59**	6.20	8.37	
33		709.36	702.60**	6.76	9.17	
04	34,578	702.56	692.55**	10.01	9.97	10.0 ± 0.4
14		701.06	691.88**	9.18	9.12	
24		720.36	710.44**	9.92	10.06	
34		680.62	669.88**	10.74	10.75	
05	43,603	688.42	678.44†	9.98	7.88	8.6 ± 0.4
15		693.37	683.00†	10.37	8.20	
25		675.86	664.94†	10.92	8.63	
35		699.76	687.75†	12.01	9.52	

* Stewart, Sergeant, Unglik, 1998
** Sergeant, Stewart, 2001
† Stewart, Unglik, 2002

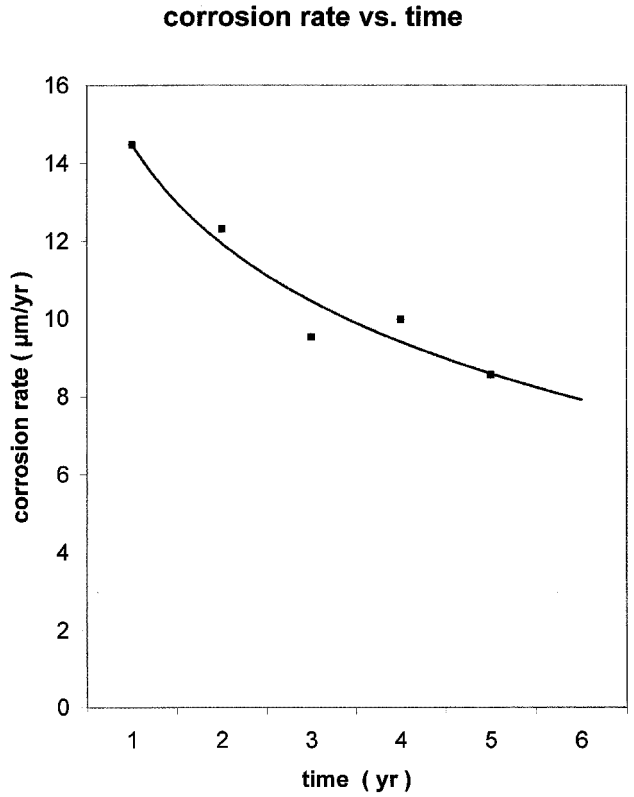

Figure 5: Graph of corrosion rate vs. time

4. Discussion

In his compilation of atmospheric corrosion rates for carbon steel, Einar Mattsson reported rates in rural areas of 4 to 65 µm/yr and in marine environments of 26 to 104 µm/yr. (Mattson, 1982) In comparison, the rate of 8 µm/yr for grey cast iron at Prince of Wales' Fort is relatively low, confirming the anecdotal observations made of the cannon. This was anticipated since the cannon were in fair condition considering they have been at the Fort for almost 250 years and grey cast iron is known to have a low corrosion rate. The environment around Prince of Wales' Fort has low chloride ion concentration, low sulphate ion concentration, and low temperatures combining to produce atmospheric corrosion rates in the range of those typically found in rural, non-marine sites. Extrapolation of the short-term data suggests a long-term corrosion rate of 6 –7 µm/yr. The experiment will continue for another 22 years to confirm the long-term rate.

It is a luxury to follow an atmospheric corrosion test instead of a program of accelerated testing. The atmospheric testing removed the need to precisely determine the environment at Prince of Wales' Fort and reproduce it at elevated temperatures in a laboratory chamber. The coupons are exposed to the same conditions as the cannon. On a microscopic scale, the metal ions and corrosion contaminants are able to react and migrate at a natural speed.

Now that there are short-term results and a long-term study underway, there is

the question of how low a corrosion rate is low enough? Is conservation intervention required? For example, extrapolating the corrosion rate to 7 μm/yr predicts the cannon could lose 3 – 4 mm from their surfaces in 500 years. The cannon will still be in place half a millennium from now, but will their markings have survived? The royal cyphers, proof marks, and weight marks are only about 3 to 5 mm thick. In 300 years they will be difficult to read, in 500 years they will be gone. If that information is lost, all that will be left will be basic tubes of cast iron. Bare tubes of metal are not sufficient to convey the significance of the Fort. Although the corrosion rate of the cannon at Prince of Wales' Fort is very slow, it is still enough to endanger the existence of a cultural resource worth preserving and commemorating.

5. Conclusions

The short-term rate of corrosion of grey cast iron at Prince of Wales' Fort was a relatively slow 8.56 μm/yr after five years. This quantitative data can be used for decision-making meetings with the Prince of Wales' Fort staff and other cultural resource professionals working at the Fort. It can communicate the rate of deterioration in a very concrete form: in 500 years the markings will be obliterated All of the people involved in the care and interpretation of Prince of Wale's Fort can now make more enlightened decisions on future preservation regimes for the cannon.

The results would suggest that conservation treatments are required to maintain the historical significance of the cannon at Prince of Wales' Fort. Monitoring the long-term study and determining the best conservation intervention and maintenance regimes for the artefacts at this remote site pose further challenges.

Acknowledgements
The author would like to thank Lyndsie Selwyn and Nancy Binnie of the Canadian Conservation Institute for their assistance with the experimental design. Thanks also go to the many Parks Canada staff who gave their time to this project. Henry Unglik's contribution included experimental design and metallurgical analysis of the cannon and coupons. John Stewart and Chris Sergeant performed the stripping of the coupons for the mass loss analysis. The staff of the Manitoba North Field Unit installed the coupon rack and provided polar bear guards during coupon retrieval. John Watt, Colleen Day, Craig Hinchey, and Lyndsie Selwyn gave helpful comments on the text.

References

American Society for Testing and Materials (1992), *G1-81 Standard practice for preparing, cleaning, and evaluation of corrosion test specimens*, Annual Book of ASTM Standards (Philadelphia, ASTM)

American Society for Testing and Materials (1992), *G50-76 Standard practice for conducting atmospheric corrosion tests on metals*, Annual Book of ASTM Standards, pp 201-205 (Philadelphia, ASTM)

American Society for Testing and Materials (1992), *G92-86 Standard practice for characterization of atmospheric test sites*, Annual Book of ASTM Standards, pp 371-374 (Philadelphia, ASTM)

Busse, E., (1997), *The Manitoba North cannon stabilization project*, MacLeod, Ian D., Pennec, Stéphane L., and Robbiola, Luc (eds.), METAL 95, pp 263-268 (London: James & James)

Environment Canada (2004), *Canadian climate normals or average 1971-2000*, http:/climate.weatheroffice.ec.gc.ca/climate_normals/index_e.html

Green, R., Singh, S. M., Hicks, B., McCuaig, J. M.,. (1983), *An Arctic intertidal population of Macoma balthica (Mollusca, Pelecypoda):* Genotypic and Phenotypic Components of Population Structure, Cdn. J. of Fisheries and Aquatic Sciences, vol. 40, #9, pp 1360-1371

Mattsson, E., (1982), *The atmospheric corrosion properties of some common structural metals - a comparative study*, Materials Performance, July 1982, pp 9-19

Sergeant, C., Stewart, J., (2001), *Examination of corrosion test coupons, Prince of Wales' fort NHS*, Ontario Service Centre #2001-0007 (Ottawa: Parks Canada)

Stewart, J., Sergeant, C., Unglik, H., (1998), *Examination of corrosion test coupons, Prince of Wales' fort NHS*, Ontario Service Centre #98-662 (Ottawa, Parks Canada)

Stewart, J., Unglik, H., (2002), *Examination of cast iron corrosion test coupons from Fort Prince of Wales*, Manitoba, Ontario Service Centre # 2002-303 (Ottawa, Parks Canada)

Thomson, D.H., (1971), *General Tests and Principles*, Ailor, W.H. (ed.), Handbook of Corrosion Testing and Evaluation, pp 115-141 (New York: J. Wiley)

Unglik, H., (1995), *Metallurgy and corrosion of cast iron cannons from Fort Prince of Wales, Manitoba*, in Vandriver, Pamela B., Druzik, James R., Madrid, Jose Luis Galvan, Freestone, Ian C., and Wheeler, George Segan (eds.), Material Research Soc. Symp. Proc., vol. 352, pp 351-363 (Pittsburgh: MRS)

Unglik, H., (1999), *Metallography of cast iron corrosion coupons from Fort Prince of Wales, Manitoba*, pp 4-11, Ontario Service Centre #96-1062 (Ottawa: Parks Canada)

Unglik, H., Barbour, A., (1992), *A metallurgical and corrosion study of the 18th Century cast iron cannons from Fort Prince of Wales, Manitoba*, pp 224-230, Ontario Service Centre #89-2193 (Ottawa: Parks Canada)

Registered Trade Items

CONQUEST® tannate soln
HOSTACOR® inhibitor
MARVELSEAL® pouches
TREMCLAD® paint

Analyses of Joe Byrne's armour

D.C. Creagh [a*], G.D. Thorowgood [b], M. James [b], D. L. Hallam [c]

[a] Division of Health, Design & Science, University of Canberra, CANBERRA ACT 2601 Australia

[b] Division of Materials Science & Engineering, Ansto, PMB 1, MENAI NSW 2234, Australia

[c] National Museum of Australia, GPO Box 1901, CANBERRA ACT,2601 Australia

Abstract

Ned Kelly was a notorious Australian bushranger (outlaw). His gang was active in Victoria (Australia) in the 1880s. Joe Byrne was a member of his gang. The armour worn by Joe Byrne in the gang's final encounter with the police was made available for analysis prior to its display at the National Museum of Australia. Neutron and x-ray diffraction, gamma x-ray fluorescence, and optical metallography were used to determine the method of manufacture of the armour. This paper extends our earlier investigation of the steel in the armour, and reports on the origin of a round mark found on the breastplate.

Keywords: xrd, γ xrf, neutron diffraction, Ned Kelly,armour.

1. Introduction

Bushrangers were outlaws: initially they were escaped convicts, but, later, they tended to be misfits in the society of the day. The most notorious gang was that led by Ned Kelly (http://www.nedkellysworld.com.au) which was active in northern Victoria (Australia) in the 1880s.

The gang was regarded by the society of the day as horse thieves and police murderers, though many would argue this was a rebellion against the inequities in Victorian society. Because they robbed banks, and distributed some of the proceeds amongst the people they came to be regarded by some to be latter day "Robin Hoods".

In an act of bravado the Kelly gang took over the town of Glenrowan, holding more than forty of the townspeople hostage in a pub (hotel). The four members of the gang (Kelly, Joe Byrne, and two others) were involved in a gun-battle with police. They wore suits of armour which had been fabricated in the months prior to the gun-battle. The battle between the armoured gang and the police at the Glenrowan pub has become a significant event in Australia's history and much folklore has grown up as a result of this. Many stories exist about the fabrication of the armour, and many families now claim that their forebears were involved in the manufacture of the armour.

This work seeks to determine which of the many stories about the manufacture is correct. To be decided were the origin of the steel used, and the method of manufacture. (Were they made by a blacksmith at a smithy? Or were they the work of unskilled workers in a large camp fire?)

The armour (Figure 1) examined belonged to Joe Byrne, Ned Kelly's second-in-command. This was made available for examination by Rupert Hammond, the owner of the armour, prior to display at the special "Outlaws" exhibition at the National Museum of Australia.

This paper extends our earlier investigation of the steel in the armour (Creagh et al, 2004), and reports on the origin of a round mark found on the breastplate.

* Corresponding author: TEL: +61 2 62012410: FAX:+61 2 62012048: email:Dudley.Creagh@Canberra.edu.au

Figure 1. Joe Byrne's armour. This comprises: a cylindrical helmet to which the face-guard is attached by bolts; a breastplate made from two pieces of metal crudely riveted together, with holes in the metal filled by metal rod which has subsequently been burred over; a similarly constructed backplate; a lap-plate fashioned from one piece of metal. All the former pieces were fabricated from thick sheets of metal. The two protective side-plates were made from much thinner metal.

2. Experiments

The experiments, undertaken at laboratories of the Australian Nuclear Science and Technology Organization (Ansto), were: neutron diffraction (using its Medium Resolution Powder Diffraction system); x ray diffraction (using a Scintag diffractometer fitted with an energy dispersive detector); a Thermo Measure Tech gamma x-ray fluorescence system (Mercury II); optical metallography of replicas taken from small regions which had been cleaned and electropolished; transmission electron microscopy of the replicas (and EDAX of particles adhering to the replica); Vickers hardness testing.

In this paper we deal, in the main, with neutron, x ray and gamma-xrf measurements.

2.1 Neutron Diffraction

Neutron diffraction reveals the structure of the bulk material. Powder neutron diffraction measurements were made on the Medium Resolution Powder Diffractometer using thermal neutrons (λ = 1.6664 Å) from the HIFAR nuclear reactor at ANSTO.

The diffractometer operates with 32 detector channels and gives medium resolution over an angular range (2θ) from 4° to 138° whilst maintaining a high neutron flux at the sample position. The monochromator consists of eight germanium crystals in a vertically-focussing arrangement, providing a neutron flux of up to 4 x $10^5 ncm^2s^{-1}$ at the sample position. The range of useable neutron wavelengths is from 1.06.Å to 5.0.Å. Complete diffraction patterns typically take about two hours to collect. Data were collected using a bank of 32 ^{3}He detectors over the full operation, in 0.1° steps. Structural refinements were carried out by the Rietveld method using the Hunter's RIETICA program (1998), with pseudo-Voigt peak shapes and refined backgrounds. All parts of the armour gave similar neutron diffraction patterns, which subsequent Rietveld analysis showed to have residual preferred orientation and residual strain. Figure 2(a) shows the neutron diffraction pattern taken from the helmet, and Figure 2(b) shows the diffraction pattern from the lap sash. The detailed differences in these patterns indicate the extent to which residual strain exists. The difference between the computed intensities and the observed intensities are shown in Figures 2(a) and 2(b) as the bottom curve on each of the graphs. There is some indication that preferred orientation exists in each component.

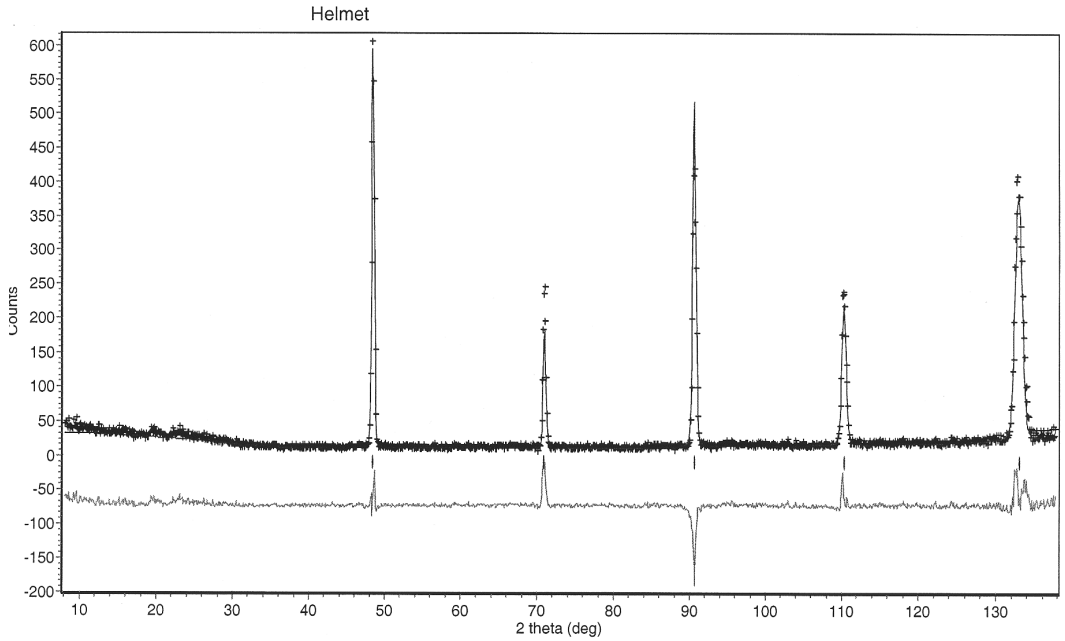

Figure 2(a).
Neutron diffraction pattern of the helmet.

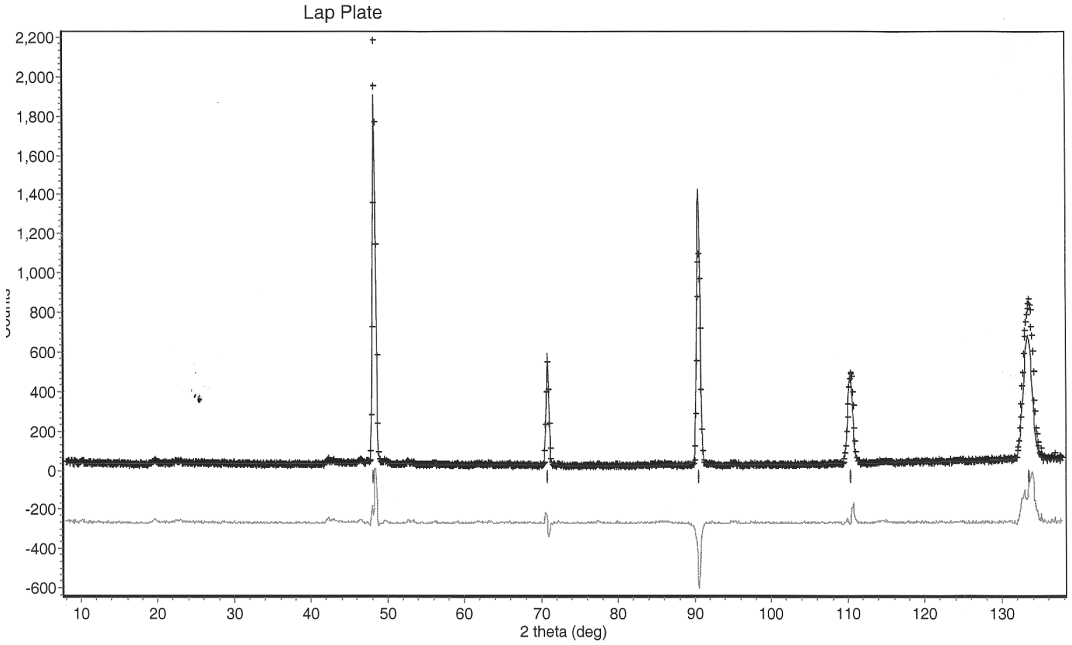

Figure 2(b). Neutron diffraction pattern of the lap-plate.

By comparing the diffraction patterns of all the components of the armour with the JCPDS Data file (JCPDS, 2003) the conclusion was reached that the diffraction patterns from the material are very similar of rolled carbon steel (JCPDS data file number 06-0696).

2.2 X-ray Diffraction

Whilst neutron diffraction yields information related to the physical state of the bulk material, x-ray diffraction reveals the structure of the material close to the surface, since the depth of penetration of the x-rays is only about 10 nm. Most of the components were too large to be examined in the Scintag diffractometer. Only one of the side plates was examined. As well, because of the lack of diffracted beam intensity the data acquisition times were long. The Scintag diffractometer was operated with the specimen horizontal and on the diffractometer axis, using the θ–θ mode of operation and $CuK_{\alpha 1}$ radiation. Figure3 shows an xrd pattern from the side plate. The diffraction pattern is typical of steel (bcc structure: a_o=28.672 nm). The poor peak heights relative to background and distorted line shapes which were observed were caused by surface strains. This is evidence that the metal had been cold worked. Peaks other than from iron are seem in Figure3. These are due to the surface coating and surface oxidation. We were not permitted to clean the surface.

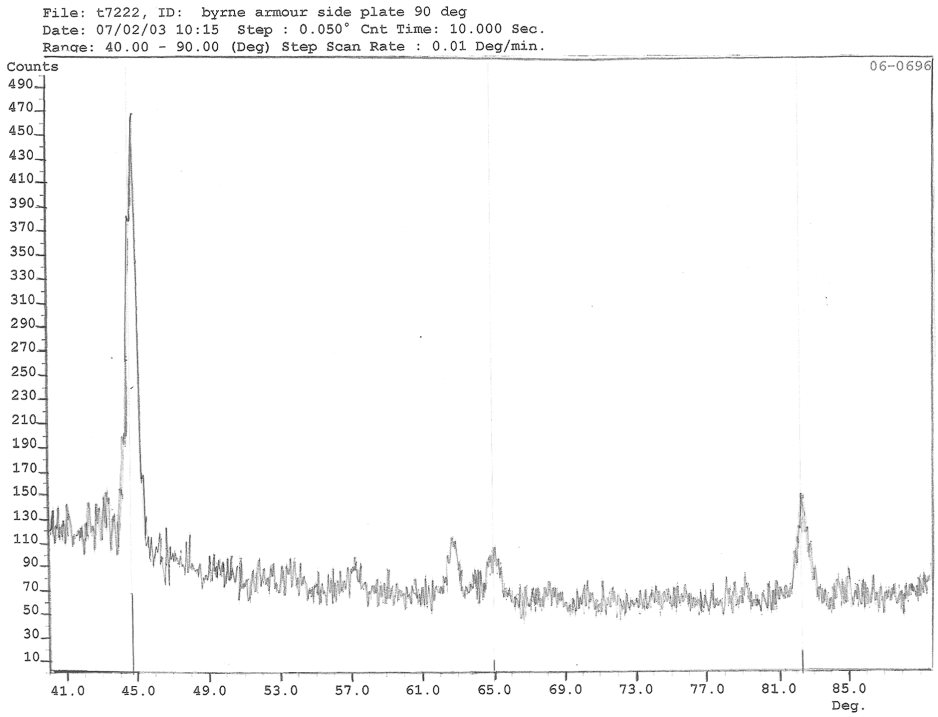

Figure 3. X-ray diffraction pattern from a side-plate. Note the weakness of the diffraction pattern and the width of the diffraction peaks. The solid lines at the bottom of the graph represent the diffraction peaks recorded in the JCPDS datafile for a rolled carbon steel (PDF number 06-0696).

2.3 Gamma x-ray fluorescence spectroscopy

Gammax-ray fluorescence spectroscopy was undertaken on all parts of the armour using a Thermo Measure Tech Metallurgist Pro Mercury II Probe. In this γ-x fluorescence spectrometer two radio-isotope sources (cadmium and iron) are used to excite electronic transitions in the material under examination. The resulting fluorescent radiation from the material is detected by a solid state detector. The charge released by a fluorescent photon in the detector is converted in a preamplifier and passes into a pulse height analyser. The height of the voltage pulse is proportional to the energy of the fluorescent photon. With appropriate calibration it is possible to determine these energies and, by comparison with an internally stored table, to determine the atomic species present in the material. To a good approximation the amplitude of the peak is proportional to the atomic concentration. The use of internal algorithms to compensate for matrix effects enables the display of

data which represents the true atomic concentration of a particular species. From this the weight concentration can be deduced.

In Table 1 results for the "helmet" and "breastplate" are shown. As well, measurements are shown for a round mark on the front of the breast-plate ("mark front") for a location at the back of the breastplate, immediately behind the mark ("mark back"). Figure4 shows the mark the origin of which needed to be assessed.

Figure 4. The circular mark on the breastplate at the centre of the picture is what is referred to as "mark" in Table 1. Also to be seen are two rivets holding the two parts of the breastplate together, and two plugs filling what were boltholes in the original material.

In Table 1 the compositions of most materials can be seen to be rather similar. The technique of analysis cannot detect carbon. The major element present in all components is iron. Most of the components contain as minor constituents: manganese, arsenic, tin, and lead.

Several items do not contain manganese, notably the cylindrical helmet, the side panels, and the rivets. It might be therefore be inferred that these were taken from different stock materials from the rest of the steel pieces in the armour. Certainly the side panels were much less thick than the rest of the pieces, and the rivets seemed to come from steel rod.

Table 1. Weight percentage compositions of the major atomic species in materials examined by gamma-xrf spectroscopy. Note that this technique cannot determine carbon content. The comment "general" means that the reading is the average reading taken from various locations on the piece. Minor trace elements have been omitted from the table in the interests of simplicity. Experimental error is typically 0.01%.

LOCATION		Mn	Fe	As	Sn	W	Pb
HELMET	**Faceplate**	0.32	96.56	0.17	1.80		0.18
HELMET	**Cylinder**		94.6	0.1	2.6		0.18
BREASTPLATE	**General**	0.33	96.85	0.07	1.48		0.14
BREASTPLATE	**Mark, front**	**0.27**	**75.35**	**3.15**	**1.14**	**3.17**	**14.4**
BREASTPLATE	**Mark, back**	**0.48**	**97.88**		**0.48**		**0.20**
BACKPLATE	**General**	0.32	96.56	0.17	1.80		0.18
LAP PLATE	**General**	0.31	94.29	0.10	2.6		0.18
SIDE PANEL 1	**General**		95.33	0.11	2.6		0.18
SIDE PANEL 2	**General**		98.14	0.25	0.47		0.09
RIVET	**Typical**		97.65		1.34		
MILD STEEL	**Kiandra**	0.44	98.6				
MILD STEEL	**Modern**	1.07	94.57		2.15		

Note the presence of arsenic, tin, and lead in all the components made from sheet metal. All but the side panels and, remarkably, the helmet, contain significant amounts of manganese. For comparison, the compositions of a modern mild steel and a sample of mild steel typical of artefacts from the Kiandra goldfields are shown (Myles, 2004). The Kiandra goldfield was worked at the time of Ned Kelly and is in a region of Australia not far to the north of Glenrowan.

Questions as to the origin of the steel and the cause of the "mark" need to be answered using different techniques.

2.4 Estimating the thickness of the "mark"

Measurements of composition of the steel in the breastplate were made at the "mark" and on the breastplate directly behind the "mark". The incident γ ray beam is monochromatic (80 keV) and its intensity I_0 remains constant throughout the experiment ($t_{1/2}$ = 330 days). The incident beam is at an angle of 45^o to the surface, and the exit angle from the surface is also 45^o.

Without the surface layer the intensity received at the detector for the iron K-edge radiation is

$$I_2 = I_0 F_s \quad (1)$$

Where F_s is the fluorescent yield for iron with 80 keV radiation into the solid angle defined by the detector slits.

With the surface layer (thickness = t) present the incident radiation I_0 passes through the layer and is attenuated by the lead (linear attenuation coefficient = μ_{L1}) according to the Beer-Lambert Law. The intensity available to excite fluorescence radiation is given by

$$I_1 = I_0 \exp - (\mu_{L1} t/\sin\theta) \quad (2)$$

The fluorescent iron radiation is attenuated by the lead (linear attenuation coefficient = μ_{L2}) as it travels to the detector, and the intensity at the detector, I_3, is given by

$$I_3 = I_0 F_s \exp - ((\mu_{L1} + \mu_{L2})\, t/\sin\theta) \quad (3)$$

The ratio of the intensities with and without the "mark" is given by

$$I_3/I_2 = \exp - ((\mu_{L1} + \mu_{L1})\, t/\sin\theta) \quad (4)$$

Since I_3 and I_2 are known, θ = 45^o, and μ_{L1} and μ_{L2} can be calculated to good accuracy (Creagh and Hubbell, 1998; Chantler, 1995), the layer thickness can be estimated.

The average thickness of the layer was estimated to be 0.4 ± 0.2 μm.

3. Results

The neutron and xrd measurements show that the material from which the armour was fabricated was a typical rolled carbon steel (similar to JCPDS 06-0696). Both showed that significant residual strain and preferred orientation in the components of the armour. This is consistent with the visual appearance of the armour (Figure 1). Individual hammer blows are readily identified: indeed, the armour is so crudely fabricated that it would seem to be unlikely that it could be the work of a professional blacksmith.

The existence of manganese in the gamma-xrf results indicates that, for all of the components the steel was manufactured after the Bessemer process was invented (1856), and, for most of the components, after 1858, because the process of adding manganese to steel to de-oxidize it was invented in 1857 by Mushet. The presence of manganese sulphide globules was confirmed by Thorogood et al. (2003) using an acetate replica technique in conjunction with a JEOL 2000FXII transmission electron microscope. The TEM study sought to investigate the existence of non-carbide phases. The traces of lead, arsenic, and tin found in the γ-xrf examination, were confirmed in the TEM experiment. These impurities were not in separate phases but as a solid solution. Their origin has yet to be explained. One possibility would be the addition of scrap galvanized iron to the melt in the Bessemer process. To date it has not been possible to determine whether the steel was made in Australia, or imported from England. Optical metallography (Thorogood et al., 2003) showed that

regions of pearlite structure associated with the original structure still exist, and that these regions were not affected by subsequent heating. In other regions spheroidization consistent with heating to dull red was observed.

Visual inspection of the armour has shown the existence of bolt holes (filled in the armour by steel rod) the spacing between which is consistent with spacings in plough shares. As well some makers' marks were seen. To date these have not been properly identified.

The circular mark (Table 1) is an impregnation of lead in the steel, consistent with the impact of a lead projectile, perhaps a low velocity bullet. This indicates that perhaps at least one bullet hit the armour. Using x ray attenuation arguments based on the decrease of intensity of the lead peak in the xrf spectrum, it is possible to determine that the average thickness of the impregnated lead to be 0.4± 0.2 μm. Tungsten is found with the lead. The presence of tungsten is odd if the mark were to have been made at the time of the Glenrowan siege, because tungsten was not introduced into ball ammunition until World War 1. This suggests that the mark was not contemporaneous with the stand at Glenrowan.

4. Conclusions

The armour was made from good quality rolled steel similar to that found in plough-shares. It was fabricated under a low heat (dull red, 600 to 700^{o}C) for several hours, and not to white hot as would have occurred in a blacksmith's forge. This gives support to the belief that the armour was fabricated over a bush fire and formed over fallen trees. The nature of the hammer blows and the degree to which cold-working has occurred supports the notion that the armour was made by amateurs. There is no evidence of bullet impact on this armour, except for the "mark" which might have arisen from the impact of a bullet, but if so, this occurred almost certainly at a later date (after World War 1).

A great deal of effort was expended by the Kelly gang and their assistants in the manufacture of this armour, and three other similar (but not identical)sets of armour. It is reported in some folk-histories that there was some dissent in the gang about the production of the armour. Contemporaneous sketches show men in armour, standing in front of the Glenrowan pub, firing at the police. The armour worn by the gang members must have been hit by bullets, yet, for this armour there is no evidence of bullet impact occurring.

For the record: Joe Byrne died whilst drinking at the bar of the pub whilst wearing the armour. He died of a bullet wound to the groin. A stray bullet had penetrated the walls. His last words were reported to be: "I told Ned that the armour would be the death of us".

Acknowledgements

The authors wish to thank the owner of the armour, Rupert Hammond, for allowing the measurements to be made, the National Museum of Australia for its support, and Australian Nuclear Science and Technology Organization for the use of its research facilities.

References

Chantler,C.T. (1995). *Theoretical Form Factor, Attenuation and Scattering Tabulation for Z = 1-92 from 1-10 eV to E = 0.4- 1.0 MeV*. J. Phys. Chem. Ref. Data 24, 71-643.

Creagh, D.C., Hubbell, J.H. (1998*). X-ray Absorption (or Attenuation) Coefficients*. In International Tables for Crystallography, Volume C. Edition 2. Section 4.2.4. International Union of Crystallography. Kluwer: Dordrecht. pp 220-236. [International Union of Crystallography: ISBN 0-7923-5268-8]

Creagh, D.C., Thorogood, G.D., James, M., Hallam, D.L. (2004). *Diffraction and Fluorescence studies of bushranger armour*. Radiation Physics and Chemistry. Proofs corrected. In press.

JCPDS (2004). *PDF4 Set of Relational Databases*. International Commission for Diffraction Data. Newton Square, Pennsylvania, USA

Hunter, B.A. (1998). *Rietica – A Visual Rietveld Program*. Commission on Powder Diffraction Newsletter, 20, p. 21.

Myles, V. (2004). *An archaeological survey of the Chinese miners' camp at Kiandra*. MA Thesis. Australian National University. Submitted.

Thorogood, G.J., Creagh, D.C., James, M.,Smith, G., Mitchell, D.R.G. (2003). *The Legend of the Kelly Gang - Distilling fact from fiction*. Science. In preparation.

Proceedings of Metal 2004 National Museum of Australia Canberra ACT 4–8 October 2004
ABN 70 592 297 967

Metallurgy of armour exhibited at the Palace Armoury Valletta, Malta.

D. Vella[a], C. Degrigny[a], M. Grech[b], A. Williams[c]

[a] Diagnostic Science Laboratories, Malta Centre for Restoration, Bighi, Kalkara, CSP 12, Malta

[b] Faculty of Engineering, Department of Materials and Metallurgy, University of Malta

[c] The Wallace Collection, Conservation Department, Manchester Square, London, W1U 3BN, UK

Abstract

The metallurgy of ten armour pieces from the Palace Armoury Collection in Malta was examined. Results showed that out of ten artefacts examined, six were produced in low carbon steel, one from a high carbon steel and three were made from wrought iron. One of the wrought iron armour pieces was fabricated from a phosphoric iron, an unusual material for these artefacts. All the steel artefacts exhibited a ferrite-pearlite microstructure. In their manufacture, no attempts had been made at producing martensite by full or slack quenching. All metal fragments contained slag inclusions. The elongated nature of the latter suggested that these artefacts were forged into shape.

Keywords: Metallurgy, armour piece, inverted metallographic microscope, microstructure phosphoric iron, steel, quench.

1. Introduction

This paper outlines the methodology behind the sampling of armour artefacts and presents results of a metallographic examination of a selection of armour pieces dating from the 16th - 17th century. The armour pieces belong to the Palace Armoury collection in Valletta, Malta and were kindly made available for research by Heritage Maltaτ

From a metallographic examination of armour plates, the following information may be gained:

(i) Confirmation of whether the armour is made from wrought iron or steel.

τ The Maltese national agency on museums and cultural heritage

(ii) *Knowledge on the technology of manufacture.* Amour plates were forged into shape. What were the temperatures employed to manufacture these objects? Were there any attempts at hardening the material to make it more resistant to blows during combat?

(iii) *Authentication of the armour pieces.* Slag is a good marker for authenticating a historic iron. However, the shape and orientation of the grains constituting the microstructure should also be considered when attempting the authentication of these artefacts (Williams, 1980).

Unfortunately a completely non-invasive technique capable of elucidating the microstructure of an artefact is not available. For this reason, any information related to the latter must be obtained through an invasive intervention such as sampling. In this case, a small fragment is extracted from the artefact, embedded in resin, prepared into a cross-section, treated with etchant, and examined under the metallographic microscope.

A *quasi* non-invasive technique for examining armour pieces was developed by Williams (Williams, 2003). In this method, a flattened plate edge is identified on the armour piece. This edge is embedded in polyester resin (reversible), ground, polished and etched to reveal the microstructure. Notwithstanding the geometrical complexity of these artefacts, it is usually possible to identify a suitable edge for examination on most armour components making up the suit armour. The microstructure is examined on an inverted metallographic microscope. This microscope is configured to allow the whole artefact to be examined 'in-situ'. The advantages of this technique are easy to comprehend. Most curators of armour museums are reluctant to allow the extraction of fragments from their armour exhibits, but are usually intrigued by the relatively benign ' in-situ' method.

Bonomi used a similar technique to study an Etruscan anthropomorphic bronze handle (Bonomi et al, 2003). The bronze artefact was polished at different points to expose the metal and then treated with etchant to reveal the microstructure. Examination was carried out 'in-situ' over an inverted metallographic microscope.

No embedding procedure was employed in this case as evidenced by the fact that the photomicrographs obtained were slightly out of focus at the extremities.

Metal plates employed in the manufacture of armour are usually very heterogeneous. This, coupled with the fact that these objects are frequently very large and manufactured from a number of plates makes it difficult to rely on a single site of examination. Whatever the examination technique employed (direct sampling or in-situ method), the question remains whether the site under investigation is representative of the whole armour piece. The level of confidence can be increased if several sites on the same armour piece are examined, but this is usually not feasible.

The 'in-situ' method of examining armour is an ideal technique for use on armour pieces that are relatively free of corrosion layers. However, for the case of armour covered with corrosion material, the reversible embedding procedure is likely to cause the detachment of the loosely bound corrosion layers. Since we are interested in these layers (specifically how they develop onto armour metal) the fragment extraction method was employed as a precautionary measure in order to conserve these delicate layers.

2. The Palace Collection and microstructure of steel armour

2.1 The Palace Armoury Collection

The Grand Masters' Palace in Valletta holds the remnants of what was once the main armoury of Knights of St. John. The knights occupied the island of Malta during the period 1530-1799. The Palace was built in the new fortress city of Valletta in the year 1570 soon after the Great Siege. Grandmaster Alof de Wignacourt established the Armoury on the first floor of this building in 1604 (Spiteri, 1999).

The Palace armoury exhibits a large variety of armour pieces dating from the 16th and late 17th century. Unlike many Armour museums in Europe, which are famous for their fine collections of armour pieces, the Palace Armoury is renowned for the fact that it is one of a few armouries in the world that has survived 'in-situ' (Spiteri, 1999). Excluding a few armour pieces (or full suits of armours) belonging to the Grand Masters or some famous Knights, the majority of artefacts exhibited at the Palace are field armour belonging to the infantry.

Unfortunately armours surviving from the period and which are presently exhibited as museum objects, suffer unhindered corrosion attack. The latter results from a combination of factors:

(i) *Atmospheric*: an aggressive Mediterranean atmosphere laden with chloride and characterized by large daily fluctuations of relative humidity and temperature (Chetcuti et al, 1992).

(ii) *Site relocation*: in 1975 the armoury was transferred from the first floor of the Palace (a site it had occupied since inception) to the ground floor level (originally the Palace stables). This transfer has possibly accelerated the degradation processes of the artefacts since the walls of the 'new' exhibit halls suffer from rising damp (Spiteri, 1999).

(iii) *Human resources:* A severe problem of lack of trained conservation/restoration staff.

As a result, the collection today is in a very poor state of conservation. Several protective systems were applied over the years in an attempt to slow down the deterioration processes. These include boat varnish, wax and various trade named anti-corrosion oils. None of these applications were very successful in the long-term protection of these artefacts. Upon ageing, varnish yellows, becomes brittle and eventually detaches from the metal. Wax traps dust, spores, and salt rich aerosols eventually breaking down. Anti-corrosion oils have proved to be aesthetically unacceptable.

Concerned with the poor state of conservation of the armoury, we decided to embark on a PhD research project that could eventually lead to the preparation of a new protective coating for these metal artefacts. This coating is applied via plasma assisted physical vapour deposition (PA-PVD). Apart from respecting the standards of conservation ethics (i.e. reversibility, transparency and corrosion protection) the protective coating will be designed to outlive conventional protective systems with minimal maintenance requirements. The coating is currently under development and will be designed for application onto the various armour pieces.

Since we are dealing with priceless objects, tests conducted on the PA-PVD coating will be carried out on coupons designed to mimic armour metal. The test coating will be applied onto both clean and partly oxidized metal. In the latter case,

the metal coupons will be artificially corroded inside a climatic chamber. The corroded coupons will be cleaned of superficial corrosion in a manner normally performed by conservators working on real armour artefacts. The PA-PVD coating will be tested on this modified surface.

The choice of metal used to reproduce armour plates is an important step in this study. The composition and microstructure of the chosen material will markedly influence its corrosion behaviour. A preliminary characterization of the microstructure and corrosion typology of a number of representative armour pieces from the Palace collection was therefore required.

2.2 Microstructure of steel armours

If an armour plate is made of relatively pure iron, the microstructure will be composed of a random arrangement of ferrite grains (white) distinguishable by their grain boundaries (black lines).

For a hypoeutectoid steel plate that has been fabricated in the austenite range, i.e. above the upper critical temperature of the metal (carbon content in the range 0.02-0.77 wt %, curve (a), Figure 1), and then allowed to cool slowly (equilibrium cooling), the microstructure will consist of grains of ferrite and lamellar pearlite (γ-austenite → α- ferrite + pearlite).

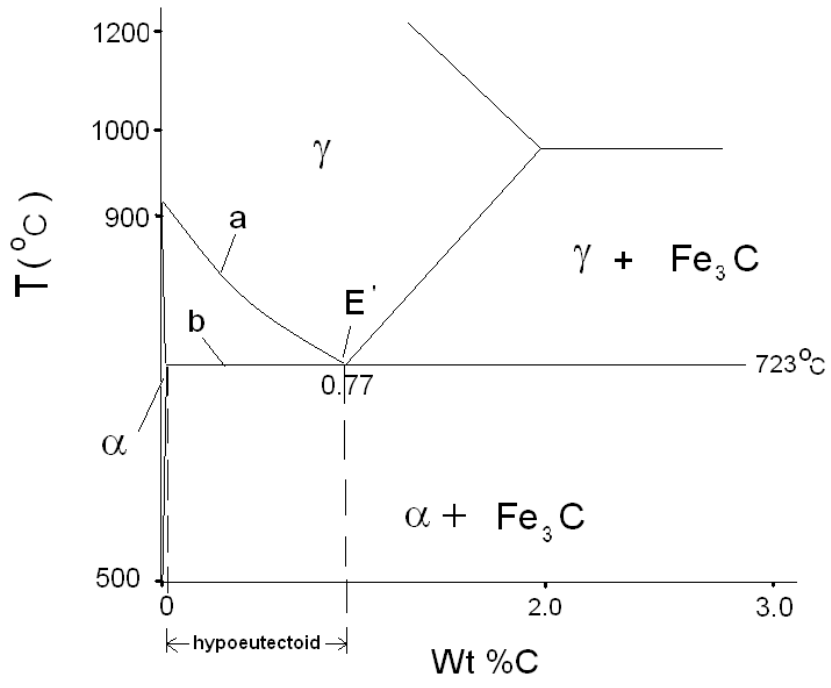

Figure 1: Detail of the equilibrium phase diagram for iron –iron carbide system showing the eutectoid point (E'), austenite (γ), ferrite (α) and pearlite (α + Fe_3C). Curve a and b represent the upper and lower critical temperatures.

Pearlite is made up of alternating bands of ferrite (pure iron) and cementite (dark grey phase of iron carbide, Fe_3C), and forms when adequate time is allowed for carbon

present in solution (in prior austenite) to crystallise as iron carbide. Upon cooling from the austenite range, the first phase to form is pro-eutectoid ferrite. The morphology of the latter is partly determined by the cooling rate and the relative size of prior austenite grains. Slow cooling in air and small prior austenite grains favours the formation of equi-axed ferrite. In contrast, large prior austenite grains and rapid air-cooling allows for the formation of Widmanstätten ferrite. These grains assume acicular and/or wedge-shaped shaped structures (Garagnani et al, 1996; Bhadeshia, 1985).

If the steel plate is forged below its upper critical temperature (curve (a), Figure 1), the ferrite grains obtained will be distorted. This occurs because ferrite crystals would have already been formed below the critical temperature (Williams, 1980).

Another possible microstructure for steel occurs when an armour plate is given a 'full quench' that is, when the plate is cooled rapidly to ambient temperatures by dipping in cold water directly from forging temperatures. This is a case of non-equilibrium cooling. The iron-iron carbide equilibrium diagram given in Figure 1 will not be useful in describing the microstructure since iron carbide will not have had enough time to separate out of solution. The steel will transform at a lower temperature into a phase consisting of plate-like or needle-like grains of martensite. Martensite is exceedingly hard but unfortunately very brittle. Quenched armour would therefore not serve any good use on the battlefield. The armour craftsmen of the 15th century were quite knowledgeable of this fact and devised different routes to circumvent the problem (Williams, 2003). For the case of quenched steel, the material was subsequently subjected to a heat treatment or tempering. Tempering causes the non-equilibrium martensite grains to transform into ferrite and carbides. During heat treatment, carbides are dispersed evenly in a ferrite matrix and material toughness is enhanced at the expense of hardness. This technique was mastered in the southern cities of Germany, primarily Augsburg and Landshut. An alternative to the 'full quench' is the 'interrupted quench'. Red hot metal is plunged in cold water (few seconds), taken out in air and allowed to cool for a few more seconds and is then reintroduced into cold water where it is allowed to continue cooling. Overall the cooling rate is less than that for a full quench and ferrite and pearlite phases form together with martensite. Another method involved varying the cooling rate of hot worked armour to obtain something in-between a full quench and equilibrium cooling. The resulting microstructure contained ferrite, pearlite as well as martensite. The latter process is known as slack–quenching and was performed by cooling armour in oil or molten lead. The cooling rate is intermediate between that following quenching in water and cooling in air (annealing) and can also be referred to as normalizing.

The presence of slag inclusions is a common occurrence in armour metal. Slag originates from impurities present in the iron ore. Hammer scale (iron oxides) from forging activity and the sand (silicates added to serve the purpose of flux during forge welding) also contribute to the volume fraction of slag in the finished product (Williams, 2003). Slag is a brittle glassy material containing iron silicate (fayalite). During hot forging, slag is plasticized and shaped into elongated stringers in a direction perpendicular to that of the direction of beating of the hammer (Williams, 2003).

3. Methodology

3.1 Choice of Artefacts

For this project, it was essential to select a number of artefacts that would represent the whole Palace collection. This proved very difficult to achieve since the collection is very heterogeneous (design, dating, provenance, functionality etc). Aware of this problem, we carried out a survey of the armour collection. The survey focused on dating and provenance, corrosion typology and past protective applications. On completion of the survey we were in a position to choose a small (10 pieces) but representative group of armour artefacts for further investigation. Table 1 lists and describes these artefacts.

Artefact	Inventory No	Provenance	Date	General state
Upper right leg protection (tasset)	PA RC 29	N/a	N/a	Artefact is part of a tasset. The artefact is heavily corroded.
Left shoulder protection (pauldron)	PA RC 166	North Italian	1600-1650	Artefact is part of a pauldron. The artefact is heavily corroded. The artefact is decorated by a brass rivet motif.
Backplate	PA 329	North Italian	ca. 1570	Artefact is a complete armour piece. It is damaged on one side (a small section has been cut through the metal). Reticular corrosion occurs on the external horizontal surface.
Neck protection (gorget)	PA RC 25	North Italian	ca. 1670	Artefact forms the back part of the gorget armour piece. The artefact is complete but is covered with a thin layer of corrosion. Original metal etching decoration is still visible under the corrosion layer.
Upper right leg protection (tasset)	PA RC 80	Probably German	N/a	Artefact forms a complete tasset armour piece that is slightly corroded.
Protection of right the upper arm (cannon)	PA RC 20	North Italian	ca. 1670	Artefact forms a complete armour piece and suffers from general corrosion. Original metal surface was decorated with etching. This decoration is still visible under the layers of corrosion.
Right shoulder protection (pauldron)	PA 317	North Italian	ca. 1570	Artefact forms a complete armour piece. Corrosion occurs on the external horizontal surfaces.
Left shoulder protection (pauldron)	PA 316	North Italian	ca. 1570	Artefact forms a complete armour piece. Corrosion occurs on the external horizontal surfaces.

Full arm (left) comprising pauldron, upper and lower cannon and elbow piece.	PA RC 88	North Italian	ca. 1620	Artefact made up of several armour pieces, which serve to protect the left arm of the wearer. Investigative work was carried out on the pauldron.
Right shoulder protection (pauldron)	PA RC 165	North Italian	1600-1650	Artefact is part of a pauldron. A thin layer of corrosion covers the artefact. The artefact is decorated by a brass rivet motif.

Table 1 – Inventory number, provenance and approx. dating of armour artefacts selected for further investigation. N/a means " not available"

3.2 Sample Preparation

Each armour piece was examined visually in order to identify a proper site for sampling. Fragment extraction was carried out in accordance to the following requirements:

(i) The site of sampling must be easily accessible. The cutting device is of a certain size and some space is required for maneuvering.
(ii) The fragment size is kept to a minimum (ca. 10 mm^2 max.)
(iii) Armour artefacts are complicated 3-dimensional objects comprising an external and an internal surface. Where possible, the fragment is extracted from the interior of the armour piece
(iv) For the case of corroded armour pieces, fragments are preferably extracted from corroded areas.
(v) Sampling is performed in such a way that important features on the surface of the armour are not damaged nor lost (e.g. decoration - etching or embossing, loss of curved features etc…)
(vi) Sampling was carried out with the prior consent of the curator.

Fragments were cut out from the armour plate using a jeweller's saw. Distilled water was applied onto the fragment and surrounding metal during the extraction process so as to avoid overheating the metal which could alter the microstructure.

Each fragment was attached to the bottom of a mould (25mL volume plastic cup) using a minimum amount of Superglue. Fragments were positioned in such a manner that permitted the armour plate from which the sample was extracted to be viewed in cross-section. Once fixed, fragments were embedded in an epoxy-based resin (Epoplast by Buehler). Liquid resin was slowly poured over the fragments to avoid trapping air bubbles and allowed to solidify overnight in a fume hood.

Grinding of the polymer surface and embedded metal was carried out on a turntable using successively 100, 200, 300, 400 and 600-grade silicon carbide grinding paper. Grinding was performed in a direction parallel to the embedded metal section. Tap water was used as lubricant. For each grinding step, the exposed metal surface was cleaned thoroughly to remove traces of silicon carbide particles that detach from the grinding paper and remain stuck to the surface. Cleaning involved

applying a layer of concentrated liquid surfactant (e.g. non-ionic Triton X-100) onto the exposed metal and surrounding polymer surface, dipping into hot running tap water for a few seconds, washing with an alcohol/methylated spirit mixture and drying rapidly with a heat gun (hair-dryer). Sections were then checked under a magnifying lens to evaluate the consistency and direction of the grinding marks before proceeding to finer grade paper.

Polishing was carried out on a polishing turntable using 6-micron followed by 1-micron diamond paste. An alcohol-based lubricant (Buehler) was used for polishing. During polishing, the treated surface was counter rotated in the direction of motion of the turntable. This allows for homogenous polishing of the whole surface. On switching from six to one micron, the metal was washed thoroughly to remove the coarser particles. A final cleaning was performed following polishing with 1-micron diamond paste. When dealing with historic or archaeological metal containing slag inclusions and/or corrosion layers, it becomes relatively difficult to obtain a metallic surface that is completely free of scratch marks. Insisting with polishing is likely to induce further scratches.

3.3 Observation, etching and examination

Polished sections were examined optically using a metallographic microscope equipped a white light source. A preliminary observation was carried out prior to etching. Features such as slag inclusions, corrosion layers and corrosion pits are easily identifiable against the white unetched background. In comparison, an etched matrix may render the identification of these microstructural features more difficult. The polished metal was then etched chemically in 2% Nital-Picral solution (2% nitric acid in ethanol, containing a trace amount of picric acid; the latter is added to enhance the effect of the Nital etch; etching time < 5 seconds) and is followed by an alcohol rinse and drying in warm air. The etched samples were re-examined under the metallographic microscope. For the metal cross-section extracted from PA RC 165 (pauldron), Oberhoffer's reagent (500mL distilled water, 500mL ethanol, 0.5g tin(II) chloride, 1g copper(II) chloride, 30g iron(III) chloride and 50mL nitric acid) was used as a second etchant.

Not more than a few minutes were allowed to elapse between the final polishing step and etching. Longer times lead to the formation of a thin layer of iron oxide on the metallic surface that tends to slow down the etching process. This effect is not desirable when dealing with metal fragments covered with corrosion layers. A longer exposure to the etching solution is likely to cause dissolution of corrosion material, which will, in turn, stain the grains forming the microstructure.

An estimate of the carbon content in ferrite-pearlite steel can be obtained from an evaluation of the ratio of dark and white areas in the photomicrograph. This can be carried out using an image analysis computer program. The software evaluates the ratio of black and white areas on a digitized microphotograph and calculates an approximate value for the concentration of carbon. Unfortunately this software was not available at the time of this study and we had to resort to an approximate estimate of the carbon content based on visual inspection of the microphotographs at low magnification.

4. Results

A description of the microstructure of armour elements is listed in Table 1. Microstructures are described starting with the simplest and proceeding to the more complex structures.

Tasset (Inv. No. PA RC 29) and pauldron (Inv. No. PA RC 166)

(a)

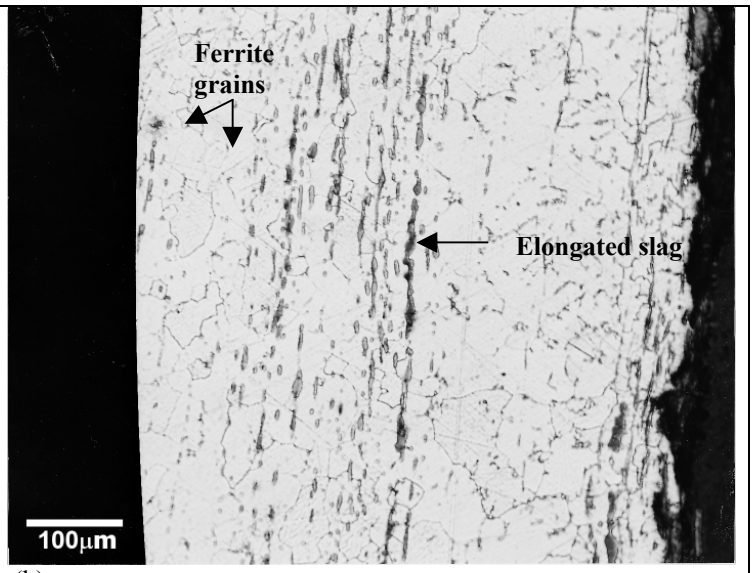

(b)

(c)

Figure 2: (a) part of a tasset armour piece (PA RC 29) (b) photomicrograph showing etched area of sample extracted from artefact shown in (a). The microstructure consists of ferrite grains. Elongated slag inclusions run the length of the section. (c) part of a pauldron armour piece (PA RC 166). Enclosed area indicates the site of sampling.

Artefacts PA RC 29 (upper leg protection, Figure 2a) and PA RC 166 (shoulder protection, Figure 2c) form parts of armour pieces and both are heavily corroded. For PA RC 29, the sample fragment was extracted from the backside of the artefact. The microstructure comprises of ferrite grains and a large volume fraction of slag (Figure 2b). The abundance of slag inclusions suggests that this armour piece was manufactured from very poor quality metal. Artefact PA RC 166 exhibits the same microstructure. The armour piece and site of sampling are shown in Figure 2c.

ABN 70 592 297 967

Backplate (Inv. No. PA 329) and gorget (Inv. No. PA RC 25)

(a)

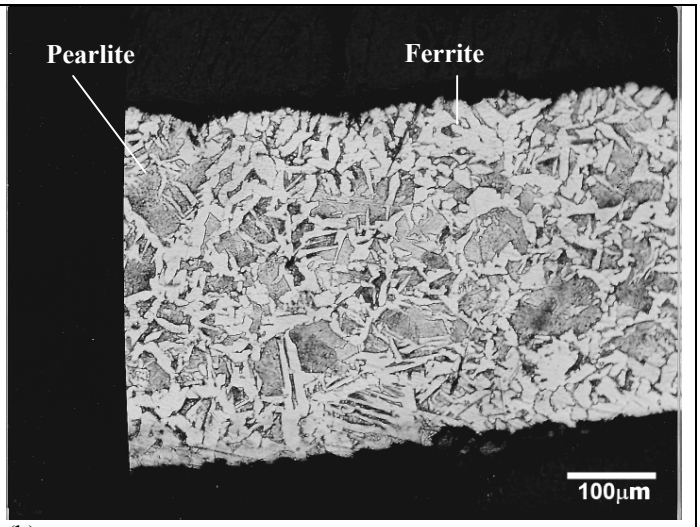

(b)

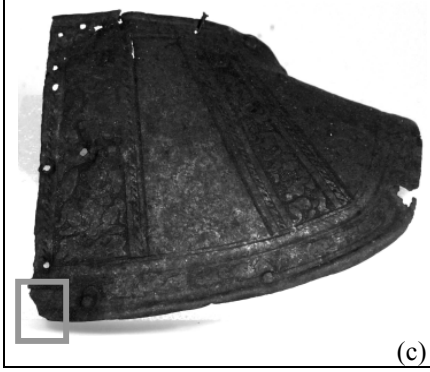

(c)

Figure 3: (a) backplate (PA 329) (b) photomicrograph showing etched area of sample extracted from backplate given in (a). Microstructure comprises of coarse ferrite grains (some acicular) and pearlite (c) part of a gorget (PA RC 25). Enclosed area indicated the site of sampling.

The backplate is a complete armour piece (Figure 3a). The sample was extracted from a damaged area of the armour piece. The microstructure consists of coarse ferrite grains surrounding islands of pearlite (Figure 3b). Widmanstätten ferrite plates having an acicular or wedge shaped structure are present in some areas (Garagnani et al 1996; Badeshia, 1985). The content of carbon in this hypoeutectoid steel is estimated at ca. 0.3-0.4-wt %. The ferrite and pearlite microstructure indicates that the plate was air cooled after fabrication.

Artefact PA RC 25 is a part of the armour piece forming a gorget (neck protection). The plate is decorated by an etching motif. The decoration is still visible in spite of a thin layer of corrosion material that covers the whole artefact. The site of sample extraction is indicated in Figure 3c. The microstructure of this hypoeutectoid steel is the same as for the backplate except that this artefact has more elongated slag inclusions. The carbon content is estimated at ca. 0.1-0.2 wt %, slightly lower than that obtained for the backplate. The microstructure suggests that the armour plate was air cooled after fabrication.

Tasset (Inv. No. PA RC 80)

(a)

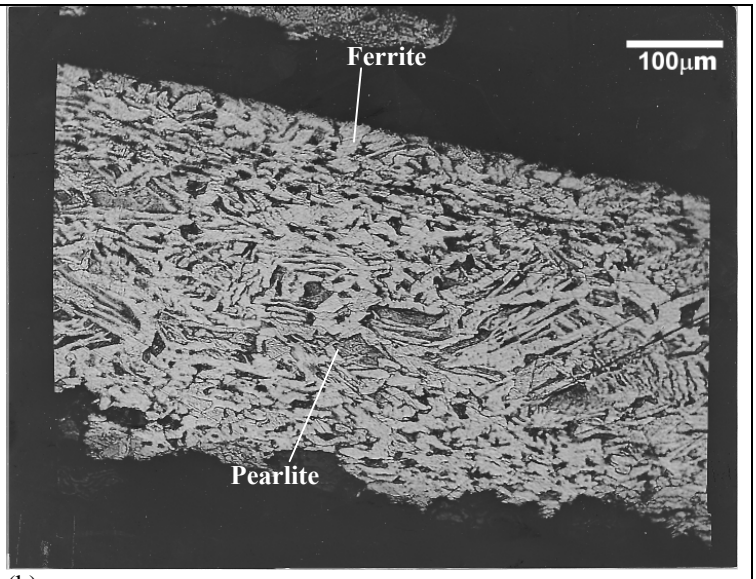

(b)

Figure 4: (a) tasset (PA RC 80) (b) photomicrograph showing etched area of sample extracted from tasset shown in (a). The microstructure is ferrite and pearlite with elongated slag inclusions. The ferrite grains are slightly distorted.

The artefact forms a whole armour piece (Figure 4a). A sample was extracted from the backside. The microstructure consists of coarse ferrite grains and pearlite. Some ferrite assumes a Widmanstätten structure (Figure 4b). The steel is a hypoeutectoid with a carbon content estimated at 0.1-0.2-wt %. Ferrite grains are slightly distorted indicating that the plate was subject to some amount of cold working (performed below curve (a) in Figure 1). The microstructure suggests that the artefact was air cooled after fabrication.

ABN 70 592 297 967

Cannon (Inv. No. PA RC 20) and pauldron (Inv. No. PA 317)

(a)

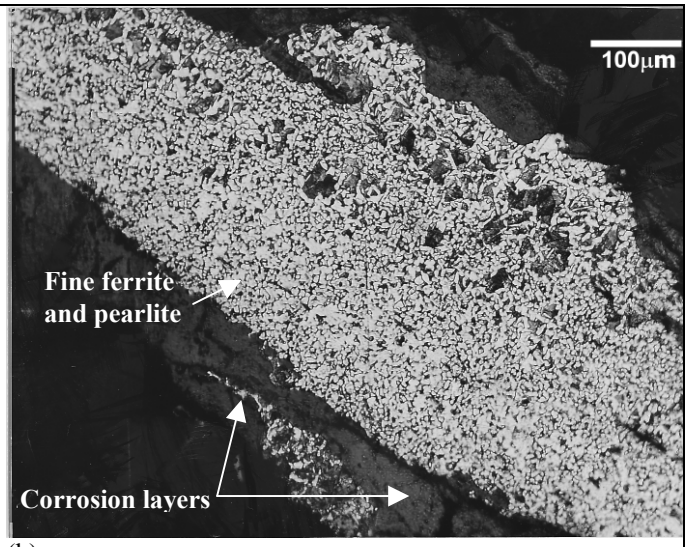

(b)

(c)

Figure 5: (a) upper cannon (PA RC 20) (b) photomicrograph showing etched area of sample extracted from cannon given in (a). The microstructure comprises of ferrite and pearlite with slag inclusions. Corrosion layers are visible in light grey (c) pauldron (PA 317).

Artefact PA RC 20 (protection of the upper arm, Figure 5a) is decorated by an etching motif and suffers extensive corrosion attack. A fragment was extracted from a corroded area. The microstructure consists of fine-grained equi-axed ferrite grains (ca. 5-10 microns in diameter) and a small amount of pearlite (Figure 5b). The carbon content of this hypoeutectiod steel was estimated at 0.1-0.2-wt %. Elongated slag inclusions run the length of the cross-section. The metal cross-section is extensively corroded and in some places corrosion has penetrated deep within the metal. The microstructure indicates that the armour piece was left to cool in air after fabrication. Pauldron PA 317 (Figure 5c) exhibits a very similar microstructure to PA RC 20.

ABN 70 592 297 967

Pauldron (Inv. No. PA 316)

(a)

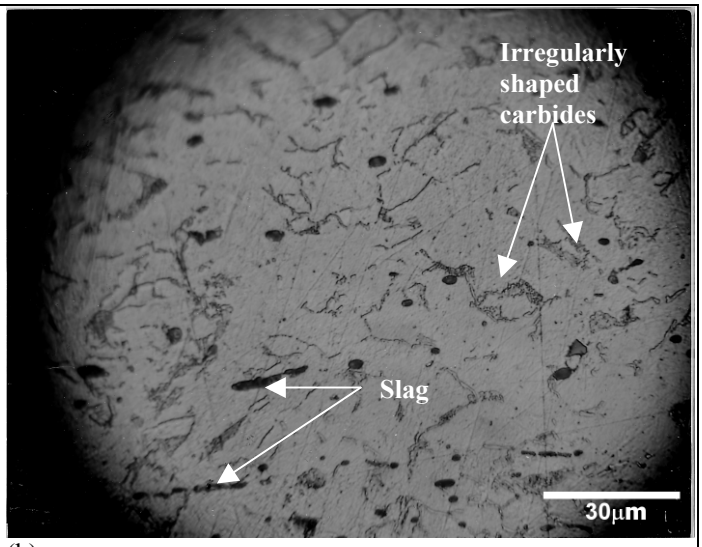

(b)

Figure 6: (a) pauldron (PA 316) (b) photomicrograph showing etched area of sample extracted from (b). Microstructure showing ferrite, carbides and elongated slag inclusions.

A fragment was extracted from within the armour piece (Figure 6a). The microstructure consists of ferrite grains and patches of pearlite. This is a hypoeutectoid steel with a carbon content estimated at 0.2-0.3 wt %. When the section was examined at higher magnification, it was noted that pearlite was transformed into carbides ('divorced' pearlite). The lamellar nature of the pearlite was converted into irregularly shaped carbide stringers. Slag inclusions (circular and elongated morphology) are clearly identifiable from carbides in the photomicrograph (Figure 6b). This may have occurred as a result of sustained heating below the lower critical temperature (below curve (b), Figure 1). Perhaps the armour piece was repaired at some stage.

Pauldron (Inv. No. PA RC 88)

(a)

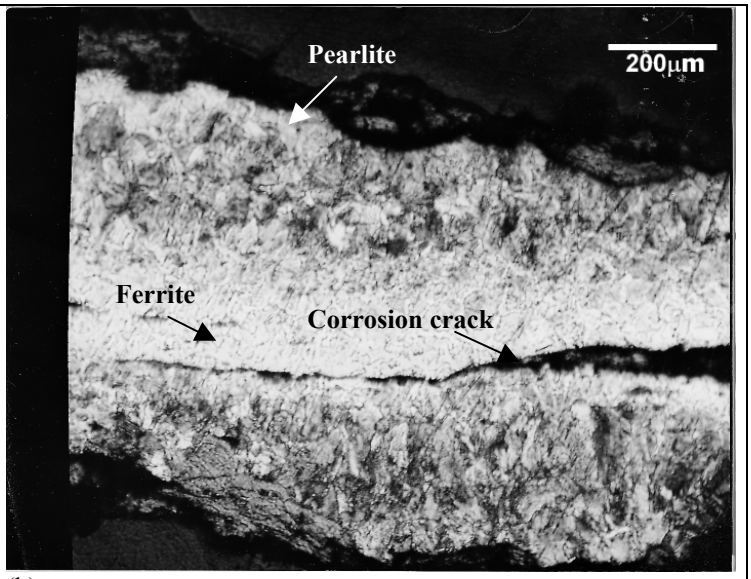

(b)

Figure 7: (a) full arm comprising of a pauldron, upper and lower cannon and elbow piece (PA RC 88) (b) photomicrograph of sample extracted from (a). The microstructure is primarily pearlitic. A large corrosion crack has developed. A ferrite band lines the corrosion crack.

A sample was extracted from inside the pauldron (Figure 7a). The microstructure is predominantly pearlitic (near eutectoid steel, carbon content 0.6-0.7 wt %) with a band of ferrite running through the middle part of the metal section. The ferrite grains line a large corrosion crack (Figure 7b). The corrosion crack seems to be following elongated slag inclusions (galvanic effect). It is very probable that the crack had developed at a weld zone, since forge welding is likely to leave a row of slag inclusions trapped along the weld line (Williams, 2003). The ferrite phase formed along the crack further supports this hypothesis. In fact, the formation of the ferrite probably resulted from the decarburization (loss of carbon) of the metal in the weld region.

ABN 70 592 297 967

Pauldron (Inv. No. PA 165)

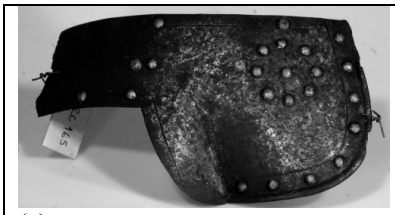

(a)

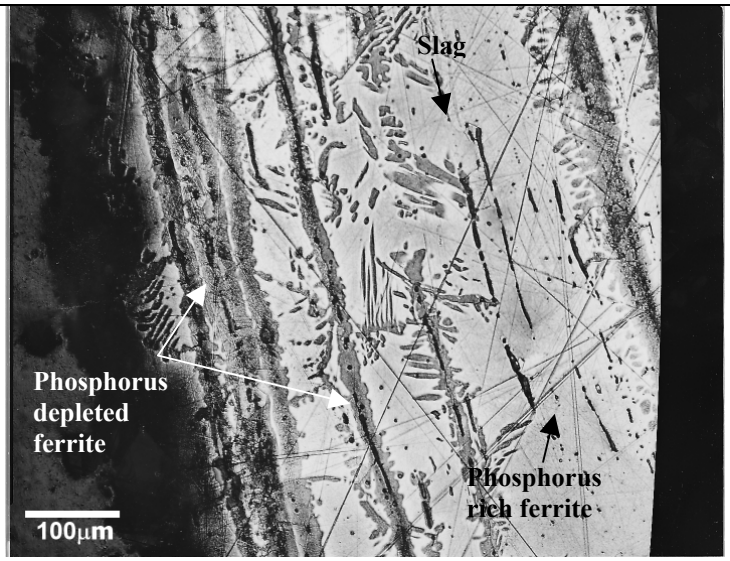

(b)

Figure 8: (a) part of a pauldron (PA RC 165) (b) photomicrograph showing etched area of sample extracted from (a). Phosphorus rich iron shows in white while phosphorus depleted zones show in dark grey.

The plate formed part of a pauldron that was decorated by brass rivets (Figure 8a). The microstructure consists of ferrite grains and slag. Furthermore, the Nital etch incurs a water shimmer appearance on some of the ferrite grains. This effect is referred to as ghosting and occurs in case of irons containing ca. 0.1-0.5% phosphorus (Stewart et al, 2000). Nital etches phosphorus rich iron zones to a lesser extent than pure ferrite leading to surface relief effects. The ghost microstructure is revealed by slight adjustments of the fine focus of the optical microscope (Stewart et al, 2000). In order to confirm the presence of phosphoric iron, Oberhoffer's reagent was applied subsequent to Nital etchant. The reagent deposits copper on the surface of pure ferrite grains. This causes the grains to appear dark under the optical microscope. Less copper is deposited in regions rich in phosphorus so that these appear bright (Stewart at al, 2000). A photomicrograph of the metal section treated with Oberhoffer's reagent is given in Figure 8b.

5. Discussion

Table 2 summarizes the general microstructural features of the armour pieces investigated.

Armour piece	Inv No.	Microstructure	slag	Wt % carbon	Cooling rate	Comments
Tasset	PA RC 29	Ferrite	+++	N/a	Air cooled	
Pauldron	PA RC 166	Ferrite	+++	N/a	Air cooled	
Backplate	PA 329	Ferrite and pearlite	+	0.2-0.3	Rapid air cooling	Widmanstätten ferrite
Gorget	PA RC 25	Ferrite and pearlite	++	0.1-0.2	Rapid air cooling	Widmansttäten ferrite
Tasset	PA RC 80	Distorted ferrite and pearlite	++	0.1-0.2	Rapid air cooling	Widmanstätten ferrite.
Cannon	PA RC 20	Ferrite and pearlite	+	0.1-0.2	Air cooled	Equi-axed ferrite
Pauldron	PA 317	Ferrite and pearlite	+	0.1-0.2	Air cooled	Equi-axed ferrite
Pauldron	PA 316	Ferrite and pearlite	+	0.1-0.2	Air cooled	'Divorced' pearlite
Pauldron (full arm)	PA RC 88	Ferrite and Pearlite	++	0.6-0.7	Air cooled	Pearlitic steel with ferrite lining a corrosion crack
Pauldron	PA RC 165	Ferrite with ghost microstructure	+++	N/a	Air cooled	iron containing phosphorus in the range 0.1-0.5 wt%

Table 2- Inventory number, microstructure, wt % carbon and cooling rate. Low (+) medium (++) and high (+++) slag content. N/a means "not available".

Slag inclusions were present in all the armour plates examined. This indicates that the metal (steel or wrought iron) utilized in the manufacture of these armour plates was produced from its ore via pre-modern techniques such as the Bloomery hearth. Wrought iron produced from the reduction of cast iron, and steel obtained directly from the reduction of the ore allowed for an amount of slag to remain in the finished bloom (Williams, 2003). Hence the armour pieces used in this study could be authenticated from the presence of slag. Furthermore, the elongated nature of slag suggests that these armour plates were forged into shape at relatively high temperatures (Williams, 2003). Out of ten artefacts examined, three pieces were made of wrought iron (ferrite) and seven were made in steel. As indicated in Table 2, the highest amount of slag was obtained in the wrought iron armour fragments. Excessive quantities of slag cause the metal to become brittle (Williams, 2003). The high amount of slag obtained in wrought iron artefacts indicates armour of lower quality.

For steel armour, the carbon content varies within the range 0.1 to 0.3 wt %. The metal utilized in the production of these artefacts would classify as low carbon steel. An exceptional case is artefact PA RC 88 which is a higher carbon steel containing 0.6-0.7wt % carbon. The size and shape of the ferrite grains vary considerably from one steel to another. Artefacts PA RC 20 and PA 317 exhibit fairly

fine equi-axed grains (5 - 10μm) while PA RC 25, PA 329 and PA RC 80 show coarse ferrite grains, some featuring an acicular shape. The latter microstructure was first described in meteoric iron by Widmanstätten (Tylecote, 1992). The acicular ferrite grains tend to isolate pearlite into separate patches, so that both the strength and toughness of the final material are unevenly distributed. Such a structure therefore renders the steel plate weak and brittle (Garagnani et al 1996; R.A. Higgins, 1993). Williams describes armour with this type of microstructure as being of inferior quality. The armour pieces were probably maintained at very high temperatures (allowing the formation of large austenite grains) and then cooled relatively rapidly in air.

Armour piece PA RC 165 was manufactured from a phosphoric iron. This was confirmed by the Oberhoffer's reagent. The microstructure consists of bands of phosphorus-rich and phosphorus-depleted zones. For an iron that contains phosphorus in the concentration range (0.1-0.5) wt %, a temperature domain exists where austenite and ferrite co-exist (900-1400 ^{o}C). The solubility of P in austenite is lower than in ferrite. Thus, if the metal is maintained in the two phase region for a sufficiently long enough time, regions of low and high P will appear, corresponding to prior austenite and ferrite zones respectively. The armour plate section revealed a banded microstructure with regions of high (white) and low (dark) phosphorus zones. This banding arrangement was encountered in a number of archaeological and historic artefacts examined by Vega. (Vega et al, 2002). The banded arrangement (phosphorus rich zones alternating with phosphorus depleted zones) was attributed to forging activity. Williams has performed metallographic examination of a large number of armour suits and separate armour pieces. He argues that although phosphoric irons are frequently found in archeological irons, they are seldom found in armour metal (Williams, 2003). Phosphorus renders the steel 'cold short' that is when cold worked the resulting material has inferior mechanical properties and is relatively brittle (Stewart, 2000). A phosphorus-rich armour plate would therefore not serve much use on the battlefield and it seems that the armourers of the time were aware of this fact. It is therefore very likely that this particular armour piece was produced from recycled material (iron objects other than armour), or from an iron billet that contained phosphorus. Phosphorus is commonly found in iron ore but might also find its way into iron from the fuel during the reduction process. Whatever the case, the armourer or blacksmith was probably unaware of the poor quality of the metal that was used.

Williams conducted an extensive study of the metallurgy of European armour. Italian armour manufactured before the year 1510 was often subject to heat treatment. In an attempt to harden the metal slack quenching was often used. This practice seems to have been stopped abruptly shortly afterwards. This applies to both good quality armour as well as field armour. Williams attributes this sudden change to the introduction of fire gilding (Williams, 2003). Out of six Italian steel armour plates investigated in this study, all were produced after 1510 and none showed any sign of quenching. Fast cooling would have provoked the formation of martensite, a phase that was not detected in any of the samples examined. This is in agreement with the general trend observed by Williams. However, given the small number of armour artefacts examined, a more comprehensive study involving many more pieces would have to be performed in order to draw more definite conclusions.

6. Conclusion

The metallurgy of several armour pieces from the Palace Armoury collection was examined for the first time in the collection's history. The metallurgy is quite heterogeneous. Of the ten armour elements investigated, three pieces were made in wrought iron, six classified as low carbon steels and one was made of high carbon steel. One of the wrought iron armour pieces was made of a phosphoric iron, an unusual material for such artefacts. All the armour pieces were forged into shape as evidenced by the elongated morphology of the slag inclusions. None of the artefacts seemed to have been quenched (full or slack) in order to obtain steel of superior strength and quality. From this preliminary investigation, we have concluded that the best material for use in the preparation of coupons will be plain low carbon steel with minimal alloying elements.

Acknowledgments

Heritage Malta and the Palace Armoury Collection for allowing us to sample the armour artefacts

Cost Action G8 for funding a short-term scientific mission (STSM) to the Wallace Collection in London.

The Wallace Collection for hosting the STSM.

Mr. Stephen C. Spiteri for helping out in the dating and provenance of the armour pieces

The Malta Centre for Restoration for supporting this work

References

Bhadeshia H. K. D. H. (1985) *Diffusional formation of ferrite in iron and its alloys* Progress in Material Science*, 29*, 321-386.

Bomomi, S., Martini, C., Poli G. and Prandstraller, D. (2003) *Modernity of Early Metallurgy: Studies on an Etruscan Anthropomorphic Bronze Handle*, International conference, Archaeometallurgy in Europe, Milan, Italy September 24-26th, 467-472.

Chetcuti, D., Buhagiar, A., Schembri, P. J. and Ventura, F. (1992) *The Climate of the Maltese Islands: A Review* (University Press, Malta).

Garagnani, G. L., Zucchi, F., Tommesani L. and Brunoro, G. (1996) *Metallurgical investigations on 16th –17th century iron armours from the Museo Nazionale of Ravenna*, Science and Technology for Cultural Heritage 5 (2), 83-94.

Higgins, R. A. (1993) *Engineering Metallurgy – Volume 1, Applied Physical Metallurgy* (Edward Arnold, UK).

Spiteri, S. C. (1999) *The Palace Armoury, A study of a Military Storehouse of the Knights of the Order of St. John* (Print Services Ltd, Malta).

Stewart, J. W., Charles J. A. and Wallach, E. R. (2000) *Iron –phosphorus- carbon system Part 1 – Mechanical properties of low carbon iron-phosphorus alloys*, Material Science and Technology, 16, 275-282.

Stewart, J. W., Charles J. A. and Wallach, E. R. (2000) *Iron –phosphorus- carbon system Part 2 – Metallographic behaviour of Oberhoffer's reagent*, Material Science and Technology, 16, 283-290.

Stewart, J. W., Charles, J. A. and Wallach, E. R. (2000) *Iron –phosphorus- carbon system Part 3 – Metallography of low carbon iron-phosphorus alloys*, Material Science and Technology, 16, 291-303.

Tylecote, R. F. (1992) *A History of Metallurgy 2nd edition*, (Institute of Materials, UK).

Vega E., Dillmann P., Lheritier M., Fluzin P., Crew P. and Benoit P. (2003) *Forging of phosphoric iron. An analytical and experimental approach*, International conference, Archaeometallurgy in Europe, Milan, Italy. September 24-26th, AIM 337-346

Williams A. (1980) *To what extent can forgeries be detected by metallurgical analysis, A study of some helmets, Institut Suisse d'Armes Anciennes* , Rapport 3 and 4, Grandson 61.

Williams A. (2003) *The Knight and the Blast Furnace, A History of the Metallurgy of Armour in the Middle Ages and the Early Modern Period* (Lieden, Netherlands).

